The Impact of Desalination and Climate Change on Salinity in the Arabian Gulf

F.L. Dols

Deltares
Enabling Delta Life

UNIVERSITY OF TWENTE.

Impact of Desalination and Climate Change on Salinity in the Arabian Gulf

By

F.L. Dols

Student nr: S182227

In partial fullfilment of the requirements for the degree of

Master of Science
in Civil Engineering & Management

at the University of Twente,
Faculty of Engineering Technology

July 2019

Keywords: Desalination, Climate Change, Climate-change, Arabian Gulf, Persian Gulf, Delft3D FM, Delft3D Flexible Mesh, future water supply.

Supervisors:

Prof. dr. K.M. Wijnberg	University of Twente
Dr. ir. G.H.P. Campmans	University of Twente
Ir. R. Morelissen	Deltares
Ir. R. Hoekstra	Deltares
Ir. R. Vlijm	Deltares

Postboxes: University of Twente, P.O. Box 217, 7500 AE Enschede, Nederland

Deltares, P.O. Box 177, 2600 MH Delft, Nederland

Preface

A year and a half ago, I chose to research this topic because of the potential to contribute in a relevant public debate on the sustainability of desalination. The power of science and engineering to solve societal problems has driven me during my 7 year journey as a student and the societal usability of the skills I was learning was always the motivation to put in the necessary hard work.

Over the past ten months, I've had the luck to cooperate with Kathelijne and Geert from the University of Twente. The meetings with Kathelijne showed me a long-term perception on the progress, which I'd lost sight of while being caught up in the day-to-day challenges. The biweekly discussions with Geert were mainly on the technical aspects, pushing me to delve deeper into physical and numerical aspects of the model. On a daily basis, I benefitted enormously from the collaboration with Deltares, because Robin, Roderik and Roland formed such an effective team. Robin always stimulated me to look at the bigger picture, Roderik helped me to keep a clear focus on the objectives and Roland was my knight in shining armour in times of need.

In the course of the project, I learned that work is not a stand-alone thing, but rather integrated in daily life. When I was feeling good, I produced and progressed, while both production and progression suffered from lesser moods. Vice versa, work also affected my mood. Experimentation with balancing work and off-work has been insightful and made me a little bit more mature. I want to thank my family and friends for inspiration and relaxation. With specific mention of my roommate in Rotterdam: Guus, you are the most authentic person I know. To call upon the biggest cliché of all times: without you guys this piece of work would not have been what it is. My eternal gratitude to all of you!

Summary

In the Arabian Gulf region, growth in population size and water use per capita causes a growing trend in water demand over the last decades. The trend of increasing fresh water demand is projected to continue, while groundwater resources are projected to be depleted by 2050. Desalination is currently the only viable solution to fresh water deficiency and new desalination plants are installed at an increasing rate, together adding up to a significant capacity of fresh water extraction from the Arabian Gulf. Another trend of increased fresh water extraction is the rate of evaporation, which is projected to increase as a result of global climate change induced air temperature rise.

Salt is conserved during water extraction by desalination or evaporation, causing salt accumulation in the Arabian Gulf. The Gulf is more saline than the ocean and that density gradient drives lateral exchange. Year round, an equilibrium is reached in which the amount of salt in the Gulf is stable. Little is known about the future impact on the development of salinity in the Arabian Gulf of large scale desalination capacity increase and air temperature rise is. This research provides a gross combined impact assessment of desalination and climate change on salinities in the Arabian Gulf.

The main objective is to identify the significance of the impact of the desalination industry combined with and relative to the impact of climate change on salinity in the Arabian Gulf. Increased salinities affect ecology and the efficiency of desalination plants. The most vital ecology and desalination is concentrated in and at the shallow coastal area, which is the reason the focus of the research is on this region. Impact is measured in year averages, seasonal variations and weekly variations of salinity.

The software package of Delft3D FM is used to conduct numerical experiments that simulate hydrodynamic flow and salt distribution for a reference case and numerous alternative forcings on the Arabian Gulf. The numerical model accurately represents water temperatures and processes of importance, like geostrophic circulation, seasonal stratification and meso-scale eddies. Salinities seem to be overestimated compared to the available field data. The research focusses on salinities of alternative conditions relative to the reference case, for which absolute values are of lesser relevance.

Climate change, in this research defined as increase in atmospheric and oceanic water temperature, drives the evaporation rates. Increased evaporation rates did not cause increased Gulf wide salinity. Due to climate change the temperature of the oceanic inflow increases more than the temperature of the bottom outflow. The resulting increase in density gradient through the Strait stimulates lateral exchange, which dampens the salinity increase due to increased rate of evaporation. Combined, desalination capacity increase and climate change barely influence the Gulf's average salinity.

On a local scale, both desalination and climate change cause salinity increases bigger than 1 PSU. The areas prone to extreme salinity increase are typically shallow and sheltered. The simulated salinities at these locations are extreme in the reference case too. Seasonal salinity extremes typically increase with double the year averaged salinity increase. Weekly variation only increases slightly in specific cases. In general, the simulations indicate that extreme salinities tend to become more extreme due to desalination capacity increase and climate change.

In the centre and north of the Gulf, increased desalination capacity and climate change barely affect the salinities, except for sheltered locations. The Bay of Iran is prone to salinity accumulation as a result of climate change driven increase in evaporation. In Kuwait Bay, salt accumulation is driven by climate change and increased desalination capacity, of which the latter dominates. Extreme increase of desalination (reference capacity times 10) in Kuwait Bay expands the spatial range of salinity increase to the shallow area in front of Kuwait Bay, towards and around Failaka island. The extreme salinities in the Gulf of Salwah that occur in the summer are simulated to increase significantly.

In the southeast of the Arabian Gulf a clear distinction can be made between the shallow sheltered Central United Arabian Emirates (UAE) coast and the relatively open east coast of Qatar and eastern coast of the UAE. The central UAE coastal zone is simulated to be imposed by salinity rise due to both climate change and desalination capacity increase. The more open east coast of Qatar and eastern UAE coast are more strongly affected by increase in gross oceanic inflow. Simulations show that increasing effects on salinity by increasing rates of evaporation and desalination are compensated by decreasing effects on salinity due increasing flushing rates. Future extreme scenarios show drops in salinity at locations along these open coastlines, that are remote from desalination plants.

It was found that wind fluctuations, average wind velocity and wind direction dominate evaporation and internal transport patterns in the Arabian Gulf and strongly affect the salinity distribution. Wind velocity increased by 50% provides for an increase of evaporation of the same order evaporation rate increase induced by air temperature rise of 4.5 ^{o}C. The uncertain development of the future wind climate introduces uncertainties in the simulations of future salinity distribution.

Table of Contents

1 Introduction

1.1 Background

Water scarcity is a severe global challenge, as 1.5 to 2 billion people currently live in areas of physical water scarcity and 0.5 billion people experience year-round water shortages (Jones, 2019). The increase of water scarcity is closely correlated to socio-economic development on one hand and increased extreme weather due to global climate change on the other hand (IPCC, 2014). For many regions in the world, desalination is currently anticipated as the only viable option to meet future fresh water demands the global reliance on desalinated water is projected to grow over the 21st century, see Figure 1.

In the arid Arabian Gulf region desalination of seawater has helped overcoming water shortages since the 1950's (Loutatidou et al., 2017). Since then the population has grown rapidly (World Bank, 2005), the water use per capita has increased (UN water, 2012) and natural fossil groundwater resources are being depleted (Mazzoni et al., 2018). The increasing fresh water shortage in the Arabian Gulf region has led to construction of numerous desalination plant, increasing the cumulative desalination capacity. Today, as much as 45% of the worlds desalination capacity is situated around the Arabian Gulf (Dawoud & Mulla, 2012). The large scale application of the energy intensive method of desalination in the Gulf Region has been possible due to cheap energy and great wealth from fossil fuel export. Desalination is considered the best available method of securing the fresh water supply in the Gulf region (Mansour, Arafat & Hasan, 2017) and big increases in desalination capacity are anticipated for the coming decades.

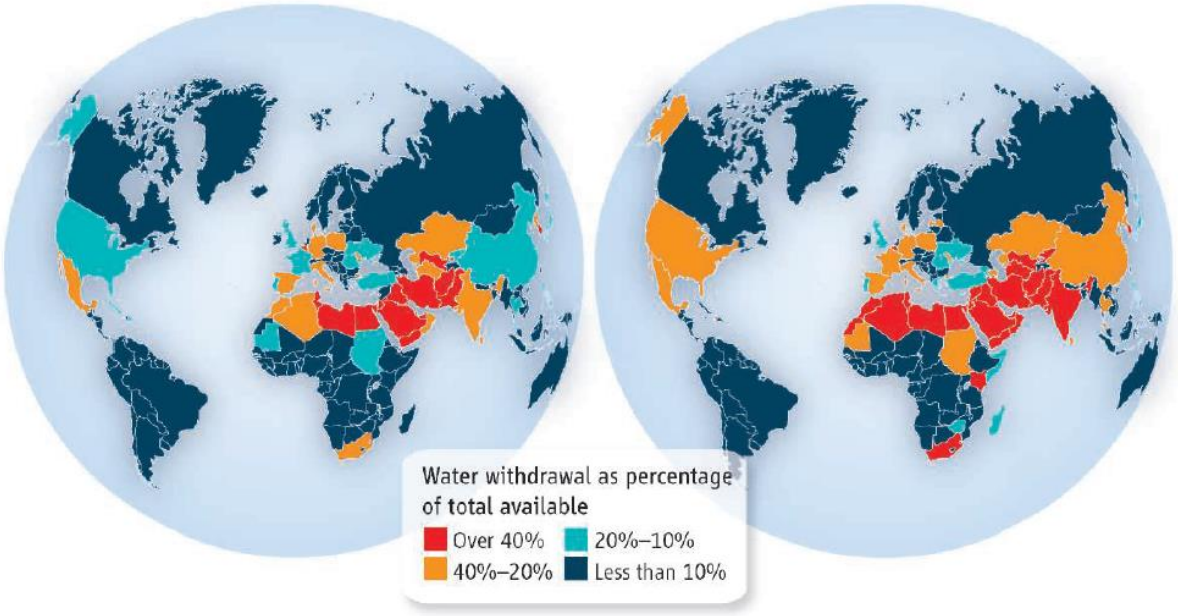

Figure 1: Maps depicting the national percentage of fresh water extracted from seawater, compared to the total fresh water supply of 1995 (left globe) and a projection for 2025 (right globe) depicting (Service, 2006).

The process of desalination extracts a volume of fresh water, but conserves salt. A brine effluent with high salinity is fed back to the Gulf, increasing the salinity of the receiving water (Hashim & Hajjaj, 2005). Increasing salinities imposes two known problems: 1) the marine ecology may be affected and 2) desalination becomes more energy consuming. The well-being of the entire marine ecology depends on the lowest links in the food chain and is therefore dependent on the quantum of phytoplankton, coral reefs and seagrass meadows (Erftemeijer & Shuail, 2012, Sheppard et al., 2010). The complex ecosystems of benthic populations (seagrass meadows and coral reefs) are negatively

affected by prolonged exposures to high salinities (Chartrand et al., 2009, Torquemada & Lizaso, 2005), because of the negative correlation between salt concentration and resolved oxygen. Rise in averaged salinity in Kuwait Bay and at an offshore location (48.6 °E 29.0 °N) in the Gulf causes a decrease in the phytoplankton population (Al-Said et al., 2017). Shrinking phytoplankton and benthic populations have negative effects on the populations of numerous marine species, which hurts fishery and tourism. The energy required for desalination increases along with increasing intake salinities. The operational costs of desalination plants with intakes in the Arabian Gulf are therefore projected to grow during the 21st century (Elshorbagy & Basioni, 2015). The complex system of external forcing on the Arabian Gulf and the impact on the marine ecology is schematically depicted in Figure 2.

The Arabian Gulf is the perfect test case to gain understanding of the sustainability of desalination of seawater because of the intensity of desalination and the sheltered geography. Insight in the sustainability of desalination is valuable for global and local policy-makers concerned with fresh water supply. The extraction of fresh water by desalination adds to the natural extraction of fresh water, by evaporation. As both natural- and anthropogenic fresh water extraction volumes are anticipated to change over the coming decennia (IPCC, 2013, Elhakeem, Elshorbagy, & Bleninger, 2015a), climate change is included in this impact assessment of increased desalination capacity on salinities in the Arabian Gulf. The topic of this research is therefore stated as:

"Impact of desalination and climate change on salinity in the Arabian Gulf."

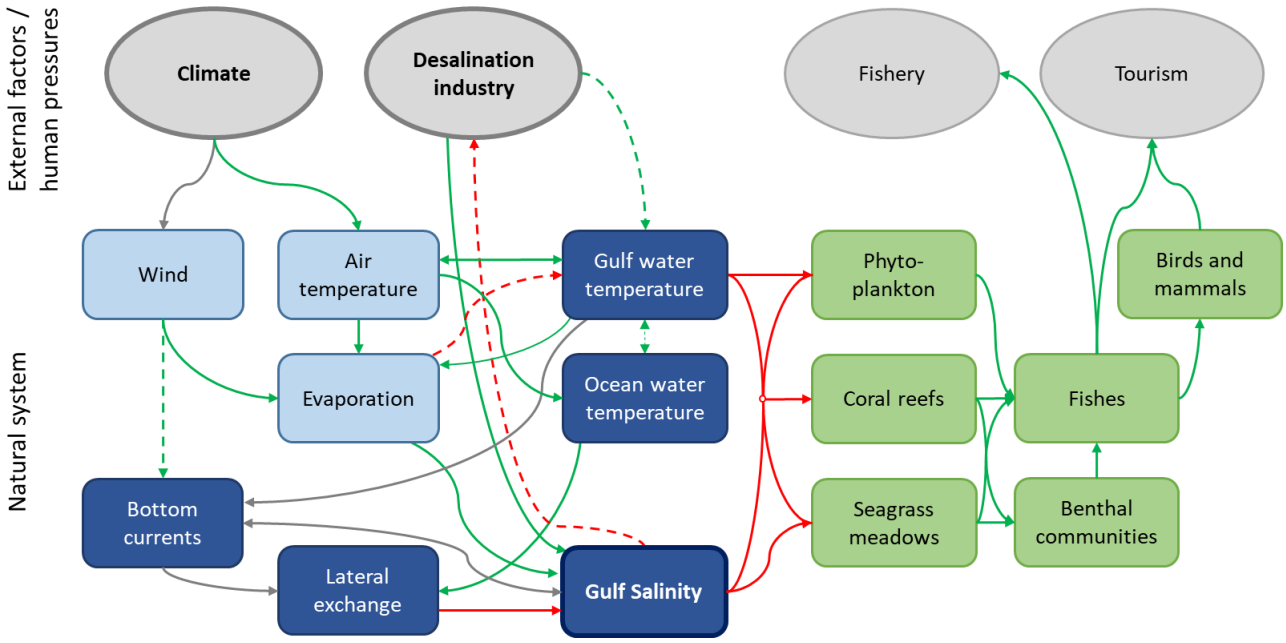

Figure 2: Schematized depiction of relevant causal relations between external factors (grey); physical drivers (atmospheric in light blue and hydrodynamic in dark blue) and marine ecology (green) in the Arabian Gulf system. The causal relations are subdivided into positive relations (green arrows), negative relations (red arrows) and bipolar relations (grey arrows) as well as strong relations (continues line) and weak relations (dashed line).

1.2 Research objective

The main objective of this research is:

"To identify the combined impact of desalination and climate change on salinities in the coastal regions of the Arabian Gulf."

1.3 Research questions

Two research questions are set up to achieve the research objective:

1. What is the combined impact of increasing desalination capacity and climate change on local salinities in the coastal regions of the Arabian Gulf?
2. How do changes in desalination capacity and climate affect salt accumulation in the Arabian Gulf?

1.4 Research scope

The scope of this report is limited to salinity, and the distribution thereof, in the Arabian Gulf. Insights in water temperature and flow patterns are used to explain the advection and diffusion of salt in the Arabian Gulf. The driving processes are analysed by means of a sensitivity analysis. To assess the effects of natural- and anthropogenic forcings this analysis will vary the values for the following parameters: desalination capacity, wind direction, wind speed, air temperature and oceanic water temperature. Precipitation is excluded in the model, because of its marginal influence and expected decreasing rate (Elhakeem et al., 2015c). The anthropogenic interference in the hydrodynamics in the Arabian Gulf is limited to the amount of water that is processed by desalination facilities along the coast and the thermal energy that is added during the process.

Experiments to answer the research questions will be executed numerically with a model as presented in Section 2.4. Field measurements are used to validate the models representability of key processes, but no real life data is used directly to answer the research questions. The numerical experiments will focus on the relations between driving physical processes and abiotic properties of the marine system: salinity and temperature in the Arabian Gulf and the Gulf of Oman, see Figure 2. The relationship between salinity and ecological components and inter-ecological relationships are outside of the scope of the numerical experiments and are rather the context for the research's relevance. Key locations of economic and ecological value: seagrass meadows, coral reefs and desalination intakes are exclusively located in shallow coastal regions. Therefore, the focus of this research is on local salinities in the coastal regions. 'Local' is defined as a spatial scale in the order of 10's of kilometres.

2 Methodology

In this chapter the approach to answering the research questions is elaborated upon. First the research outline is presented in Section 2.1, then presenting the future scenarios for desalination capacity and yearly averaged temperature in Section 2.2. Indicators to assess the impact are presented in Section 2.3. The numerical model and it's set-up are illustrated in Section 2.4.

2.1 Research outline

The research consists of four phases. Phase I is a system analysis, focussing on governing phenomena in transport of water and salt in the Arabian Gulf. Then, a numerical model is set up in Phase II to run simulations for a sensitivity analysis in Phase III. The representation of the indicative transport processes in the simulations is validated. Phase I to III (see Figure 3) are iterated until the principle physical processes are represented to satisfaction. In phase IV, model results of future projections are assessed on impact on the coastal regions in the Arabian Gulf. The eventual impact assessment is retrieved from a combination of the results from Phase III and IV.

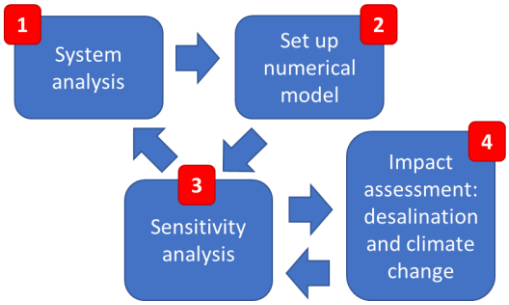

Figure 3: Flow chart, representing the research outline in schematic steps.

2.1.1 Phase I: System analysis

Hydrodynamics in the Arabian Gulf have been investigated by numerous field surveys and modelling efforts, conducted over the past four decennia. The literature covering previous efforts is consulted to find out what processes dominate mixing and residual circulation in the Arabian Gulf.

2.1.2 Phase II: Setting up the numerical model

A numerical model is set up with the Delft3D Flexible Mesh software package. A variety of sources are used to retrieve boundary conditions, see Section 2.4. Results of the present-day-forcing reference case are roughly validated to field surveys results (Reynolds, 1993, Swift & Bower, 2003). Both vertical cross sections and spatial maps of temperature, salinity and density are used for the qualitive validation to field survey result. Timelines and spatial maps of surface temperature are validated to a satellite data assimilation (Abbasi, 2018). The model simulation runs from sampled, depth-averaged initial conditions and is forced with meteorological data from 2008 to 2016. The output for the year 2016 is used for the analysis to secure sufficient spin up time, see appendix 2.

2.1.3 Phase III: Sensitivity analysis

The causal relations between physical drivers and water properties, depicted in Figure 2, are investigated by simulations of isolated parameter alternations. The effects on transport patterns of water and salt in the Arabian Gulf are considered. A model forcing as presented in Section 2.4 is used as a reference case and simulated for 9 years, starting from 2008. Alternations to the reference case will be simulated separately. Simulation will be executed with isolated air temperature rise, isolated ocean temperature rise, combined air and ocean temperature rise, alternative wind velocities and -directions, uniform and rotated uniform wind fields and alternative desalination capacities. An overview of all simulations is given in appendix 1.

The air temperature is changed by adding a constant value to the spatially non-uniform time series. The change in ocean temperature alternation is achieved by adding a constant value to the time series of all cells in the boundary cross section. The wind velocity adjustments are done by multiplying the wind forcing components in x- and y-directions by a constant value. The uniform wind field is based on monthly averaged, space-averaged wind velocity in the spatial and temporal mean wind direction, as presented by Kamranzand (2018). The uniform wind direction is rotated 20° in both clockwise and counter-clockwise direction and the results of these simulations are compared to the uniform wind field. The desalination capacity is adjusted by multiplying the discharge of all desalination plants as recorded by Latteman and Höpner (2010).

The model simulations produce spatial output twice per computed week. Lateral exchange volumes through the Strait of Hormuz (56.4 °E) are found by averaging flow velocities over the cross-section. There are too little temporal data points to effectively average out the tidal influence on the flow velocities in the Strait. Therefore, chapter 5 uses only relative volumes of lateral exchange to explain water and salt budgets in the Arabian Gulf. In the presented tables, the volume of lateral exchange is divided by the area of the Arabian Gulf, to be able to make a direct comparison between the relative gross exchange volume through the Strait and the relative extraction volume due to increased desalination capacity or evaporation. For the horizontal distribution of flow velocity the scarce spatial datapoints cause the tidal influence to be over represented. A Fourier function is used to generate a depth-averaged flow velocity map for the Arabian Gulf, averaged over the last year of the simulations.

2.1.4 Phase IV: Future impact analysis

Combined effects of climate change and desalination are simulated by mild and extreme scenarios for short and long range future impact assessment. The projections are presented in Section 2.2, from which the years 2050 and 2080 are used as scenarios. The impact of these scenarios on salinities in the coastal areas of the Arabian gulf is assessed on the impact indicators presented in Section 2.3.

2.2 Future projections

For the future impact assessment in Phase IV, two scenario paths are drawn up for both development of desalination capacity and climate change. A mild scenario and an extreme scenario. The scenarios for the development of the reference desalination capacity (Latteman & Höpner, 2010) are based on the combined prognosis of population growth (World Bank, 2005), water use per capita (Odhiambo, 2017) and depletion of groundwater resources (Mazzoni et al., 2018) in the Arabian Gulf region. Following previous argumentation, the rate in which new desalination capacity is installed is expected to increase over the next decades at a rate in the same order as projected by Edson, Wainer & Ferrero (2016). Figure 4A shows the future projection that is used to set up the scenarios for phase IV, being:

- A mild scenario for desalination capacity development, with 2 times the reference capacity in 2050 and 5 times the reference desalination capacity for 2080;
- An extreme scenario for desalination capacity, with a multiplication of 4 times the reference desalination capacity by 2050 and of 10 times by 2080.

The air temperature rise projection used for the simulations (see overview appendix 1) are based on a climate projection by the International Panel for Climate Change (IPCC, 2014), see appendix 3, and regionally observed trends (Al Sarmi & Washington, 2011). The mild scenario is based on the assumption of very active global climate policy and little carbon concentration increase. The mild projection in Figure 4B follows the IPCC's *'representative concentration pathway 2.6'* (RCP2.6). The extreme scenario is based on the assumption of a passive global climate policy and accompanying significant carbon concentration increases, it follows the IPCC projection of RCP8.5.

- A mild scenario of air temperature rise with 1.5 °C increase in 2050 and 2080 relative to 2015;
- An extreme scenario of air temperature rise with 3 °C by 2050 and 4.5 °C by 2080 relative to 2015.

Along with atmospheric temperature rise, the temperature of the ocean is expected to rise as well. In the future scenarios the water temperatures at the open ocean boundary are assumed to increase uniformly with the same temperature rise as in the atmosphere.

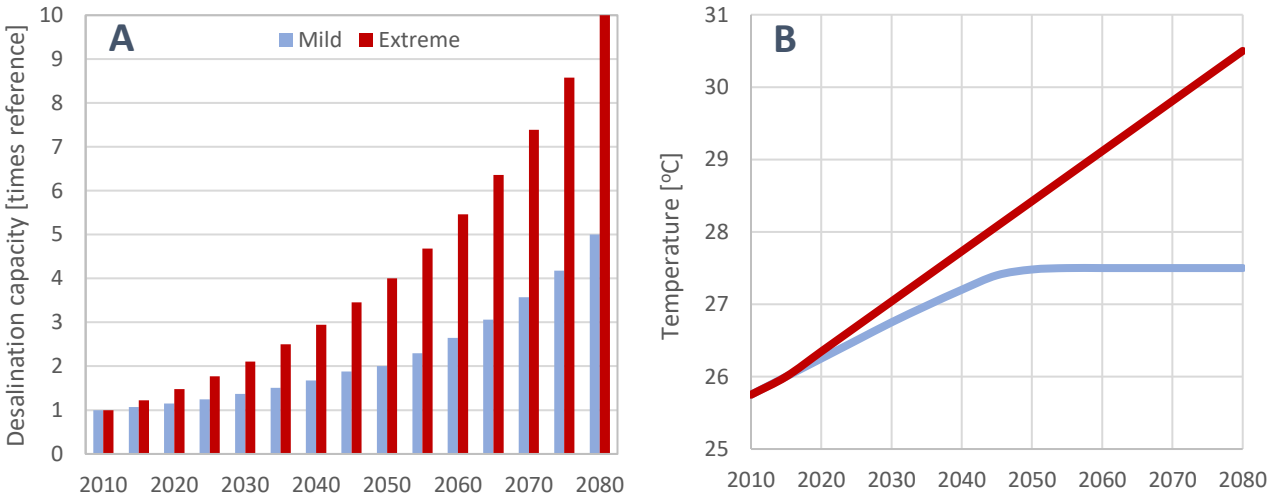

Figure 4, left panel (A): Future projections of operational desalination capacity in the Arabian Gulf, measured relative to the installed capacity in 2010 (Latteman & Höpner, 2010). Right panel (B): Future projections of year averaged air temperature in the Arabian Gulf region.

2.3 Impact indicators

Three impact indicators are chosen to quantify the impact of increased desalination capacity and climate change on coastal salinities in the Arabian Gulf. These indicators are: yearly averages, seasonal variation and weekly variation at locations of specific interest. Economic or ecological value is used as a selection criterium in this research. Locations of ecological value are seagrass meadows and coral reefs of most significance. Locations of economic value are the intakes of the largest desalination plants. The locations of the 11 biggest desalination intakes are derived from research by Latteman & Höpner (2010). The locations of the most significant seagrass meadows and coral reefs are derived from Buchanan (2015). The locations are distributed along the Gulf coasts as depicted in Figure 5.

Year averages are the most straight-forward figures to measure the accumulation of salt locally and for the Arabian Gulf in general. Local year averaged salinities are relevant when considering a location for a future desalination plant. Changes in meteorological conditions cause yearly patterns of three dimensional temperature and salinity distribution (Pous, Lazure & Carton, 2014). Seasonal variability of salinities near the bottom is crucial for the survivability of corals and seagrasses. The bigger the seasonal variability, the higher the salinity extremes that occur in summer. Exposures to extreme salinities (> 50 PSU) for longer than 2 weeks impose high mortality rates for both coral species (Coles, 2003, Chartrand et al., 2009) and seagrasses (Torquemada & Lizaso, 2005). During weeks of extreme high salinity corals or seagrasses capture oxygen whenever possible. Weekly variability is therefore important, as weekly lows can limit harm to seagrass meadows and coral reefs and contribute to its recovery of short term extremes.

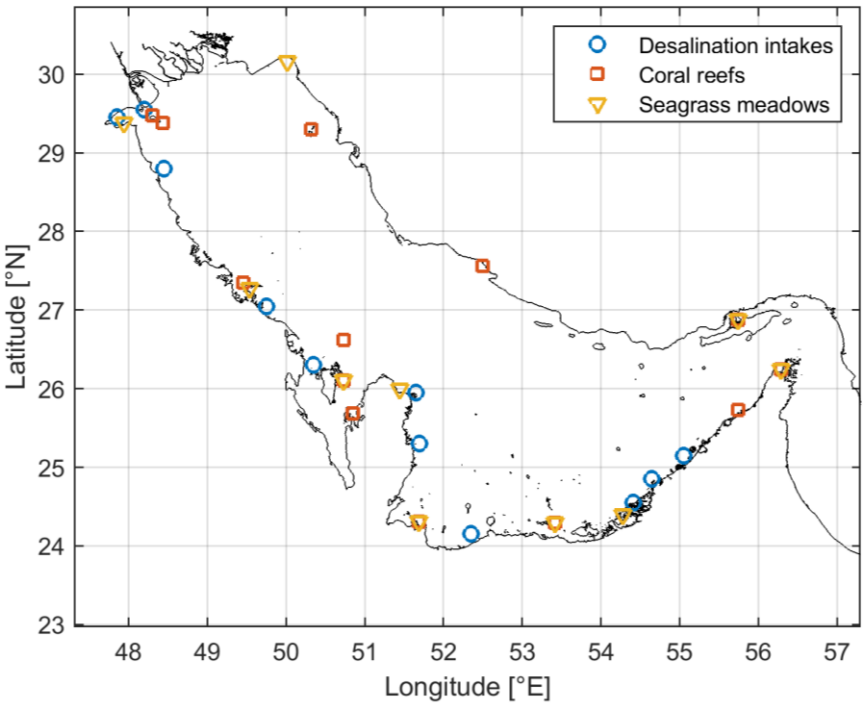

Figure 5: Map of the Arabian Gulf showing the locations of the most relevant desalination plants (blue circle); most important Coral reefs (orange squares) and most important seagrass meadows (yellow triangles).

2.4 Model set-up

In this research, a numerical approximation is used. Sub-sections 2.4.1, 2.4.2 and 2.4.3 present some of the equations that are approximated. The model of the Arabian Gulf is developed with Delft3D Flexible Mesh, abbreviated to *'Delft3D FM'* (Deltares, 2018). The core of Delft3D FM are three-dimensional non-hydrostatic momentum equations, derived from the Navier-Stokes equations (Kernkamp et al., 2011). Delft3D FM's predecessor Delft3D has been applied for numerous studies in the Arabian Gulf (Pokavanich et al., 2015, Peng & Bradon, 2016) and validated for water levels and -temperatures (Elhakeem, Elshorbagy & Bleninger, 2015b). The spatial discretization is derived from the finite volume method, where velocity components are defined at the cell surfaces and water level, salinity and temperature are defined at the cell centres. A complete overview of physical and numerical settings is provided in appendix 4.

2.4.1 Motion of water

A summation of the rate of change of some property and three dimensional advection terms is described by the *'total derivative'*, which is depicted in Equation I.

$$\frac{D}{Dt} = \frac{\partial}{\partial t} + u\frac{\partial}{\partial x} + v\frac{\partial}{\partial y} + w\frac{\partial}{\partial z} \quad \text{(I)}$$

The total derivative of velocity in three dimensions is calculated with equations II, III and IV:

$$\frac{Du}{Dt} = \frac{\partial}{\partial x}\left(v_h\frac{\partial u}{\partial x}\right) + \frac{\partial}{\partial y}\left(v_h\frac{\partial u}{\partial y}\right) + \frac{\partial}{\partial z}\left(v_v\frac{\partial u}{\partial z}\right) - g\frac{\partial \zeta}{\partial x} - \frac{1}{\rho_0}\frac{\partial p_{atm}}{\partial x} - \frac{g}{\rho_0}\int_z^\zeta \frac{\partial \rho}{\partial x}dz + fv \quad \text{(II)}$$

$$\frac{Dv}{Dt} = \frac{\partial}{\partial x}\left(v_h\frac{\partial v}{\partial x}\right) + \frac{\partial}{\partial y}\left(v_h\frac{\partial v}{\partial y}\right) + \frac{\partial}{\partial z}\left(v_v\frac{\partial v}{\partial z}\right) - g\frac{\partial \zeta}{\partial y} - \frac{1}{\rho_0}\frac{\partial p_{atm}}{\partial y} - \frac{g}{\rho_0}\int_z^\zeta \frac{\partial \rho}{\partial y}dz - fu \quad \text{(III)}$$

$$\frac{Dw}{Dt} = \frac{\partial}{\partial x}\left(v_h\frac{\partial w}{\partial x}\right) + \frac{\partial}{\partial y}\left(v_h\frac{\partial w}{\partial y}\right) + \frac{\partial}{\partial z}\left(v_v\frac{\partial w}{\partial z}\right) - \frac{g\rho}{\rho_0} \quad \text{(IV)}$$

With u, v and w the flow velocity in three dimensions (x, y, z). v_h and v_v are the horizontal and vertical viscosity. g is the gravitational acceleration. ζ is the elevation. ρ_0 and ρ_z are the densities at the water elevation $\zeta = 0$ and at $\zeta = z$. p_{atm} is the atmospheric pressure. f is the Coriolis frequency.

The Coriolis term is negligible in the momentum equation in vertical direction. The elevation and atmospheric pressure are not dependent on z. Therefore the total derivative in vertical direction (equation IV) is merely a summation of the diffusion terms and the gravitational acceleration due to density difference. The acceleration in vertical direction $(\partial w/\partial t)$ and the vertical velocity (w) are much smaller than the horizontal accelerations $(\partial u/\partial t, \partial v/\partial t)$ and velocities in horizontal direction (u, v) in shallow water flows (Tan, 1992).

2.4.2 Transport of salt

The transport of salt is incorporated in the model in similar fashion as transport of any matter or water property (such as heat). The rate of change of salinity is calculated by equation V.

$$\frac{\partial S}{\partial t} = u\frac{\partial S}{\partial x} + v\frac{\partial S}{\partial y} + w\frac{\partial S}{\partial z} + \left(\frac{\partial S}{\partial x} + \frac{\partial S}{\partial y}\right)\left(K_H\left(\frac{\partial S}{\partial x} + \frac{\partial S}{\partial y}\right)\right) + \frac{\partial}{\partial z}\left(K_V\frac{\partial S}{\partial z}\right) \qquad \text{(V)}$$

With S the salt concentration (or salinity). K_H and K_V are the background values of horizontal and vertical diffusivity. Section 2.4.1 argued that $u \,\&\, v >> w$, which results in domination of horizontal transport of salt over vertical transport. With the side note that: *length scale >> depth scale*.

2.4.3 Ocean-atmosphere mass and heat exchange

The atmosphere-ocean heat exchange consist of three major phenomena: *1) radiation*: solar radiation travels through and is partially absorbed by the atmosphere. Most of the radiative energy is absorbed by the ocean; *2) conduction*: ocean and air exchange thermal energy on a day-night and on a seasonal cycle; *3) convection*: latent heat transport from ocean to atmosphere by vaporized water molecules. Appendix 8 elaborately explains all three major phenomena, while this section will focus on evaporation, as it is the mass balance rather than the heat balance that is in the scope of this research.

Atmospheric conditions drive the rate of evaporation. Clouds partially block solar radiation, relative atmospheric humidity relates to the ease of entering the atmosphere for vaporizing molecules and wind transports the vaporized molecules, decreasing the atmospheric humidity. The heat exchange model is described more extensively in Appendix 8.

The water surface reflects part of the solar radiation, but there is a net heat flux of solar energy into the ocean. The ocean has higher year averaged temperatures than the air because of the net radiative flux from atmosphere to ocean. The temperature difference drives a net conductive energy flux from ocean to atmosphere. The outflux of convective energy (through evaporation) is much larger than the conductive flux. Evaporation is dominant in both the heat- and mass balance.

Forced evaporation

Solar radiation forces evaporation directly and indirectly. Direct forcing of evaporation means that water molecules in the surface layer absorb the solar energy until the molecule vaporizes and 'escapes' into the atmosphere. Equation VI shows that the rate (volume/time) of forced evaporation depends on atmospheric density (ρ_a), the wind velocity (U_{10}), the specific humidity of saturated air (q_s) and the actual humidity of air (q_a).

$$M_{ev,forced} = \rho_a * c_e * U_{10} * (q_s - q_a) \qquad \text{(VI)}$$

With the calibrated Dalton number c_e. Specific humidity q_s depends on water surface temperature and atmospheric pressure. The remote air humidity q_a depends on air temperature, relative humidity and atmospheric pressure, (Deltares, 2018).

Free evaporation

Evaporation may also occur through free evaporation (convection of latent heat), driven by inversed density gradients in the atmospheric boundary layer (0-10 m). Equation VII shows how free evaporation is modelled.

$$M_{ev,free} = k_s * \overline{\rho_a} * (q_s - q_a) \quad \text{(VII)}$$

With heat transfer coefficient k_s depending on the viscosity, density and molecular diffusity of air (Deltares, 2018). k_s equals 0 if the density gradient is positive in downward direction. $\overline{\rho_a}$ is the atmospheric density, averaged over the first 10 meters.

Atmospheric conditions drive the rate of evaporation. Clouds partially block solar radiation, relative atmospheric humidity relates to the ease of entering the atmosphere for vaporizing molecules and wind transports the vaporized molecules, decreasing the atmospheric humidity.

2.4.4 Bathymetry and numerical grid

The bathymetry used in the model is based on data from the General Bathymetric Chart of the Oceans (GEBCO). After construction of the grid, the bathymetry was modified to match the grid cells with the Delft3D-Quickin tool. The Bathymetry is shown in Figure 9.

Conform to the objective of this research the spatial resolution of the model is relatively rough with a 5km resolution at the boundary and in the deep part of the Gulf Oman (depth > 1000 m) and a 2.5 km horizontal grid resolution for the shallower areas. The transition between the grid resolutions (red line in Figure 6A) consist of triangles (see Figure 6B) to optimize the orthogonality. For a sea of the size of the Arabian Gulf, Coriolis forces are significant, see equations II and III. Therefore the model grid is transformed from cartesian coordinates to spherical coordinates, taking into account the earth's curvature and accompanying forces on the system.

A Z-layer formulation is applied in vertical grid direction, to avoid σ-layer artefacts of layers of over 300m thick at the open ocean boundary to affect the Gulf. A supplementary advantage is that this allows for incorporation of immediate effects of buoyancy on the vertical flow and turbulence (Deltares, 2018). Stratification in the top layers in the Arabian Gulf is strong and resulting density gradients are steep. The effects of stratification on both vertical and horizontal turbulence and circulation are significant. Therefore a layering with a thickness of 2m for the upper 13 layers is applied, with a multiplication of factor 1.3 moving downward. This results in a maximum of 38 layers in the model domain and a maximum of 24 vertical layers in the Arabian Gulf (west of the Strait of Hormuz).

2.4.5 Model forcing

Transport of heat and mass in the model is a result of external forcing at the open ocean boundary and at the water surface. The water surface is forced by atmospheric conditions: wind, air pressure, air temperature, relative humidity and solar radiation (partially depending on cloud coverage). The connection to the open ocean in the Gulf of Oman is forced by water temperature, salinity and by tide induced periodic water level deviations. The effects of surge are not incorporated in the boundary condition. The reference model forcing in a brief overview:

- Astronomical tide components at the open model boundary in the Gulf of Oman, retrieved from the FES 2014 global tide model (Carrere et al., 2015);
- Daily updated cross-sections of water temperature and salinity at the open boundary in the Gulf of Oman, retrieved from the Hybrid coordinate ocean model (HYCOM);

- Temporally and spatially varying wind, air pressure, air temperature, relative humidity and cloudiness fields, retrieved from ECMWF's 'ERA-interim' hindcast model (Dee et al., 2011);
- A total of 8 river discharges based on Al-Asadi (2017) and Alosairi & Pokavanich (2017);
- 126 desalination plants, the discharge is based on Latteman and Höpner (2010).

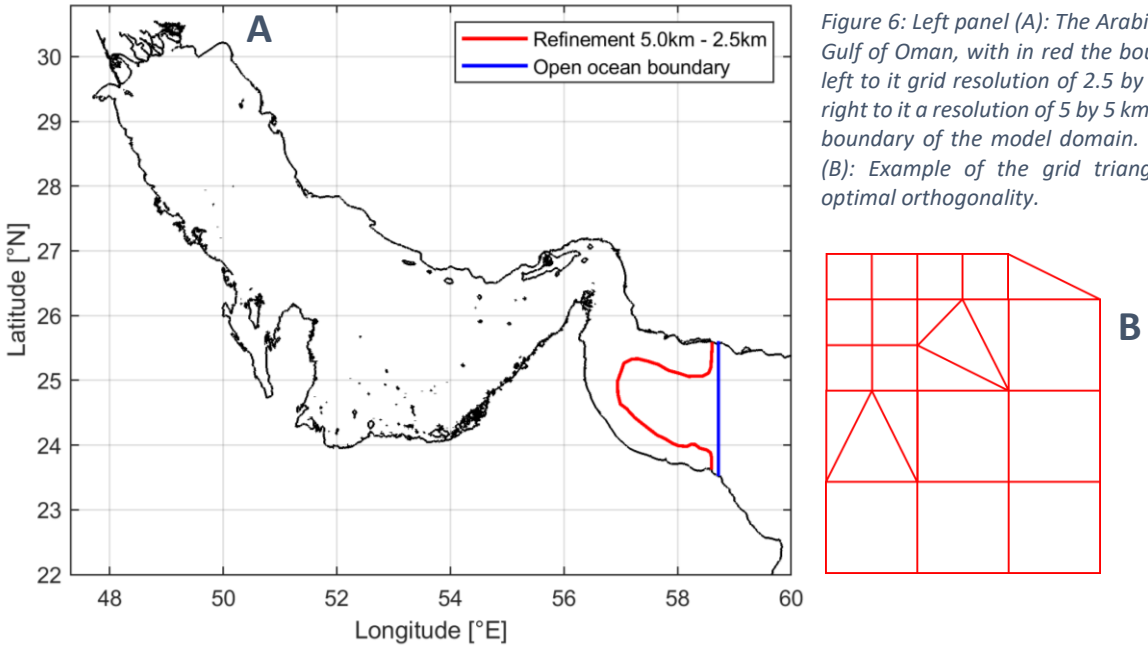

Figure 6: Left panel (A): The Arabian Gulf and Gulf of Oman, with in red the boundary with left to it grid resolution of 2.5 by 2.5 km and right to it a resolution of 5 by 5 km. In blue the boundary of the model domain. Right panel (B): Example of the grid triangulation for optimal orthogonality.

2.4.6 Open ocean boundary condition

The conditions for water level, temperature and salinity at the open ocean boundary are modelled as Dirichlet conditions. The salinity and temperature values are overruled when the flow velocity at the boundary cells is directed outward. The astronomical, or tidal, forcing is imposed as by a summation of periodical water level fluctuations, derived from the Finite Element Solution (FES) tidal model. The astronomic constituents for phase and amplitude were interpolated from the FES grid to match the coordinates of the open ocean boundary. Temperature and salinity at the boundary are based on HYCOM hindcast results. HYCOM is a primitive equation model that is accurate in approximating worldwide ocean circulation on a large time scale (Bleck, 1998, 2002), therefore ideal for providing the open ocean boundary condition for the Arabian Gulf model. In vertical direction the value of the nearest neighbouring cell is used to translate data from HYCOM output to Delft3D FM input.

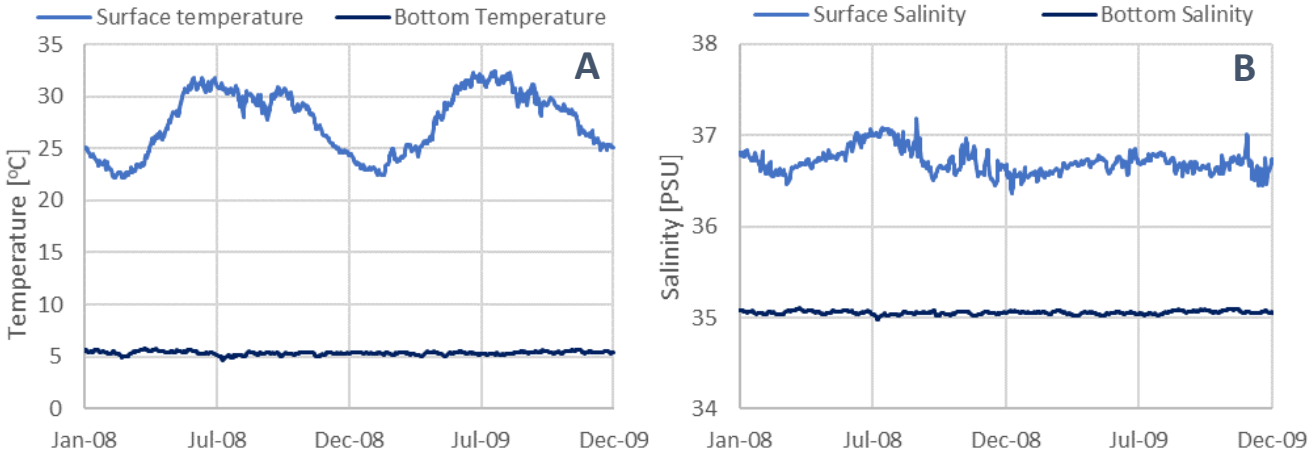

Figure 7: On the left panel (A) surface and bottom temperature and on the right panel (B) Surface and bottom salinity at the open ocean boundary condition for 2008 and 2009, retrieved from HYCOM.

Figure 7 shows timelines of cross-sectional mean values of surface and bottom temperature (A) and salinity (B). The HYCOM time series for 2008 and 2009 are extended for 10 years. Based on the depth at the boundary condition (> 3000 m), the salinity of oceanic inflow is assumed to be unaffected by the outflow and climate change. Globally, the future oceanic salinity is assumed constant.

2.4.7 Atmospheric conditions

The meteorological forcing consists of spatially and temporally varying wind climate, atmospheric temperature, air pressure, relative humidity and cloudiness. Precipitations is not included in the model. It is gained from ECMWF's *ERA-interim* hindcast model, with a temporal resolution of 3 hours and a spatial resolution of approximately 70 km. For simulations with a uniform wind field, the wind data is based on Kamranzand (2018). Precipitation is not included, due to its insignificant influence. Wind stresses at the water surface, heat fluxes and mass fluxes, resulting from evaporation can be computed with the atmospheric conditions. In Appendix 5 a distribution of wind roses shows the yearly average wind direction between 2008 and 2017. Over the majority of the gulf north-westerly winds dominate the wind climate. East of 54°E longitude the predominant wind direction starts to shift to westerly winds, following the topography of the southern Gulf. Weekly mean air temperature, cloud coverage and wind velocity of the modelled 6-hourly data is presented in section 3.2.

2.4.8 River Discharge

There are eight rivers included in the model: three in the north of the Arabian gulf, two along the Iranian coastline and three in the south of Iran, see Appendix 6. The Shatt al Arab River delta, in the north of the Arabian Gulf, is fed by the rivers Euphrates and Tigris. Combined the rivers were a major fresh water supply for the Arabian Gulf until mid-20th century (Saleh, 2010). From the 1960's onwards dozens of dams have been build, which cumulatively have reduced the discharge of all the rivers that debouch into the northern Gulf. Based on data by (Al-Asadi, 2017) the discharges at Shatt al-Arab and Karun are derived. The discharges of the Hendijan, Hilleh and Mand rivers are based on data derived from (Alosairi & Pokavanich, 2017). The discharges of the south Iranian rivers (Mehrun, Shur and Minab) are estimated to equal the discharge of the Hilleh river, due to the lack of hydrological data. The total cumulative river discharge varies seasonally from 390-890 m^3/s, while the yearly averaged discharge of 1992 was estimated to be 1300 m^3/s (Reynolds, 1993).

2.4.9 Desalination plants

There are 126 desalination plants included in the model, cumulatively representing the total capacity as presented by Latteman and Höpner (2010). A desalination plant takes water in from the Gulf (flow I in Figure 8), separates water from salt with either membrane (RO) or thermal (MED/MSF) treatment. Fresh water (flow II) is directed to end users (e.g. cities and agriculture) and the residual brine (flow III) is fed back to the Gulf. Salinity and temperature of the extracted discharge (II) is decided by the depth averaged salinity and temperature at the intake location. Salinity and temperature of the brine discharge (III) are relative to the salinity and temperature at the intake location. For a Multiple-effect distillation (MED) plant with a typical constant desalination efficiency of 1/4 *. One unit of fresh water is gained and 3 units of brine are fed back into the Gulf. Therefore the addition of salinity of the brine (II) relative to the intake (I) is 1/3 of the intake salinity. As the brine discharge is modelled as a constant relative value, the intake salinity is assumed constant at 40 PSU and the additional salinity of flow III is 13.33 PSU. The additional temperature for the brine discharge is 5 °C for all desalination techniques. The simplification of assuming a constant intake salinity introduces an deviation to reality by extracting salt when the intake salinity is other than 40 PSU. The artificial salt extraction is one third of the deviation of actual salinity compared to the assumed salinity of 40 PSU times the desalination rate.

**The efficiencies for RO and MSF plants are 1/3 and 1/8 respectively.*

Desalination brine discharges have severe impact close to the outfall (John et al., 1990, Roberts et al., 2010), the spatial distribution of the desalination plants is therefore important. Appendix 7 includes a map of the Arabian Gulf with the most significant desalination plants in the region for each of the conventional desalination methods: Multi-stage Flash (MSF), Multi-effect distillation (MED) and Reverse osmosis (RO). 95% of the desalination capacity is located at the western coast, with local high concentration in Kuwait, Bahrain and near big cities along the Saudi and UAE coast. Alternative desalination capacities of the sensitivity analysis simulations are proportionally distributed over the existing desalination plants. Thereby assuming the distribution of volume treated by a specific desalination technique to be constant as well as assuming the spatial distribution of desalination capacity to be constant.

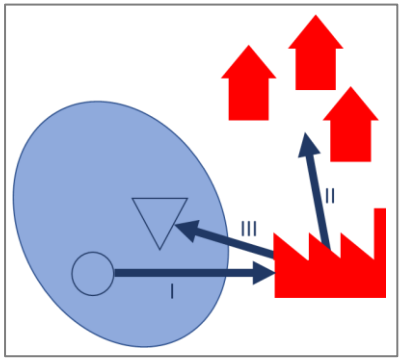

Figure 8: Schema of desalination plant. Flow I = intake; flow II = extracted fresh water; flow III = effluent brine.

Table 1: Overview of rates; salinity and temperature of fresh water extraction and brine discharge due to desalination and river discharge.

	Rate [m^3/s]	Salinity [PSU]	Temperature [°C]
Desalination: fresh water extraction	245	0	30
Desalination: brine discharge	1163	+5 (MSF) +13.3 (MED) +20 (RO)	+5
Rivers: cumulative discharges	390–890 (summer/spring)	0	20 –30 (summer/winter)

3 Case Study: the Arabian Gulf

This chapter provides a brief introduction to the system that is studied in this research: the Arabian Gulf. Section 3.1 presents the topography and bathymetry. Section 3.2 presents the Gulfs climate and section 3.3 discusses the Gulfs hydrology.

3.1 Topography and Bathymetry

Located between Saudi-Arabia in the west and Iran in the east, lies a semi-enclosed water body that is referred to as both the Arabian and Persian Gulf. Figure 12 shows the Gulf states and other key locations. Without Political motives, this water body will in this research be referred to as *the Arabian Gulf* or simply *the Gulf*. The Arabian Gulf has a freshwater inflow from the Tigris and Euphrates river delta in the northwest of the Gulf. The connection to open water is limited to the 55 km wide strait of Hormuz (56.4 °E) which connects the Arabian Gulf to the Gulf of Oman. The Gulf of Oman opens to the Indian Ocean. The average depth of the Arabian Gulf is approximately 38 meter and the depth only exceeds 100 meter at the scour around the Musandam peninsula, at the south of the Strait of Hormuz. The depth in the Gulf of Oman stretches beyond 3000 m. The south Iranian coast is much steeper than the Saudi and northern coast, see Figure 9. The nominal length of the Gulf is approximately 1000 km from northwest to Southeast and the surface area is approximately 235.000 km^2. The estimated volume of the Gulf is 8,600 km^3.

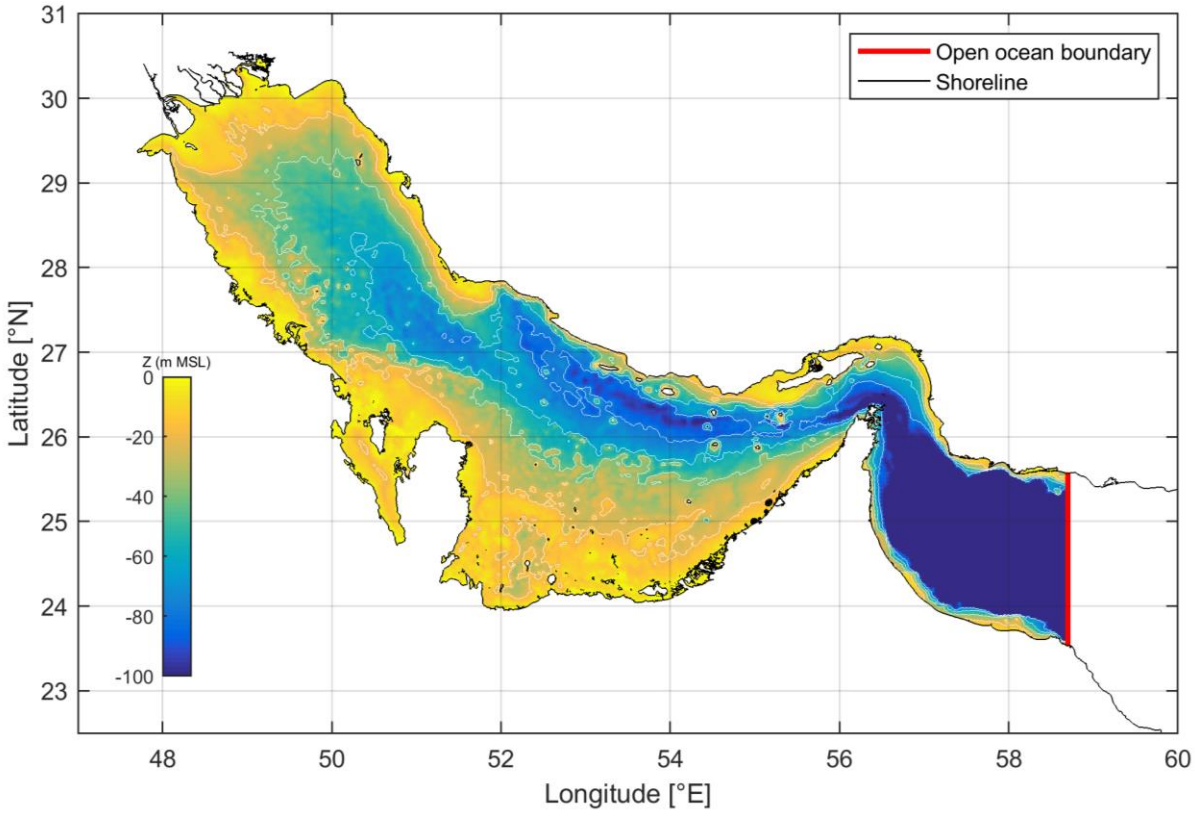

Figure 9: Bathymetry of the Arabian Gulf. With contour lines (white lines) at heights -20 m; -40 m; -60 m and -80 m and with the open ocean boundary condition (red line) at 57.72 °E longitude

3.2 Climate

The Gulf is located between 24 °N and 30 °N latitude, climatologically defined as the subtropics. The arid environment causes the Gulf climate to be subtropical in winter and tropical in summer, with transitions between these seasons (Vaughan et al, 2018). In summer, the average daytime maximum temperature is 41°C, while the mean daytime temperature during winter is 20°C, see Figure 11. The shallow waters of the Gulf adapt very quickly to atmospheric temperatures, so the sea surface temperatures have large seasonal variation, passing 35 °C during summer (John, 1990). The majority of the time the sky above the Arabian Gulf is clear, with only 20% of the days with any cloud coverage in 2016 and average cloud coverage in the summer of 5%. Figure 11 shows the weekly averaged cloud coverage and weekly averaged, minimum and maximum air temperature. The Atmospheric humidity ranges from 21% in summer to 60% in winter (Al Senafi & Anis, 2015).

The average wind speed and direction is relatively constant over the year, see Figure 5. With typical wind speeds of 5 m/s, varying between windless and strong northern wind gusts, called *Shamal* winds, till 15 m/s. The summer Shamal is caused by seasonal thermal lows lying over northwest India, Pakistan, Iran and southern Saudi Arabia (Rao et al., 2003). The winter Shamal is caused by mid-latitude disturbances that propagate to the east and typically cause extreme weather conditions (Rao et al., 2001). The strength of the summer Shamal is similar to the winter Shamal, but much more instable and varying in intensity and direction.

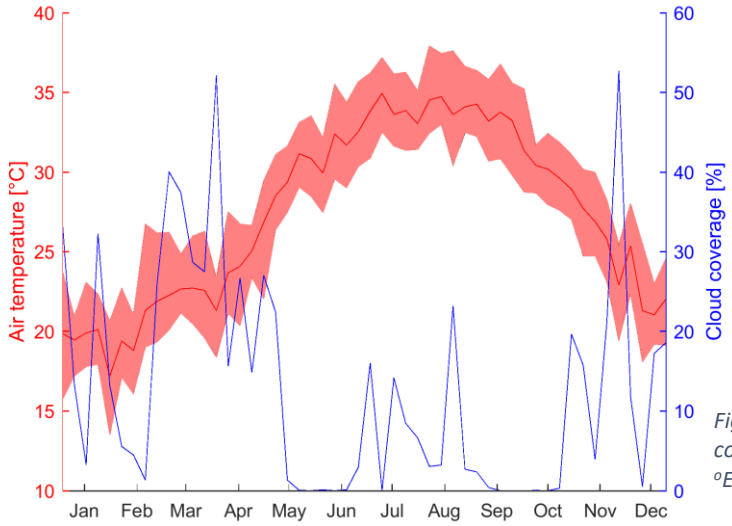

Figure 11: Week-averaged air temperature and cloud coverage. Hindcasted for 2016 by ERA5-interim for 52.5 °E 27 °N.

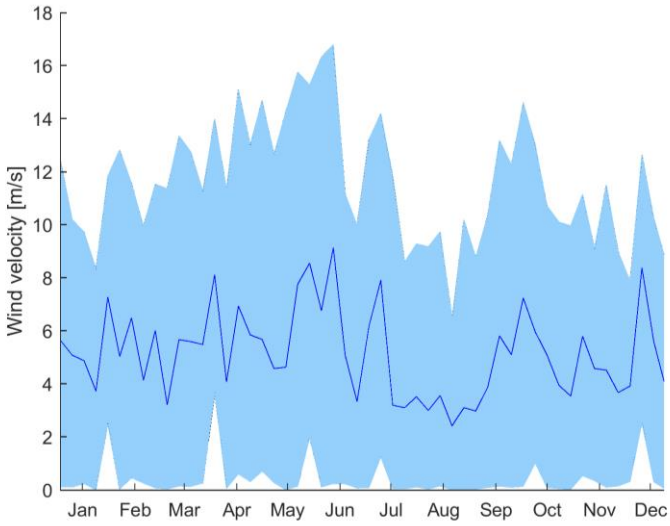

Figure 10: Week-averaged (solid line) mind speed and minimum and maximum wind speeds in 2016 (light blue bands).

3.3 Hydrology and hydrothermal

The water mass balance of the Arabian Gulf consists of fresh water outflux by evaporation and desalination, fresh water influx by precipitation and river discharge and salt water exchange through the Strait of Hormuz. The amount of precipitation and the amount of freshwater intake from river discharges into the Gulf are relatively small over the entire year. The fresh water influx from the rivers and rain is much smaller than the evaporation driven mass outflux from Gulf to atmosphere. Evaporative mass flux is on its term much smaller than the mass of the gross lateral influx through the strait of Hormuz, see Table 2 for year-averaged and appendix 12 for month-averaged hydrologic data.

The heat budget of the Gulf is controlled by solar radiation, evaporative heat flux and lateral water exchange with the Gulf of Oman. Due to high evaporative heat flux from the Gulf into the atmosphere, there is a negative net heat flux (the heat conserved in the water body decreases) through the surface, which is compensated with a positive lateral heat flux through the Strait. The positive heat flux through the strait is a result of a net influx of water mass through the (warm) surface layers, above depths of 20 meter, and a net outflux of water mass through the (cool) deep layers, at depths below 50 meter (Johns et al., 2003). The contribution of desalination to heating the Gulf on the basin-wide scale can be neglected. Wind, air temperature, relative humidity and water temperature drive evaporative heat- and mass fluxes, see section 2.4.3.

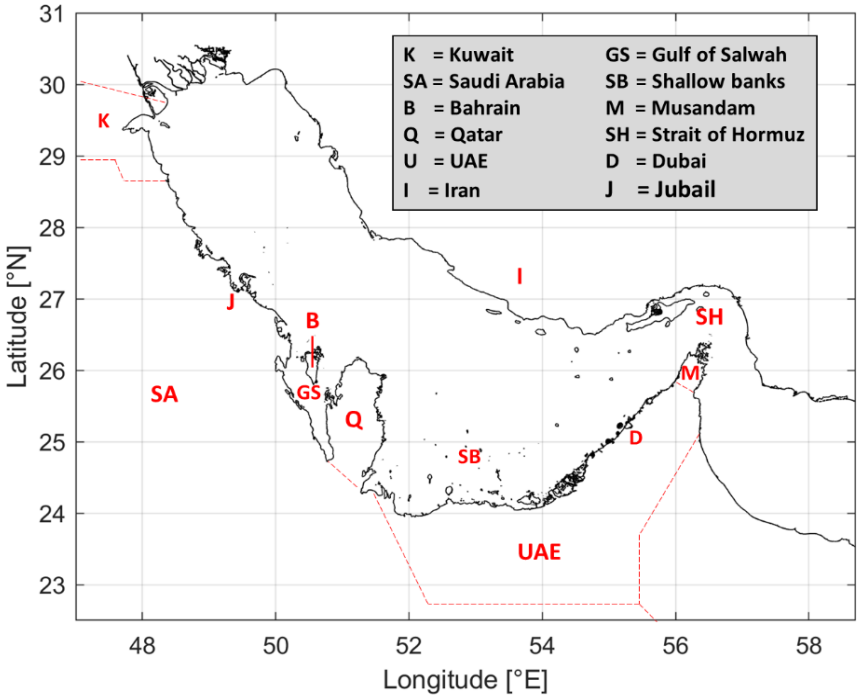

Figure 12: The Arabian Gulf, it's neighboring countries and important locations.

Table 2: Year-averaged evaporation; lateral exchange and precipitation averaged over the area of the Arabian Gulf between 1981 to 1990 (Xue & Eltahir, 2015). Desalination capacity is based Latteman & Höpner (2010). River discharge is based on Al-Asadi (2017) and Alosairi & Pokavanich (2017.)

	AVG. FLUX [M/YEAR]
EVAPORATION	**-1.84**
RIVER DISCHARGE	**+0.08**
PRECIPITATION	**+0.08**
DESALINATION CAPACITY	**-0.03**
NET LATERAL INFLOW	**+1.71**
GROSS LATERAL INFLOW	**32.2**

4 Reference case: qualitative validation

In this chapter the model results for the reference case will be introduced. The principle hydrodynamic flow is discussed in section 4.1 and the salinity distribution is discussed in section 4.2. The modelled results are compared to field survey data and outcomes of previous modelling efforts. The extended validation results are documented in appendix 13. The Discussion in Chapter 6 will elaborate upon the validity of the model and interpretation of its results.

4.1 Hydrodynamic circulation

The reference case, with model set up and forcing as presented in section 2.4 is simulated from 2008 to 2017. With a highly saline outflow and a relatively fresh oceanic inflow the flushing of the Arabian Gulf flow pattern (as presented in Figure 13B) is classified as: '*inverse estuarine flow*'. The main circulation in the Arabian Gulf is cyclonic. The seasonal variation of the inflow (the '*Iranian jet*') and its magnitude are driven by the variation in rate of lateral exchange volume through the Strait of Hormuz, see sections 4.1.1 and 4.1.6 and by the vorticity in the east of the Gulf (section 4.1.2), which is driven by fluctuations of wind and stratification of the flow (section 4.1.4 and 4.1.5 respectively). The cyclonic surface circulation is strongest in summer and weakest in late fall (Alosairi & Pokavanich, 2017). In spring and summer the basin wide circulation is strengthened by meso-scale eddies (MSE's) with a 100 km diameter in the southeast of the Gulf during summer, see section 4.1.2.

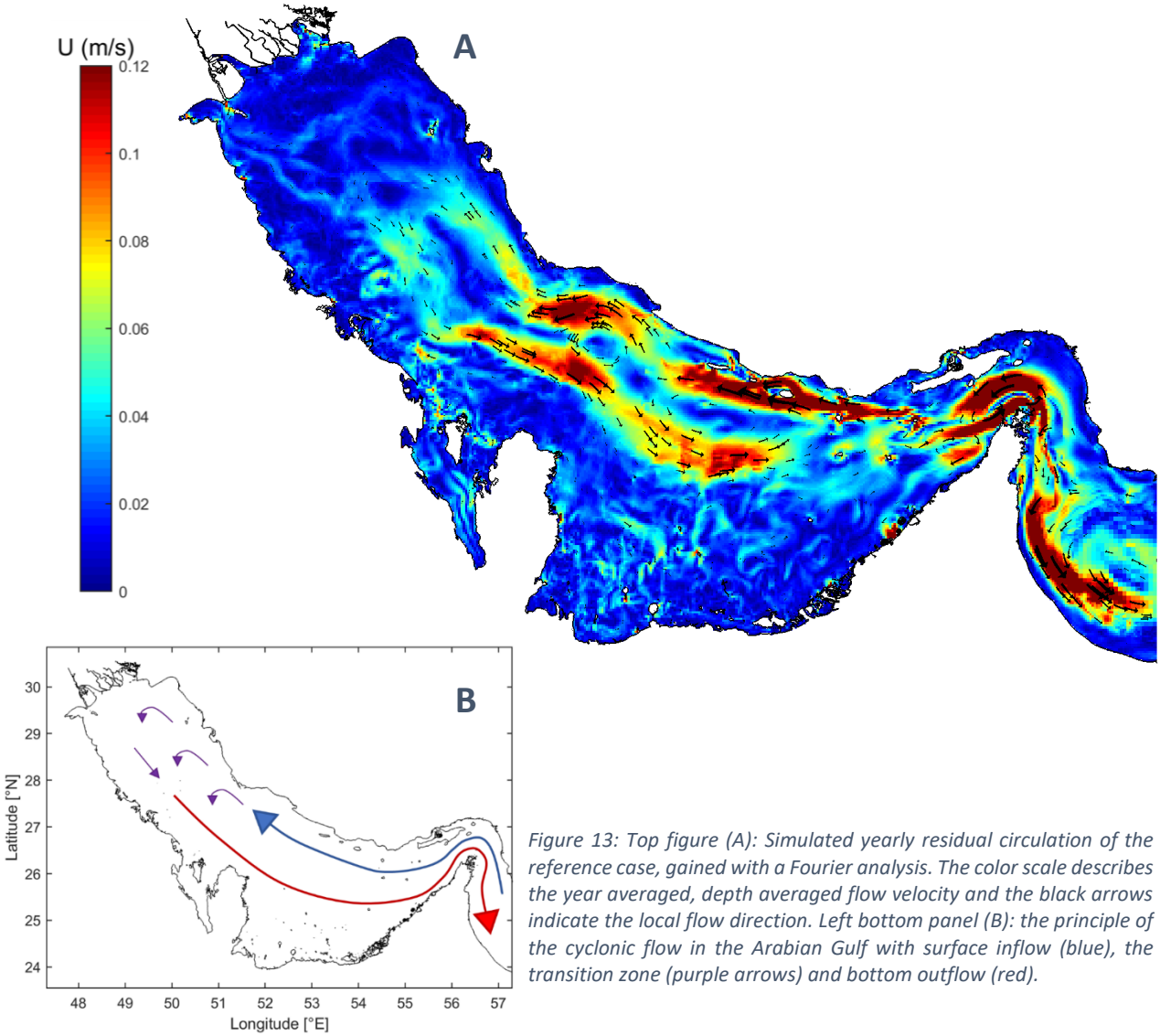

Figure 13: Top figure (A): Simulated yearly residual circulation of the reference case, gained with a Fourier analysis. The color scale describes the year averaged, depth averaged flow velocity and the black arrows indicate the local flow direction. Left bottom panel (B): the principle of the cyclonic flow in the Arabian Gulf with surface inflow (blue), the transition zone (purple arrows) and bottom outflow (red).

4.1.1 Oceanic inflow

At the Strait of Hormuz an outflowing (eastward directed) bottom current and an inflowing (westward directed) surface current of oceanic water are defined. The oceanic inflow is less saline than the bottom outflow. Temperature and salinity difference cause a density gradient across the Strait of Hormuz. The density gradient at the Strait governs the gross exchange volume (Johns et al., 2003). The oceanic water penetrates the Gulf through the Iranian jet (blue arrow in Figure 13B) and reaches the centre of the Gulf along the Iranian coast in winter and through meso-scale eddies in summer.

4.1.2 Meso-scale eddies

A combination instable atmospheric forcing and interior baroclinic instability causes vorticity of the inflowing Indian Ocean water and the Iranian Jet starts meandering in early summer in the southeast of the Gulf. A dynamically stable equilibrium is developed by a series of MSE's (Thoppil & Hogan, 2010). The horizontal vorticity in the east of the Gulf dominates the course, velocity and reach of the Iranian jet, influencing the circulation in the Gulfs interior. Therefore, well representing the MSE's is very important. The patterns of the MSE's differ per year and a direct comparison of the modelled MSE's (Figure 14A) with the typical vorticity pattern (Figure 15B) can't be made. It can be concluded that the location and size of the MSE's corresponds to earlier findings.

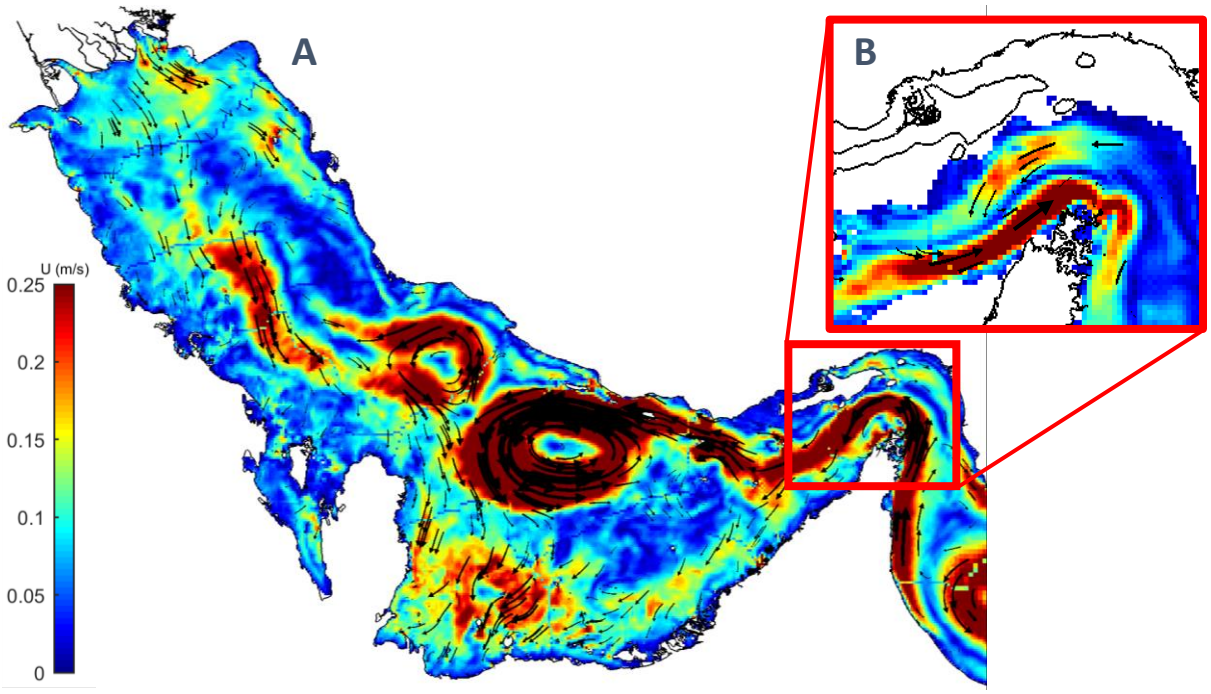

Figure 14: Left panel (A) Month-average of simulated flow velocities for July 2016 of the reference case at the surface. Right panel (B): a zoom-in on the flow through the Strait of Hormuz at a depth of 50m.

4.1.3 Wind driven flow

Wind dominates the surface flow in the north; wind dominates the evaporation rate and wind drives vorticity in the east, affecting direction and energy intensity of the inflow. Shear stress induced by the wind drives a surface flow in the predominate wind direction. Over a longer stretch (order of 100 km) the course of the flow is redirected according to the principles of Ekman dynamics (see Appendix 11). The dominating north-westerly wind along the Iranian coast, causes an Ekman transport in southwestern direction from the north Iranian coastline, see the blue arrow in Figure 15A. In the northeast of the Gulf the coastal cross section is steep and deep enough for water to be transported underneath the Ekman current at a depth of ~40 m in opposing direction. Sub-surface Ekman flow is balanced by upwelling near the Iranian coast, see the curvy, purple line in Figure 15A. In the southeast of the Gulf Ekman transport is directed towards the shallow banks.

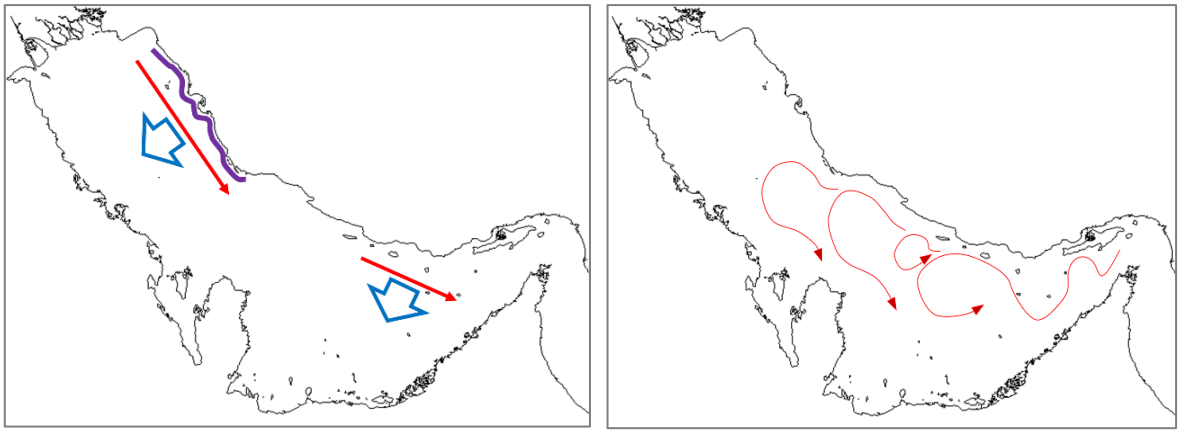

Figure 15: Left panel (A): Predominant wind direction (red); the principle direction of Ekman mass transport (blue) Ekman transport and a uplift along the shore (purple). And right panel (B): principle of the meso-scale eddies that occur during summer (Vaughan, Al-Monsoori and Burt, 2018).

4.1.4 Density driven flow

Heat and mass fluxes cause density gradients in the Gulf in 3 dimensions. Swift & Bower (2003) concluded from field data that the density field dominates the hydrodynamic circulation and long term transport processes of water and salt in the Gulf. Fresh water extraction affects local salinities and thereby affects the course of currents and the distribution of salt, see the causal relation diagram in Figure 2. In the shallow regions along the southwestern coast the salt can't sink to depths as it does in deeper regions. This introduces horizontal density gradients with high density along the shores and shallow areas of the Gulf and relatively low density in the Gulfs centre. The pressure gradient is negative in offshore direction, which introduces a gravity driven force in offshore direction. This force is balanced by the Coriolis effect, see equations II and III and Appendix 10 for a schematization. An anticlockwise (cyclonic) current along isobars and around the low density field in the centre of the Gulf is well represented by the simulated reference case, see Figure 13A.

In the north, the wind dominates the flow, resulting in a transition zone between the density driven Iranian jet at the surface (blue arrow in Figure 13B) and the density driven bottom outflow (red arrow in Figure 13B). In the deep parts of the Gulf (>30m), besides the far north, neither the salinity nor the density of water changes significantly over the year (Swift & Bower, 2003).

4.1.5 Stratification

Stratification is the formation of vertical layers of different density in a fluid. Stratification occurs when the density gradient is sufficiently steep, introducing a pycnocline (a fictive boundary between layers). In an unstratified fluid, the coupling of horizontal flow velocities of two vertically adjacent cells is dominated by viscosity. In stratified flows the turbulent exchange is dampened by the pycnoclinic boundary, which causes advection to dominate over viscosity, see equation II in section 2.4.1. This allows for a vertical distribution of flows in opposite direction (Marshall et al., 2002).

It is simulated that in spring the air temperature rises and heats the surface and sub-surface layers. Thermal stratification occurs and in summer the Gulf is fairly stratified, see Figure 18. The stratified Gulf in summer, causes the wind to be more influential to the course of the inflowing oceanic water. The stable winter Shamal winds barely influence the stable surface flow of Indian ocean water in southwestern direction, while the fluctuating summer Shamal winds cause an instable surface inflow of Indian ocean water (Yao, 2010). Decreasing air temperature and high rates of evaporation (driven by low humidity and strong winds) in fall cause cooling of the surface layer and mixing of the water column. The energy intensity of the MSE's decreases over fall until it's disappearance in winter.

4.1.6 Highly saline outflow

The rate of evaporation is dominated by seasonally varying conditions, see section 2.4.3. Evaporation rates vary from 0.11 m/month in March to 0.20 m/month in November (Xue & Eltahir, 2015). Salt is conserved during the process of fresh water extraction by evaporation. The residual highly saline water drives a year-round stable, south-eastward bottom outflow current. Both flow rate and salinity of the outflow current are relatively seasonally constant, with seasonal deviations in the order of 10% (Hunter, 1982). Properties of both the surface inflow and the bottom outflow drive the exchange of water and salt through the Strait of Hormuz and therefore drive the Gulf averaged salinity. The inflow decreases in energy intensity over its course through the Arabian Gulf, while the bottom outflow increases in intensity over its course. Both in- and outflow are most energy intensive near the Strait of Hormuz. Figure 13A does not clearly show this, because it is depth averaged. Figure 14B does show that the bottom outflow intensifies near the Strait.

4.2 Salinity distribution

Advection and diffusion of salt over the entire basin are rather slow processes, so salt transport is dominated by drifts rather than bipolar currents. The magnitude of density driven currents is much smaller than the magnitude of tidal driven currents (Lardner & Das, 1991). Considering net currents (drifts), density gradients and winds dominate, while tidal drift is negligibly small. Salt (residual to processes of fresh water extraction by evaporation or desalination) sinks and accumulates, causing locally increased salinities (Pous, 2012). Density gradients drive transport of salt from locations of accumulation to fresher locations by means of gravity currents. Geography is decisive for the equilibrium salinity of a location. Sheltered, shallow locations typically have a much higher equilibrium salinity than open, deep locations. Figure 17 shows that the northern and western coastline are more saline than the Iranian coastline, which is due to lower rates of flushing (Swift & Bower, 2003).

The seasonal difference in flow properties and behaviour causes seasonal variation in surface salinity and vertical salt mass fluxes. Solar radiation heats the surface water and results in stratification. Seasonal variation of radiated solar heat, humidity and wind climate drives seasonal variation of evaporation. In spring low evaporation rates drive a net downward flux of salt (thermal stratification). Thermal stratification increases the pycnocline and makes vertical mixing harder. The surface is less saline sand the bottom more saline in summer, relative to winter (see Figure 18D-F). Decreasing air temperature and high rates of evaporation (driven by low humidity and strong winds) enhance vertical diffusion and an upwards salt flux, which results in typical higher values for vertical flow velocity. Equation V (section 2.4.2) shows that this enhances the vertical advection of salt resulting in a near homogeneous vertical salinity distribution in winter, see Figure 18A-C.

Salt is accumulated at the southern banks due to shallowness, low flushing rates and intensive desalination. Accumulated salt is eventually transported along the bottom towards and across the Strait of Hormuz. The difference between the density of in- and outflow is decisive for the exchange volume. Wind direction fluctuation is crucial for flushing the most sheltered locations. Change in predominant wind direction, influences the direction of wind driven surface currents and can thereby influence the volume of exchange of sheltered areas. This volumetric exchange between sheltered area and relatively open water governs the salinity within the sheltered area.

Relative to assimilated data (Figure 16) the modelled salinity of the reference case is high. The deviation relative to the measured data increases when moving away from the Strait of Hormuz. More elaborate validation in Appendix 13 shows that the simulated depth profiles of salinity show correspondence with profiles from assimilated field data. Surface temperature shows correspondence in absolute values from the assimilated database.

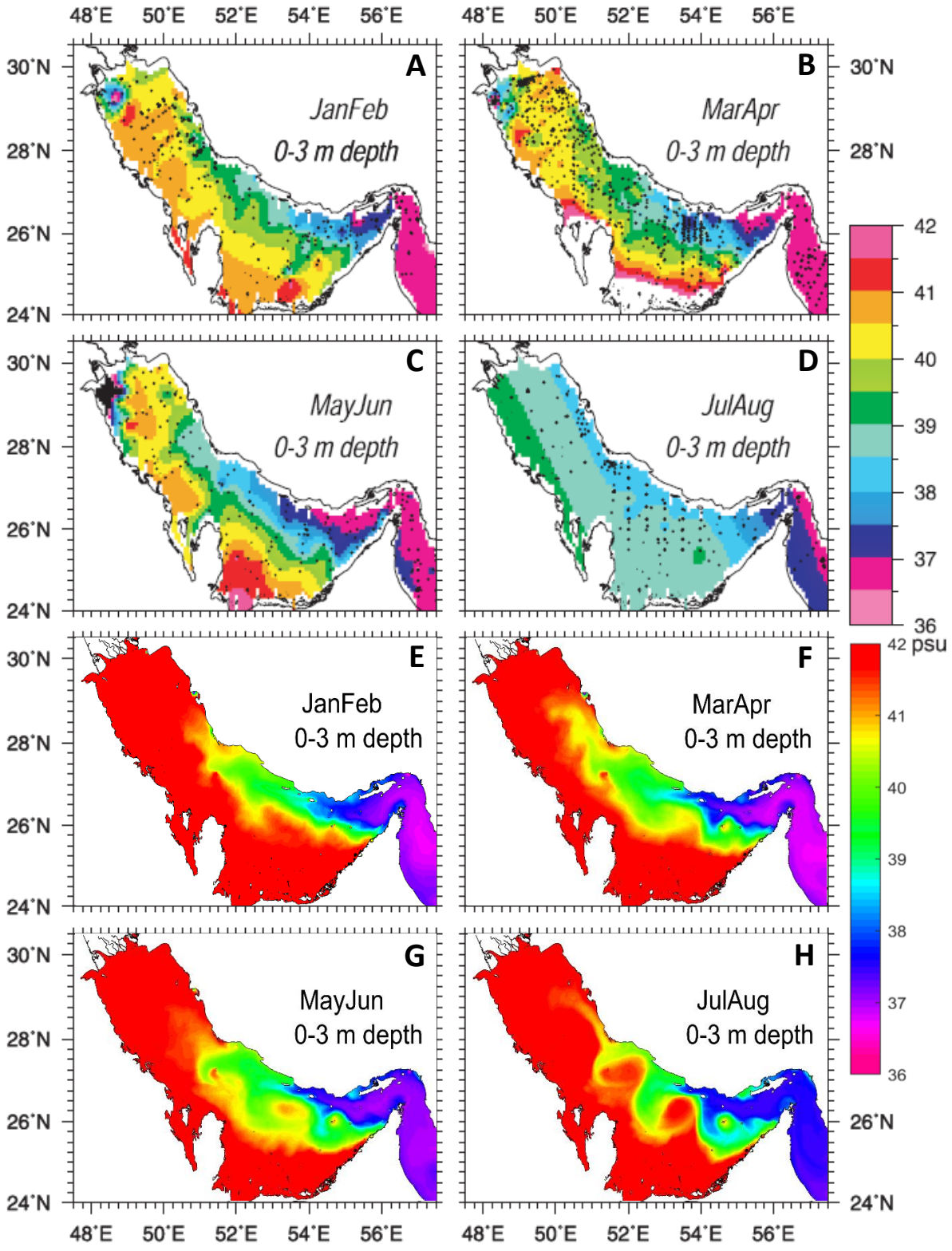

Figure 16: spatial plots of surface salinity. The upper two rows contain spatial interpolations of assimilated data from the period 1960 to 2000 from MOODS for (A) January & February, (B) March & April, (C) May & June and (D) July and August. The bottom two rows contain output data from the simulation of the reference case, for (E) January & February, (F) March & April, (G) May & June and (H) July and August.

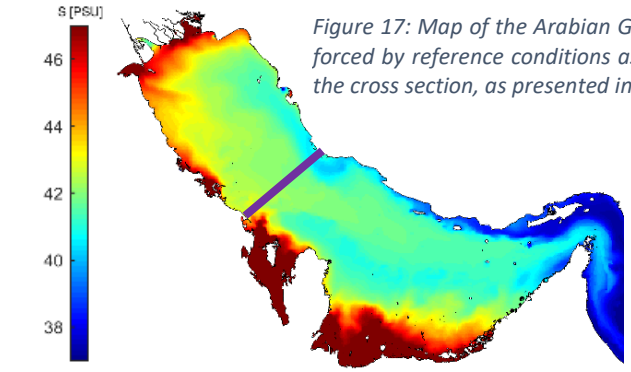

Figure 17: Map of the Arabian Gulf of simulated distribution of salinity in the Arabian Gulf forced by reference conditions as they are presented in Section 2.4. The purple line marks the cross section, as presented in Figure 18.

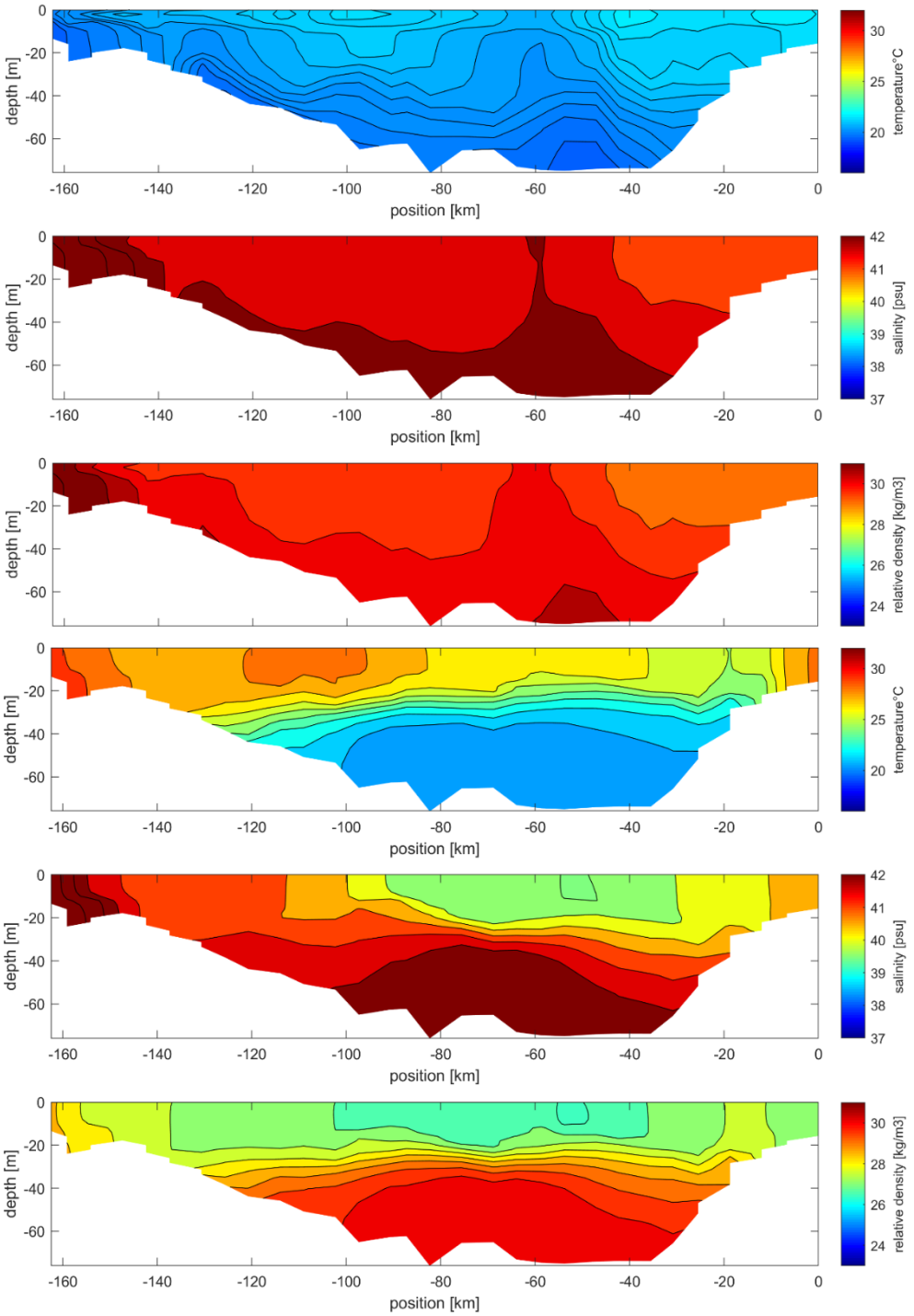

Figure 18: Vertical cross section along the line, depicted in Figure 17. Upper three panels temperature, salinity and density (respectively) averaged over February 2016 and lower three panels: temperature, salinity and density (respectively) averaged over July 2016. Retrieved from simulation of the reference case.

5 Results of alternative desalination and climate simulations

This chapter presents the results of the model simulations with alternated climate and desalination capacity conditions. Section 5.1 provides the basin-wide effects and section 5.2 elaborates upon local effects of desalination capacity increase and climate change.

5.1 Basin wide effects

5.1.1 Impact of combined desalination capacity increase and climate change

Simulations of the mild projection for 2050, results in an insignificant increase of Gulf-wide-averaged salinity. The 1.5 °C increase of temperature, causes an increase in evaporation rate by over 8% for both 2050 and 2080. The increased evaporation rate does not cause a significant rise in Gulf averaged salinity. The annual gross inflow volume has grown with over 3% by 2050 and by approximately 5% by 2080. Adding a gross annual inflow of almost 4 m/year (the gross inflow volume divided over the area of the Gulf, see section 2.1.3). The increase in gross exchange is much larger than the increase in net influx (~0.2 m/year). The net inflow increase merely balances the additional extraction of fresh water.

For the extreme scenarios, forced by both extreme desalination capacity increase and extreme climate change, the simulated evaporation rate rises by 17% in 2050 and by 27% by 2080 (till 2.57 m/year). The additional fresh water extraction is compensated by a net influx through the Strait of Hormuz of 0.5 m/year by 2050 and 0.8 m/year by 2080. The gross influx is simulated to grow with almost 7 m/year by 2050 and with over 11 m/year by 2080. The percentual increase in gross lateral inflow volume is of in the order of half the increase of fresh water outtake.

Table 3: Overview of future scenario results: basin wide salinity, evaporation and lateral exchange.

Scenario:		Reference case 2016	Extreme 2050	Mild 2050	Extreme 2080	Mild 2080
Evaporation rate	[m/year]	2.03	2.38	2.20	2.58	2.20
Evaporation relative	[%]	-	+17 %	+8.4 %	+27 %	+8.6 %
Average salinity	[PSU]	41.2	41.2	41.2	41.3	41.3
Average salinity relative	[PSU]	-	-0.07	0.00	0.03	0.05
Relative gross inflow vol.	[m/year]	-	6.86	2.59	11.28	3.68
Relative gross inflow vol.	[%]	-	9.1 %	3.4 %	15 %	4.9 %
Area +1 PSU salinity	[%]	<0.2 %	8.3 %	0.6 %	19 %	8.6 %
Area +2 PSU salinity	[%]	<0.2 %	5.1 %	<0.2 %	10 %	0.4 %
Area +3 PSU salinity	[%]	<0.2 %	0.4 %	<0.2 %	7.4 %	<0.2 %

5.1.2 Sensitivity to desalination capacity

From the results of the simulations of isolated change in desalination capacity (presented in Table 4) it is clear that the extraction by desalination and the rate of evaporation are not related. The Gulf average salinity is marginally affected by changes in the desalination capacity. The gross inflow of oceanic water is affected by increased desalination capacity, but not as straight-forward as expected. The gross inflow is simulated to be smaller for the desalination capacity cases of 0, 2 and 5 times reference capacity. For the 10 times reference capacity, the gross inflow volume has increased, which dampens the increase in Gulf averaged salinity partially.

A large part of the impact of the extreme scenario for 2080 is caused by the increase in desalination capacity till 10 times the reference capacity. Table 3 and Table 4 show that approximately 2/3 of the area of increased salinity by 1, 2 and 3 PSU in the extreme 2080 scenario is due to desalination capacity increase. The similarities between Figure 19A and B indicate that the desalination capacity dominates the spatial distribution of salinity increase in the extreme 2080 scenario.

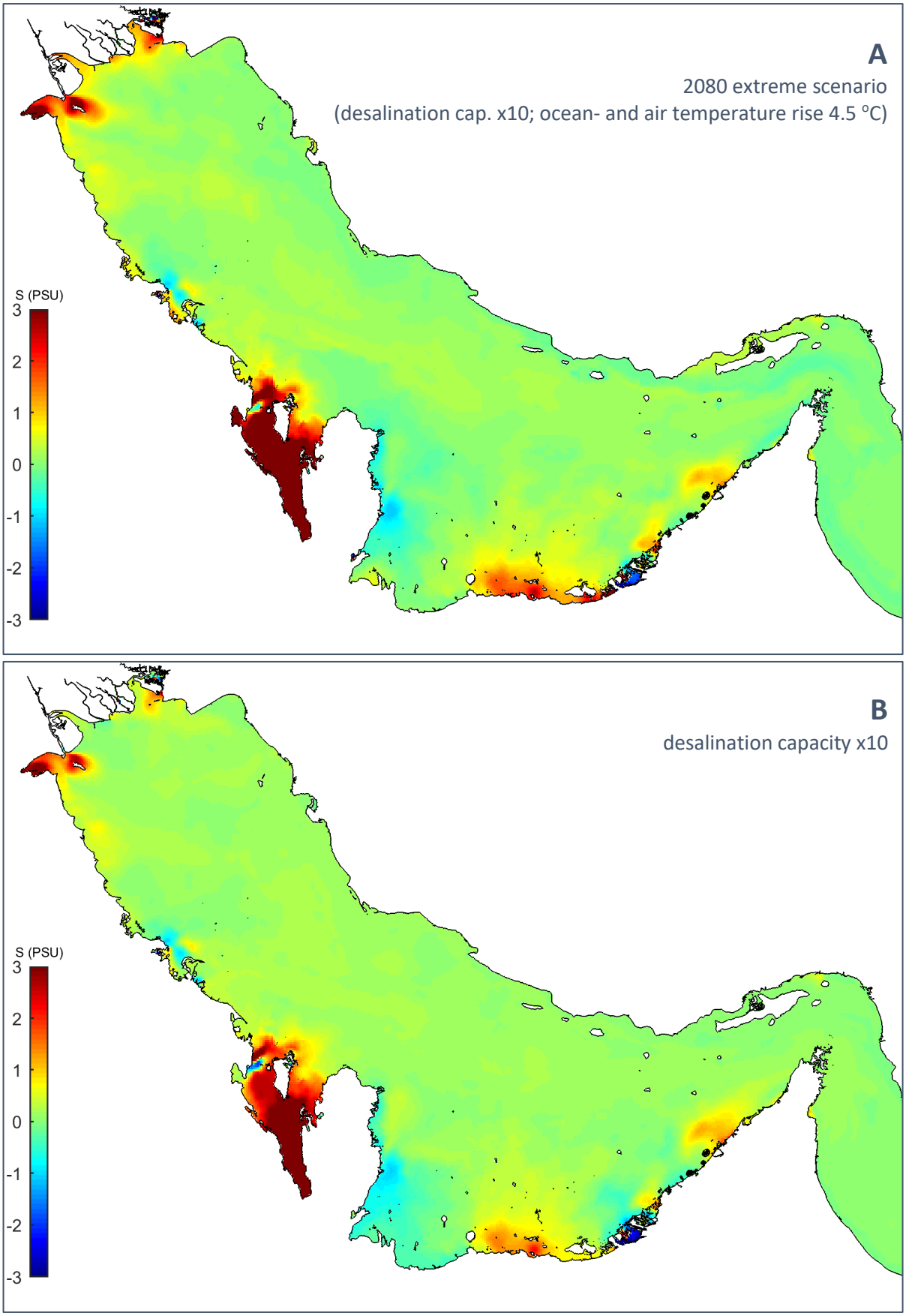

Figure 19 A&B: Maps of the Arabian Gulf of the year-averaged deviations of bottom salinities in the Arabian Gulf relative to the reference case. Simulated for A) the extreme 2080 scenario and B) the desalination capacity ten times the reference desalination capacity.

Table 4: Overview of simulated results for alternative desalination capacitie..

Desalination capacity	0x	ref. case	2x	5x	10x
Evaporation rate [m/year]	2.03	2.03	2.03	2.03	2.03
Average salinity [PSU]	41.2	41.2	41.2	41.3	41.3
Average salinity relative [PSU]	-0.04	-	+0.01	+0.08	+0.12
Relative gross inflow volume [m/y]	-2.48	-	-0.64	-1.40	+1.42
Relative gross inflow volume [%]	-3.3 %	-	-0.8 %	-1.9 %	+1.9 %
Area salinity +1 PSU [%]	<0.1 %	-	0.1 %	5.8 %	14 %
Area salinity +2 PSU [%]	<0.1 %	-	<0.1 %	0.2 %	7.2 %
Area salinity +3 PSU [%]	<0.1 %	-	<0.1 %	<0.1 %	3.8 %
Area salinity -1 PSU [%]	2.7%	-	0.2 %	0.5 %	0.9%

5.1.3 Sensitivity to atmospheric temperature

The findings in this section are based on simulations with the same oceanic temperature as for the reference case, so not increased along with increasing atmospheric temperatures. An increase in air temperature by 1.5 °C causes an increased evaporation rate (~8%) and higher Gulf averaged salinity (+0.16 PSU). An increase in air temperature by 3 °C causes an increased evaporation rate (~17%) and higher Gulf averaged salinity (+0.27 PSU). An air temperature increase by 4.5 °C causes increases the evaporation rate by ~24% and the Gulf averaged salinity is 0.44 PSU higher as a result. The air temperature seems to have a linear positive relation with the evaporation rate and a non-linear relation with the Gulf averaged salinity. There is no indication of a trend or correlation between the gross exchange rate and the air temperature. The most extreme salinity increase is concentrated in sheltered areas along the western coast, see Figure 21A. A relatively large part (19%) of the shallow region is affected by salinity rise of 1 PSU or higher due to air temperature rise of 4.5 °C. A negligible part of the shallow region is exposed to salinity increases of higher than 3 PSU.

Table 5: Overview of simulated results for cases with alternative atmospheric temperature forcing.

	Reference case 2016	Atmospheric temperature +1.5 °C	Atmospheric temperature +3 °C	Atmospheric temperature +4.5 °C
Evaporation rate [m/year]	2.03	2.18	2.34	2.51
Evaporation relative [%]	-	$+8_{.5}$ %	+17%	+24 %
Average salinity [PSU]	41.2	41.4	41.5	41.7
Average salinity relative [PSU]	-	+0.16	+0.27	+0.44
Relative gross inflow volume [m/y]	-	-0.74	0.38	0.14
Relative gross inflow volume [%]	-	$-1_{.0}$ %	$0_{.5}$ %	$0_{.2}$%
Area +1 PSU salinity [%]	-	0.6 %	8.1 %	19 %
Area +2 PSU salinity [%]	-	<0.1 %	0.5 %	7 %
Area +3 PSU salinity [%]	-	<0.1 %	<0.1 %	0.6 %

5.1.4 Sensitivity to oceanic water temperature

The findings in this section are based on simulations with the same atmospheric temperature as for the reference case, while the oceanic temperature is changed. The increased oceanic water temperature causes a small increase in the evaporation rate in the Arabian Gulf in the order of 2.5% for 4.5 °C oceanic water temperature increase (see Table 6). The effect is an order smaller than the impact of atmospheric temperature rise on the evaporation rate in the Arabian Gulf, see section 5.1.3, which can be explained with the ocean heat model as presented in section 2.4.3.

Increasing the oceanic water temperature causes an increase in temperature difference between in and outflow at the Strait of Hormuz, see Figure 20A and B. Increased temperature difference, causes an increased density gradient. Gross lateral inflow is positively related to the density difference. The bigger the volume of exchange with the ocean, the less salt accumulates in the Arabian Gulf. Resulting in lower salinities for increased oceanic temperature. Table 6 shows that the Gulf averaged salinity is simulated to drop by 0.20, 0.36 and 0.54 PSU due to increased oceanic temperatures of 1.5 °C, 3 °C and 4.5 °C respectively. The distribution of decreased salinity over the Arabian Gulf, due to increased oceanic temperature is close to spatially uniform, see Figure 21B.

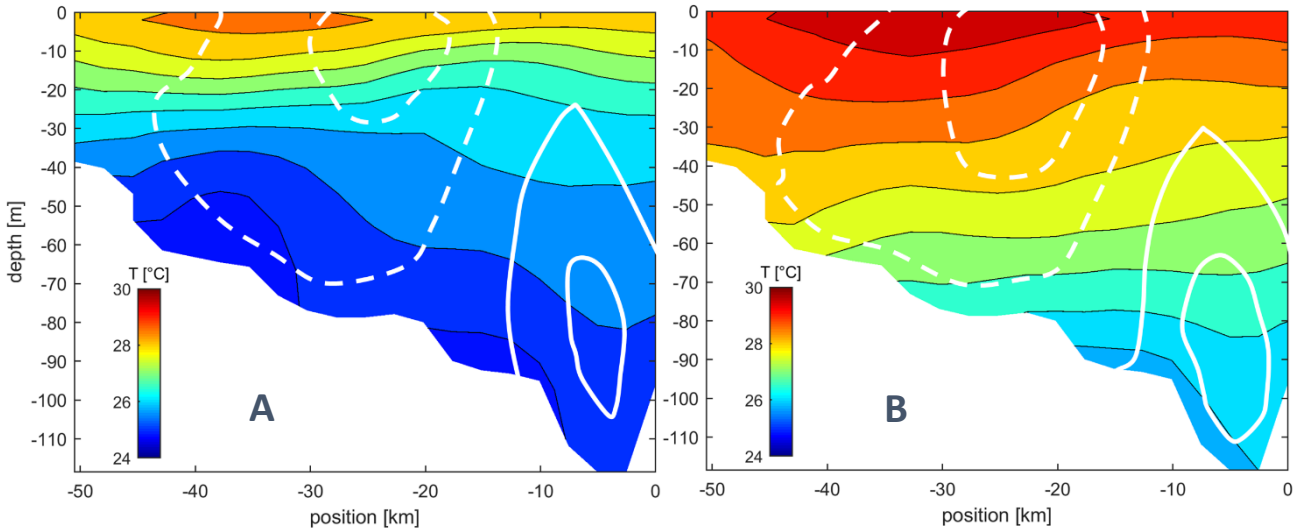

Figure 20: Cross sections through the Strait of Hormuz, showing temperatures and the schematic contours of inflow (dashed white line) and outflow (continoues white line) of A (left panel) the reference case and B (right panel) the simulation of elevated oceanic temperature by 4.5 °C.

Table 6: Overview of simulated results for cases with alternative oceanic temperature forcing.

	Reference case 2016	Ocean temperature +1.5 °C	Ocean temperature +3 °C	Ocean temperature +4.5 °C
Evaporation rate [m/year]	*2.03*	*2.05*	*2.06*	*2.08*
Evaporation relative [%]	-	*+0.9 %*	*+1.7 %*	*+2.5 %*
Average salinity [PSU]	*41.2*	*41.0*	*40.9*	*40.7*
Average salinity relative [PSU]	-	*-0.20*	*-0.36*	*-0.54*
Relative gross inflow volume [m/y]	-	*+4.68*	*+7.57*	*+8.59*
Relative gross inflow volume [%]	-	*+6.4 %*	*+10.4 %*	*+11.4 %*

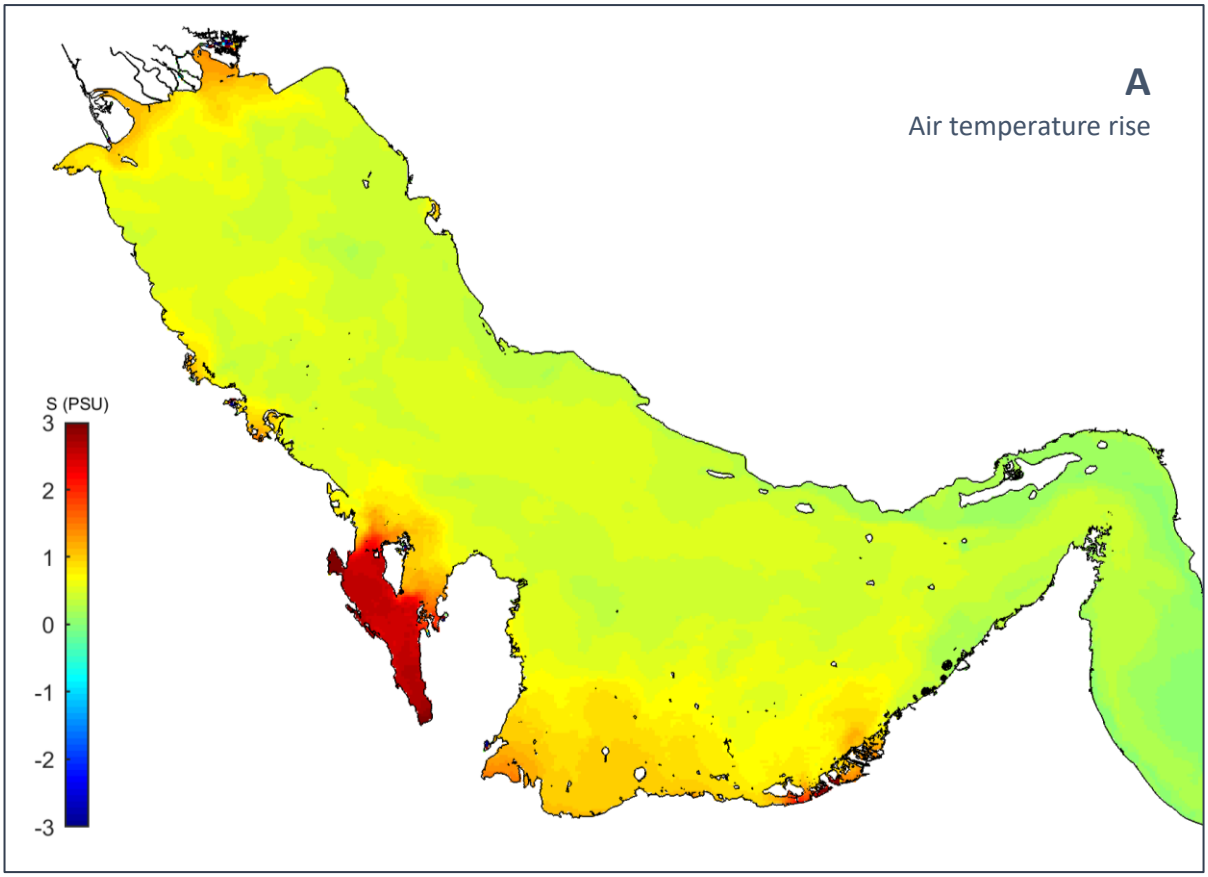

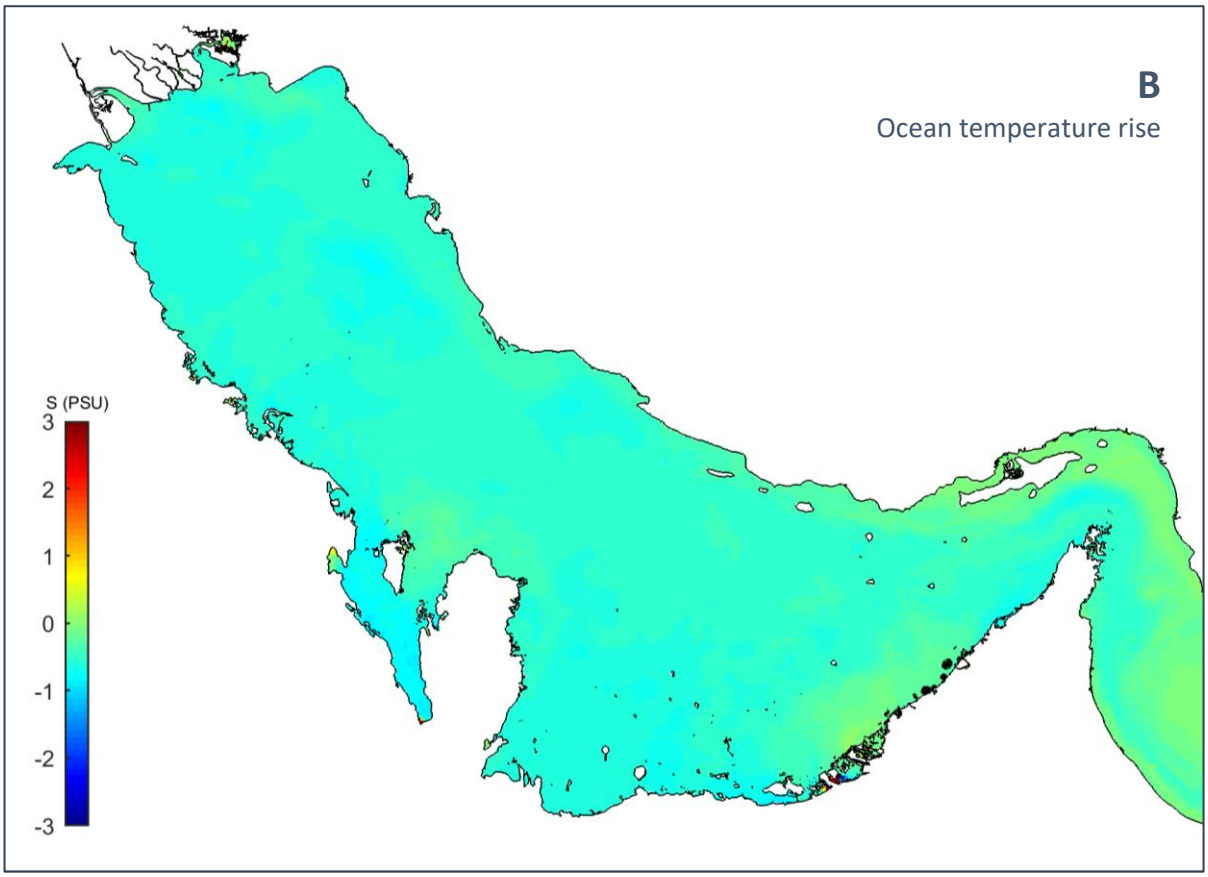

Figure 21A & B: Maps of the Arabian Gulf of year-averaged deviations of bottom salinities in the Arabian Gulf relative to the reference case. Simulated for A (top panel): atmospheric temperature rise of 4.5 °C and B (bottom panel): oceanic temperature rise of 4.5 °C.

5.1.5 Sensitivity to wind climate

This section will discuss the impact of wind velocity, -direction and fluctuations of both. In the climate change scenarios there has been no inclusion of changed wind climate. The wind climate is important for basin wide circulation (see sections 4.1.2 and 4.1.3) and evaporation rates (see section 2.4.3) which are both crucial factors for the salinity and the distribution thereof in the Arabian Gulf.

Change in wind velocity

An increase in the absolute wind velocity by 50% results in simulation of a ~25% higher rate of evaporation (see Table 7). The spatial plot of salinity deviation of the increased wind simulation relative to the reference case resembles the negative of the salinity deviation plot of the decreased wind velocity simulation, see Figure 23B & C. Increased wind velocity causes a stronger Iranian jet and a bigger volume of water reaches the north of the Gulf. The outward directed flow spreads out to the south, reaching the southern banks. The outward directed flow stagnates along the eastern UAE coast, where intensive salinity increases are simulated.

A decrease in the absolute wind velocity by 50% results in ~18% less evaporation and a strong decrease in standard deviation of evaporation than the reference case, see Table 7. The decrease in evaporation causes a decrease in salinity in the majority of the shallow regions, with the exception of specific areas that suffer from smaller rate of flushing, due to a decreased volume of wind-induced surface water transport. The decrease in wind velocity causes decreased vorticity near the Strait of Hormuz, the velocity of the Iranian jet is therefore smaller. Less oceanic water reaches the western part of the Gulf, leading to increased salinity at the southern banks and at the Centre of the Gulf. In the north of the Gulf, decreased wind velocity causes a decrease in evaporation rates, leading to a decrease in salt accumulation.

Uniform wind field

Uniformization of the wind field leads to weaker meso-scale eddies and a less dominant inflow along the Iranian coast. Instead, more ocean water flows towards the south-eastern shallow banks, where salinity drops are simulated. Due to the uniform wind direction being almost orthogonal to the entry of the Gulf of Salwah, the volumetric exchange with the Gulf of Salwah decreases due to uniformization. Fluctuations of the wind velocity and direction drive vorticity near the Gulf entry and the direction of the oceanic inflow, see Figure 22D. This affects the flushing of sheltered areas. Locally, the fluctuation of the wind is decisive for the degree of salt accumulation.

Rotation of predominant wind direction

Rotation of the uniform wind field does not lead to significant change in evaporation rate, see Table 7. Clockwise rotation of the uniform wind field causes higher flushing rates of the Gulf of Salwah and the southwestern banks, while the outflow from the desalination intensive south-eastern banks is counteracted by the wind-induced, southward surface flow, see Figure 22E. Relative to the uniform wind field the salinity of the Gulf drops by ~0.3 PSU due to the rotation in clockwise direction. The uniform wind field, rotated 20 degrees in counter-clockwise direction causes lower flushing rates and salt accumulation in the Gulf of Salwah and in front of the central UAE coast. Gulf wide salinity increases by ~0.3 PSU relative to the uniform wind field.

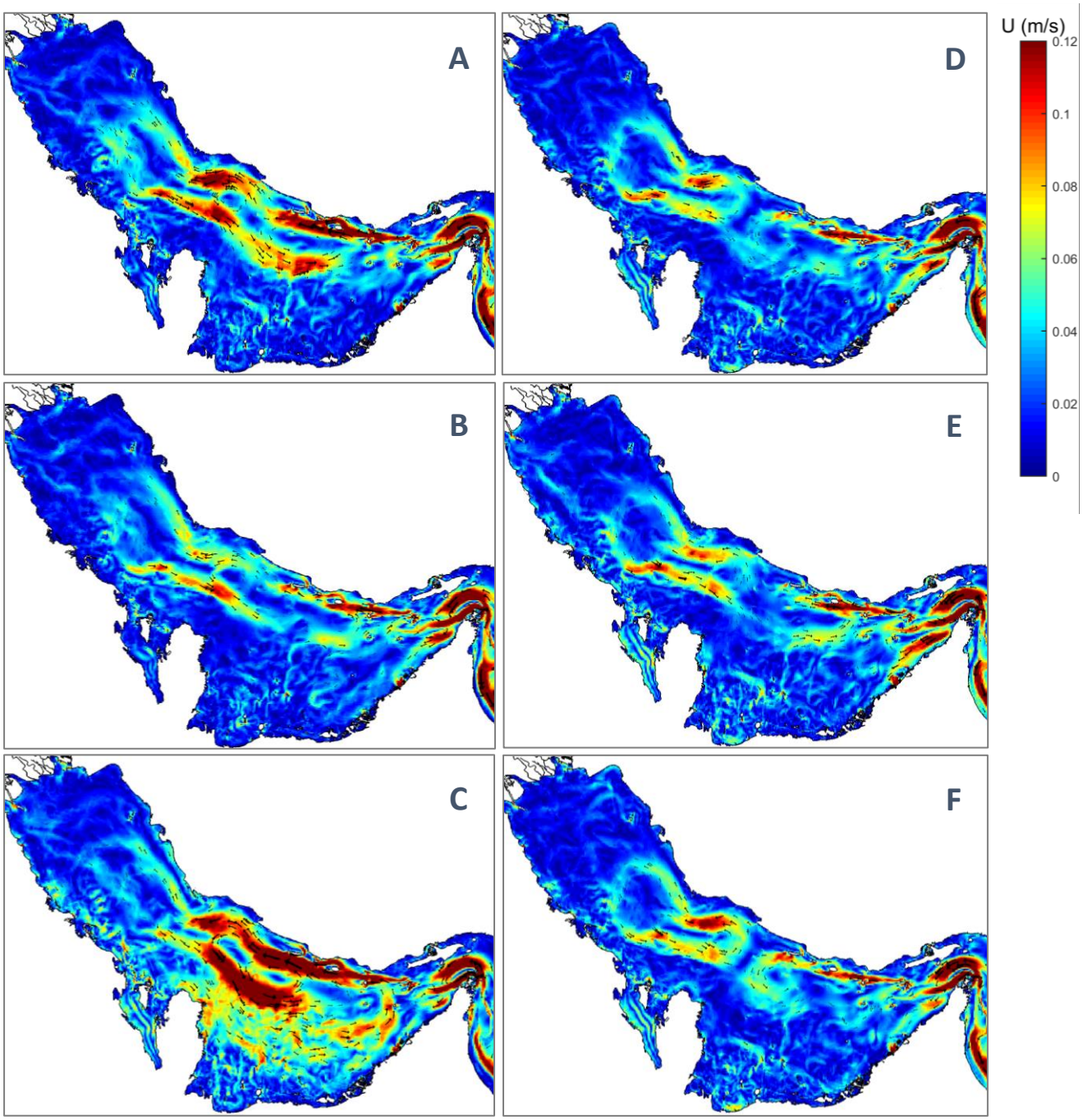

Figure 22: Maps of the Arabian Gulf, showing simulated yearly residual circulation, gained with a Fourier analysis, for left column (top-down) A: the reference case, B: mild wind velocity (-50%), C: strong wind velocity (+50%). Right column (top-down) D: uniform wind, E: uniform wind rotated clockwise, F: Uniform wind rotated counter-clockwise.

Table 7: Overview of simulated results for alternative wind velocity and -direction.

Wind -	velocity +50%	velocity 50%	direction +20 °	direction -20 °
Evaporation rate [m/year]	*2.38*	*1.66*	*1.89*	*1.88*
Evaporation relative [%]	*+25 %*	*-18 %*	-	-
Average salinity [PSU]	*41.7*	*40.9*	*41.1*	*41.7*
Average salinity relative [PSU]	*+0.45*	*-0.36*	*+0.02*	*+0.57*
Rel. gross inflow volume [m/y]	*+0.90*	*-1.35*	*-0.98*	*-5.62*
Rel. gross inflow volume [%]	*+1.2 %*	*-1.8 %*	*$-1_{.3}$ %*	*$-7_{.4}$ %*

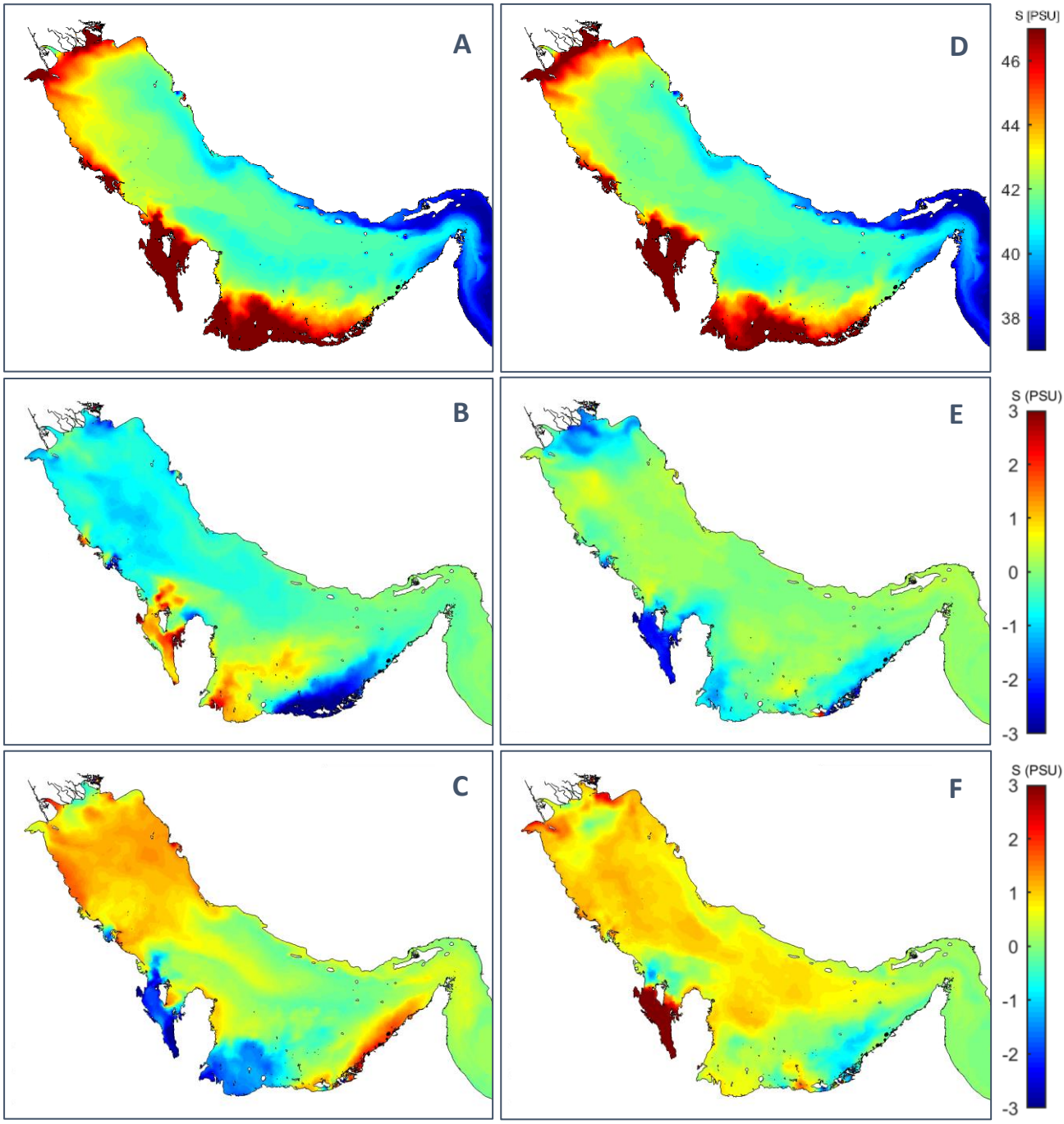

Figure 23A-F: Left upper panel (A) absolute year averaged bottom salinity of reference simulation. Left middle panel (B): Bottom salinity relative to the reference case of mild wind velocity simulation, left lower panel (C): Bottom salinity relative to the reference case of strong wind velocity simulation. In right upper panel (D): the absolute year averaged bottom salinity of the uniform wind field simulation, right middle panel (E): bottom salinity of clockwise rotated wind field relative to the uniform wind field case, right lower panel (F): bottom salinity of anti-clockwise rotated wind field relative to the uniform wind field case.

5.2 Local impact

On a local scale, the order of simulated salinity increase with respect to the reference case is much bigger than on Gulf-wide scale. In this section the effects of desalination capacity increase and climate change are considered on a local scale. Seasonal and weekly variations are thereby also regarded, see section 2.1.3.

5.2.1 Impact of combined desalination capacity increase and climate change

On a local scale, the order of simulated salinity increase with respect to the reference case is much bigger (order of 10 times) than on a Gulf-wide scale. For the mild projection for 2050, a negligible part of the coastal area shallower than 20 meter experiences a rise in salinity of over 1 PSU, but by 2080 the percentage of the shallow area that encounters a rise in salinity by at least 1 PSU is simulated to be 9% (see Table 3). For the extreme scenario simulations the results show that by 2080 over 18 % of the shallow area experiences an increase in salinity of at least 1 PSU, while over 7% experiences a salinity increase of at least 3 PSU. In general, the increase in bottom salinity in the shallow coastal zone is concentrated at the sheltered areas, where salt accumulates after intensifying the fresh water extraction driven by evaporation or desalination. Salinity drops were observed at the East coast of Qatar and the eastern part of the United Arabian Emirates (UAE) coast *(marked with green perimeters in Figure 24)*, which is discussed in section 6.1. Most extreme salinity rise was simulated at:

- Kuwait Bay and the Bay of Iran *(red perimeter in Figure 24)*
- The Gulf of Salwah *(purple perimeter in Figure 24)*
- Western coast United Arabian Emirates *(blue perimeter in Figure 24)*

The common drivers for extreme salinity increase are shallowness, a high degree of shelter and high concentrations of desalination brine discharge. The key locations imposed with the significant salinity increase (> 1 PSU) are marked red in Figure 24.

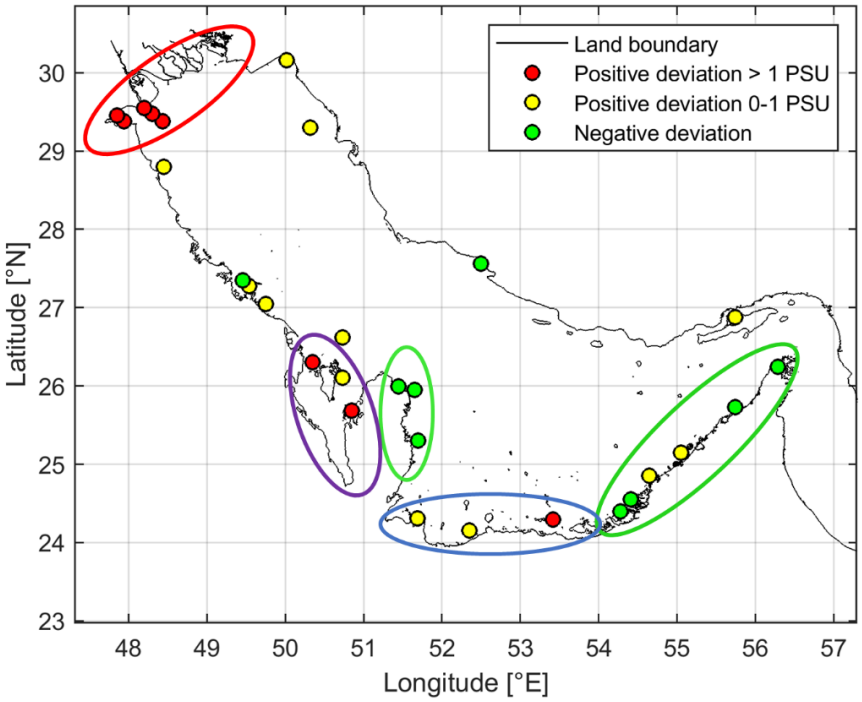

Figure 24: Locations of key interest, colored according to salinity deviation of the extreme scenario in 2080 simulation with respect to the reference case. The blue perimeter marks the western and central UAE coast; the green perimeters represent the east coast of Qatar and eastern coast of the UAE; the purple perimeter represents the Gulf of Salwah and the red perimeter marks the sheltered northern bays.

East coast of Qatar and eastern coast of the United Arabian Emirates

Simulated salinities directly near desalination outfalls along the eastern Qatar shoreline and the eastern part of the UAE coastline show no deviation of the salinity higher than 1 PSU in the extreme 2080 scenario, see Figure 24. The year-round salinity is not simulated to increase, as the local influence of increased desalination capacity and increased evaporation rate is balanced by the local effect of increased gross oceanic exchange. For locations remote from significant desalination outfalls, like Khaimah (25.8 °E, 55.9 °N), the year averaged and seasonal extreme salinities drop, see Figure 27F. In this region the impact on salinities of increased volumetric exchange with the ocean is simulated to be bigger than the direct impact of increased desalination and evaporation rates.

Kuwait Bay (northern Gulf)

In the coastal regions in the centre and north of the Gulf, neither increase in desalination capacity nor air temperature rise results in significant adaptation of the salinity (see Figure 26A & B for weekly salinities at a seagrass meadow near Bandar Siraf, north Iran). Exceptions to this are sheltered, shallow locations, like the Bay of Iran and Kuwait Bay. Salinities in the Bay of Iran are vulnerable to temperature rise. For Kuwait Bay, increased desalination capacity is simulated to be more impactful than air temperature rise (see Figure 26C & D). 50 km east of the observation point in Kuwait Bay, at a coral reef north of Failaka island (29.48 °E 48.32 °N), increased desalination capacity till five times the reference case causes increased year round salinity and increased weekly variation (see Figure 26E) that are of bigger order than the year round salinity increase caused by climate change, see Figure 26F. Figure 27C & D show that additional accumulation is forced when the desalination capacity is increased to 10 times the reference capacity. The simulation with a desalination capacity of ten times the reference capacity (Figure 27D) shows a rise in year round salinity of about five times the resulting salinity rise from the 5 times reference simulation.

Gulf of Salwah

Spatial plots clearly indicate that the salinity in the Gulf of Salwah is sensitive to changes in climate and desalination capacity, see Figure 19 and Figure 21. The reference salinity in the Gulf of Salwah is extreme, see Figure 23A. The year round salinity at the Hawar coral reef, located at the West coast of Qatar (25.65 °E, 50.87 °N), is more sensitive to changes in desalination capacity than to climate change, see Figure 25E & F. The weekly variation is not affected by changes in either climate change or desalination capacity. The seasonal variation at Hawar increases, because of a higher rate of salt accumulation during summer (see the slope from June to September in Figure 25E and Figure 27B). An increase in desalination capacity of 400% causes a salinity extreme of 2 PSU higher than in the reference case, while the year averaged increase is in the order of 0.5 PSU at Hawar, see Figure 25E. An increase in desalination capacity of 900% causes an increase in extreme salinity of ~4 PSU and forces a rise of ~2 PSU in winter salinity.

Western coast United Arabian Emirates

In the western part of the UAE coastal area, the impact of increased desalination capacity is slightly bigger than the impact of climate change (see Figure 25A & B) at a seagrass meadow near Abu al-Abyad, located close to desalination plant outfalls. Salt accumulates in front of the western UAE coast when imposed to increased desalination brine discharge. Figure 25A shows higher peaks, but more clearly a longer duration before the salt is flushed away after a peak. More distanced from large desalination outfall locations, at a seagrass meadow near Al Yasat (24.27 °E, 51.7°N), the influence of climate change induced air temperature rise dominates over the impact of additional desalination capacity, see Figure 25C & D. Neither the simulation for climate change nor desalination capacity increase show that the seasonal variation nor the weekly variation of salinity is sensitive to increasing rates of fresh water extraction.

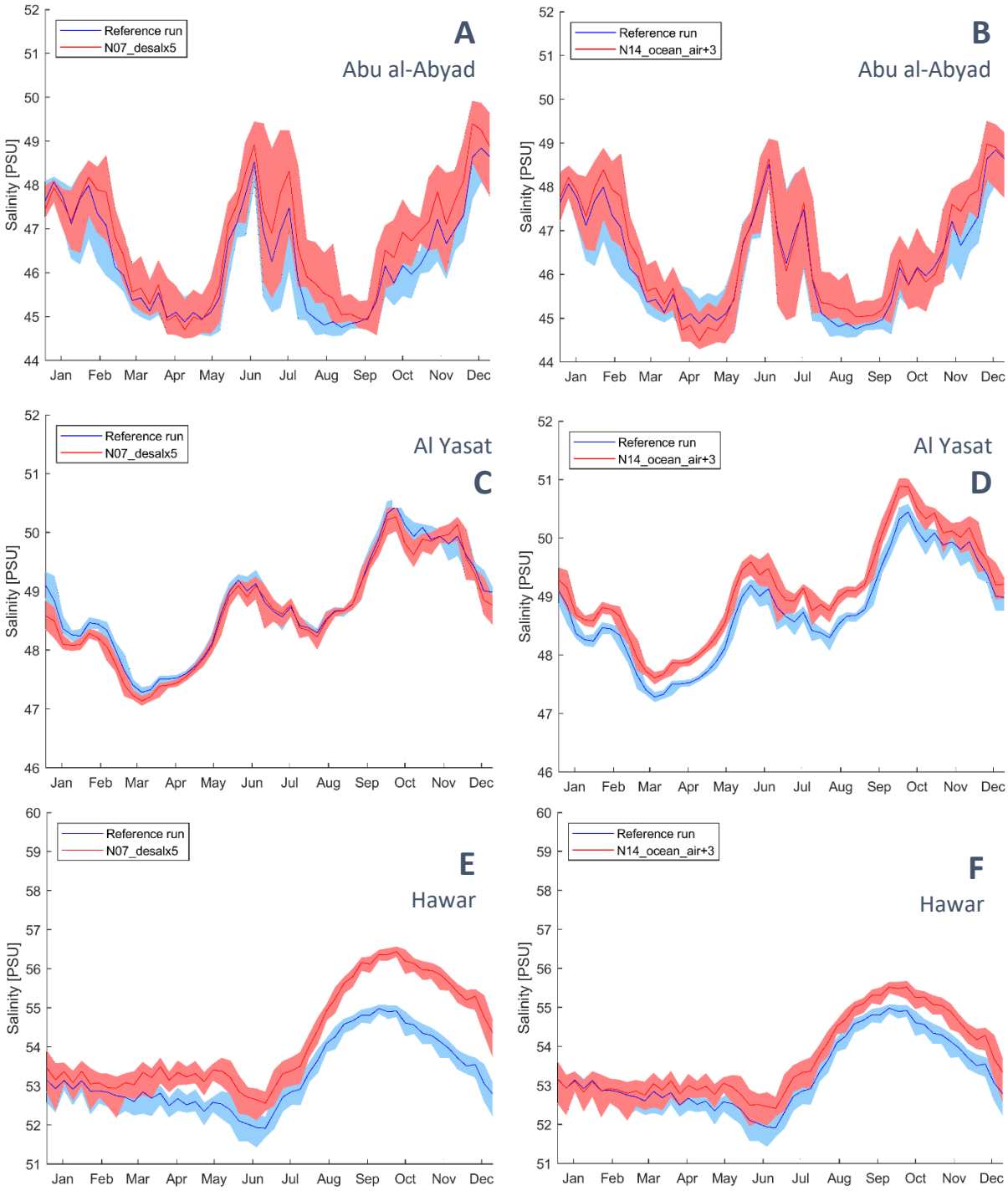

Figure 25 A-F: Week-averaged (dark lines) and weekly variation (light band) of reference simulation (blue) and simulations of increased salinity by five times (red) for the left column (A, C, E). For the right column in red are the results of increased temperature by 3 °C (B, D, F). At Abu al-Abyad (top panels: A and B), Al Yasat (middle panels: C and D) and at Hawar (bottom panels: E and F).

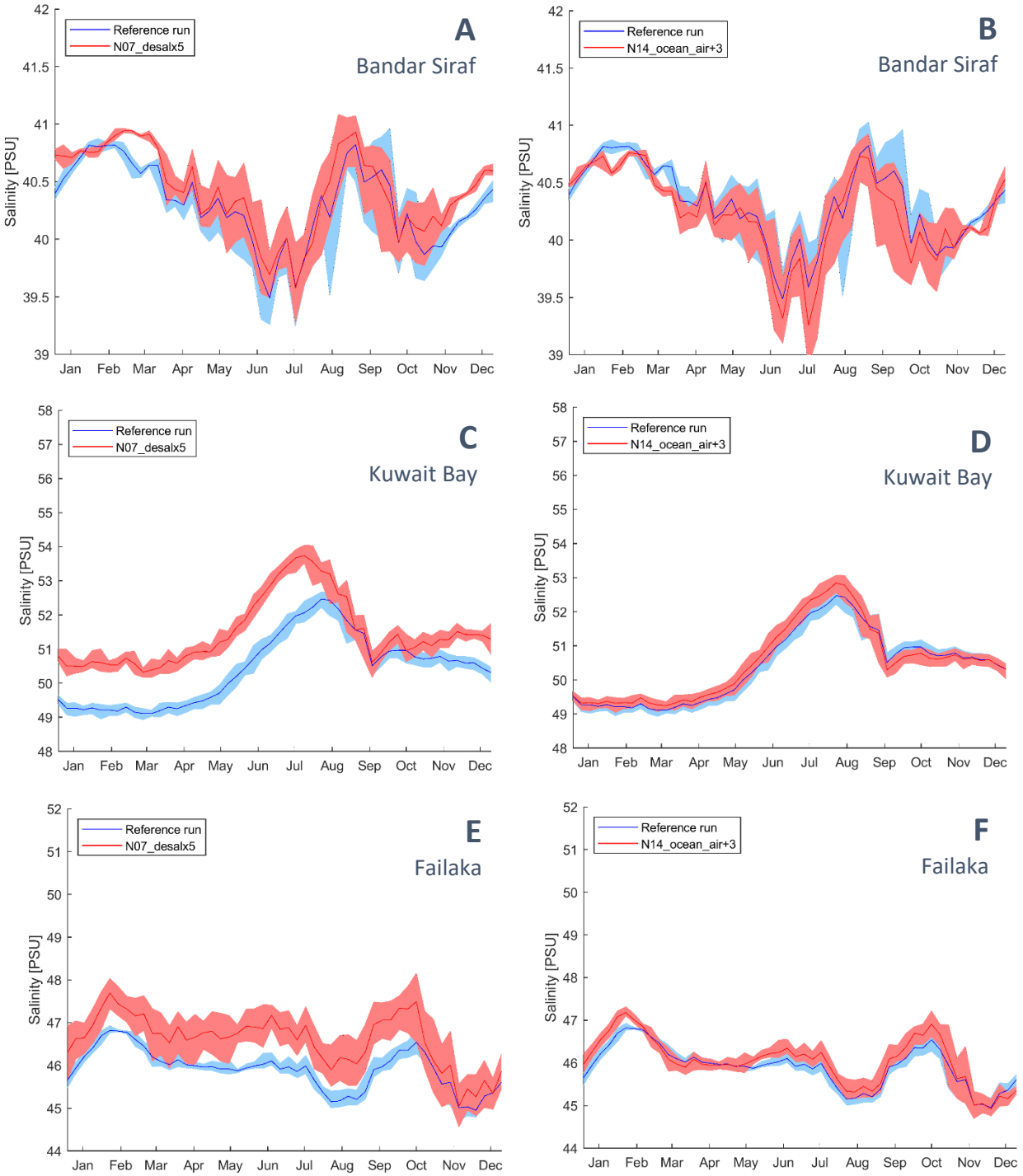

Figure 26A-F: A-F: Week-averaged (dark lines) and weekly variation (light band) of reference simulation (blue) and simulations of increased salinity by five times (red) for the left column (A, C, E). For the right column in red are the results of increased temperature by 3 °C (B, D, F). At Bandar Siraf (top panels: A and B); Kuwait Bay (middle panels: C and D) and at Failaka island (bottom panels: E and F).

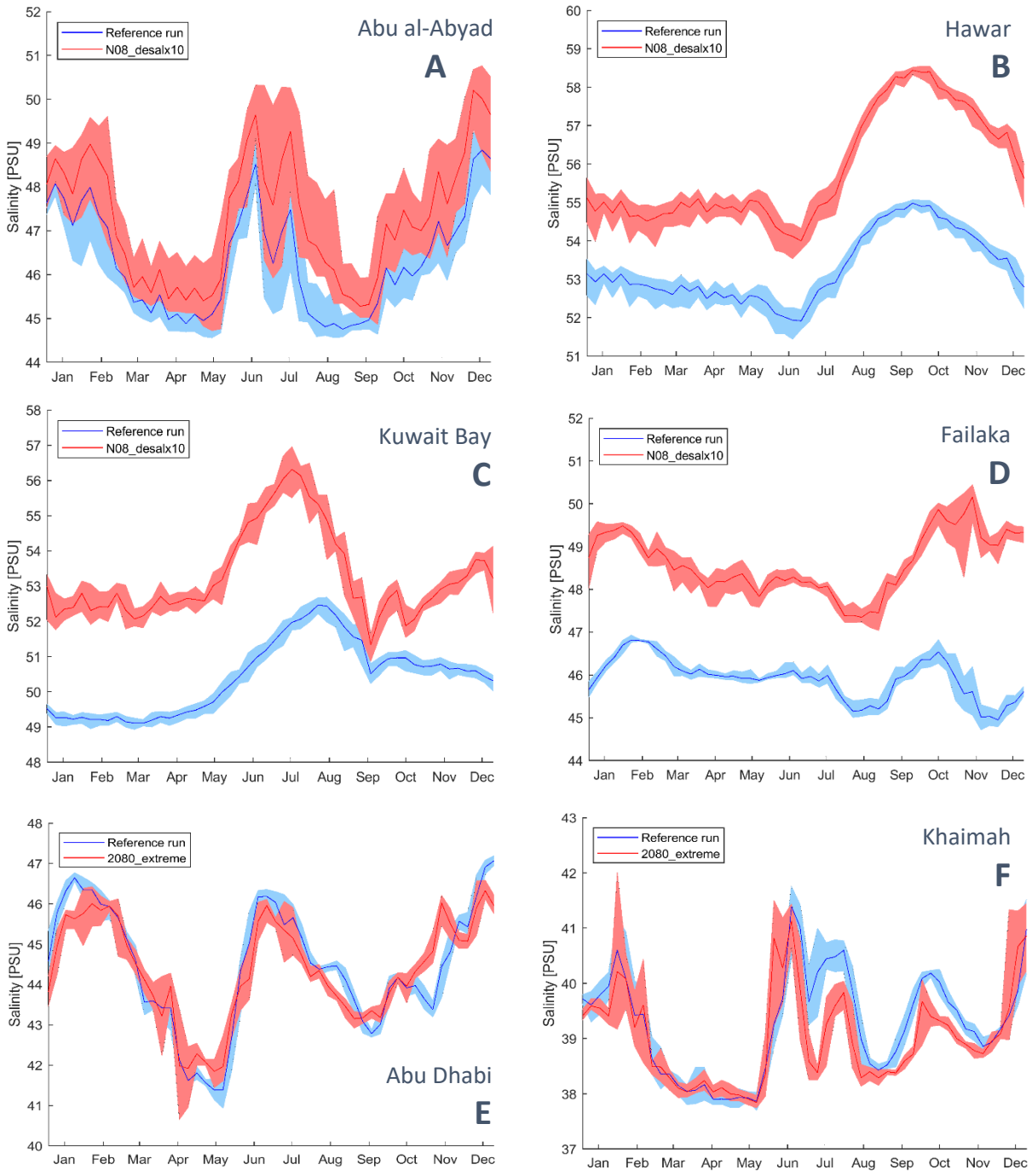

Figure 27A-F: Weekly averaged (dark lines) and weekly variation (light band) of reference simulation (blue) and simulations of increased salinity by 10 times (upper two rows: A - D) and of the extreme scenario for 2080 (bottom row: E and F). At Abu al-Abyad (A); Hawar (B); Kuwait Bay (C); Failaka island (D); Abu Dhabi (E) and Khaimah (F).

5.2.2 Sensitivity to desalination capacity

There is a positive relationship between desalination capacity and salinity, see Figure 28. The simulated impact on the shallow regions of two times reference desalination (Figure 28B) is negligible. The simulated impact of five times reference capacity (Figure 28C) on salinities in the shallow regions is severe with Table 4 showing that approximately 6 % of the shallow region is imposed by at least 1 PSU salinity rise. The simulated impact of ten times the desalination capacity (Figure 28D) of the reference case is extreme with ~14% of the shallow area imposed by salinity increase of 1 PSU, of the shallow area appr. 7% is imposed by salinity rise of at least 2 PSU and approximately 4% by salinity rise of more than 3 PSU. The bathymetry at and around a location is crucial for salinity adaptation to increased desalination capacity. The reference salinities at relatively open locations are typically mild and the local salinity is relatively insensitive to changes in desalination capacity. Typical for sheltered, shallow locations are high reference salinities and high sensitivity to desalination capacity increase.

The correlation between salinities in the reference case and salinity increase caused by increased desalination capacity is strong, based on yearly averages at the key locations (Figure 28). The locations at which salinity increase of over 1.5 PSU is modelled, are all in the sheltered shallow Gulf of Salwah and in the sheltered shallow Kuwait Bay area, see the magenta filled circles in Figure 29. The scatterplots in Figure 28 show no difference between salinities at the desalination plant intakes (blue circles) and the locations of ecological importance (orange squares and yellow triangles).

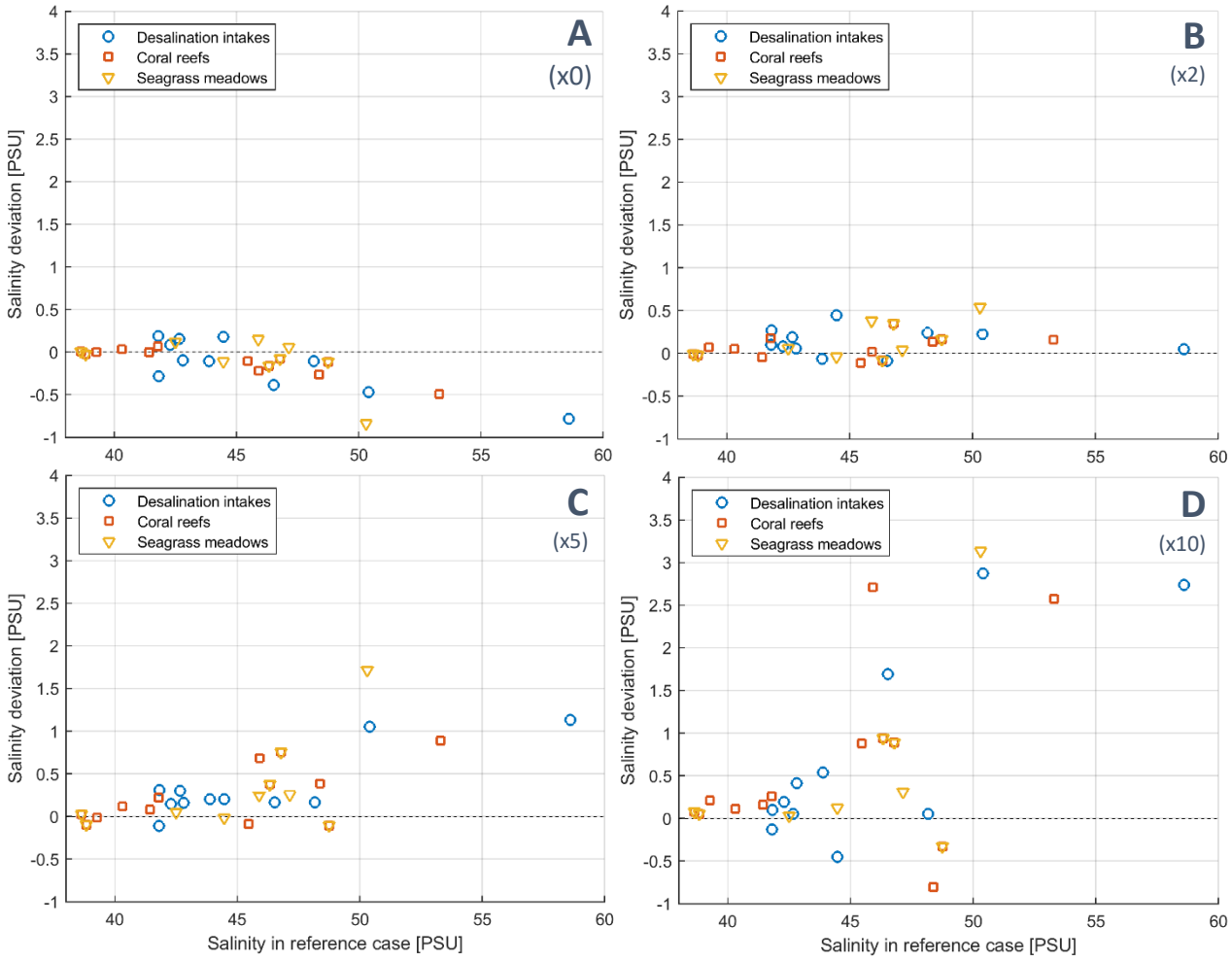

Figure 28: Scatter plots of salinity deviation relative to reference case plotted over salinity in the reference case for simulations of: A (top left panel): no desalination capacity, B (top right panel): reference desalination capacity times two, C (left bottom panel): desaliantion capacity times five, D (right bottom panel): desalination capacity times ten.

At the coral reef north of Jubail and at the seagrass meadow near Abu Dhabi (24.3 °N, 51.1 °E, see Figure 29A) extreme increase in desalination capacity (10x) is modelled to cause a salinity decrease of more than 0.5 PSU. In the discussion, section 6.2.3, the cause for salinity drops is elaborated upon.

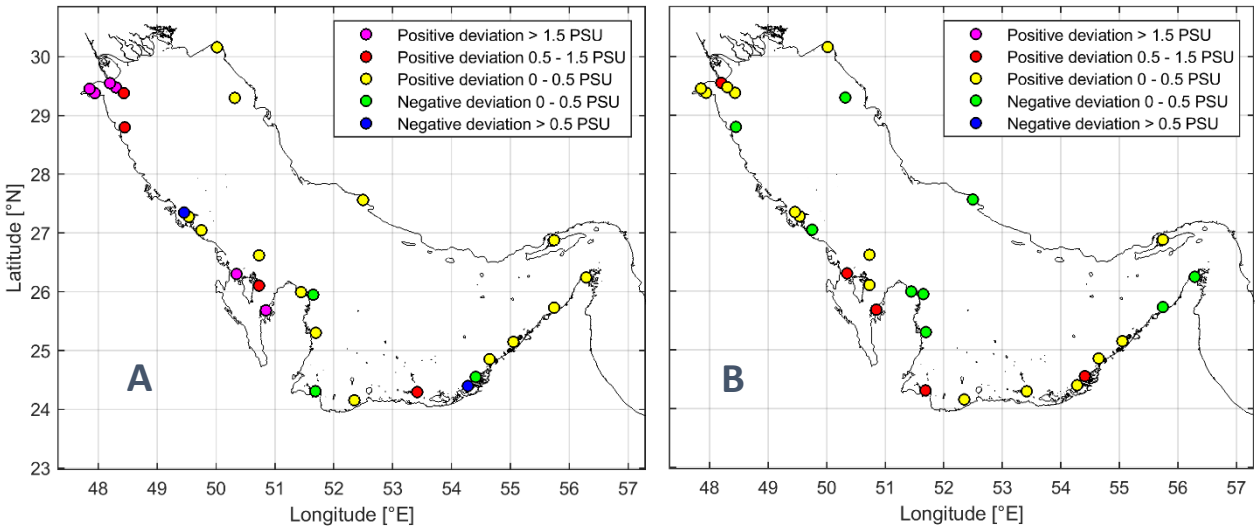

Figure 29A & B: Salinity deviations of key locations for A (left panel) desalinations capacity times ten scenario relative to the reference case and B (right panel) air temperature +4.5 °C relative to the reference case. With salinity decease of >0.5 PSU in blue, salinity decrease <0.5 in green, salinity increase of <0.5 PSU in yellow, increase of 0.5 – 1.5 PSU in red and increase of >1.5 PSU in magenta.

5.2.3 Sensitivity to atmospheric temperature

The simulations of alternated atmospheric temperature (including and excluding ocean temperature adaptation) show a strikingly linear correlation between salinity in the reference case and increase of salinity when forced by increased air temperature only (Figure 30A) or by air and ocean temperature (Figure 30B). The linearity indicates that climate change will induce a polarization of salinities in the Arabian Gulf due to air temperature rise, with local salinity extremes showing extreme salinity increases. Figure 30B is more scattered than Figure 30A, which indicates that the shelterness of locations might be altered. This makes sense as an increase in gross lateral exchange through the narrow Strait will affect the transport patterns of inflowing oceanic water.

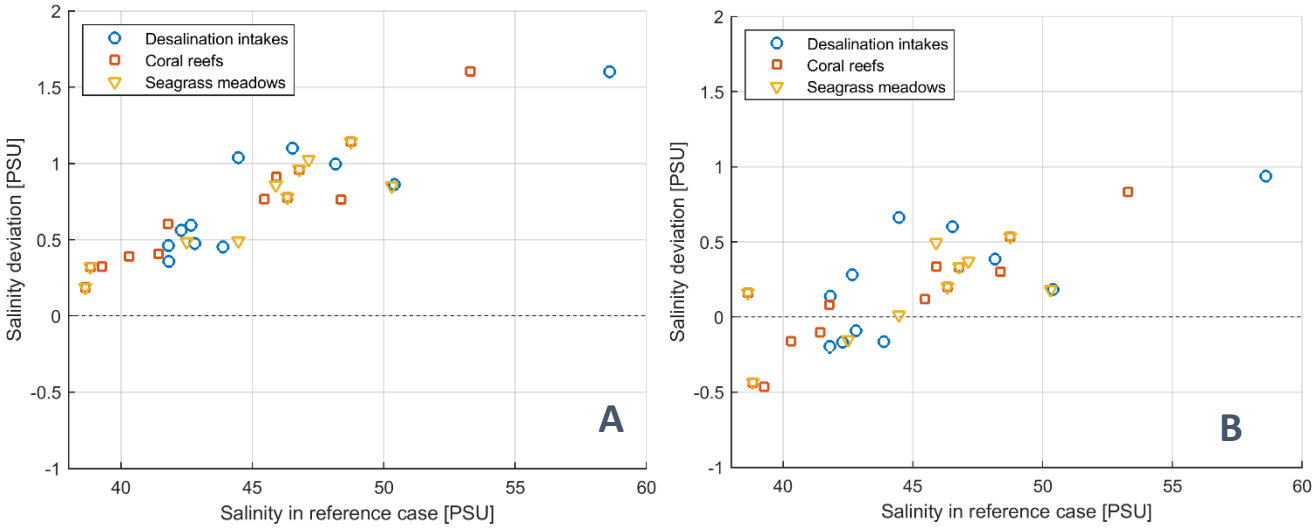

Figure 30A & B: Scatterplots of simulated salinity deviation for A (left panel) the air temperature only +4.5 °C case and B (right panel) air temperature and oceanic temperature +4.5 °C case, relative to reference case and plotted over salinity in the reference case.

6 Discussion

In this chapter, both the potential and the limitations of this research are discussed, providing the context required to interpret the conclusions, as drawn in chapter 7.

6.1 Model findings

In this section the general findings are discussed in section 6.1.1. The difference in outcome of this research, compared to a previously conducted research on the impact of desalination capacity increase and climate change is discussed in section 6.1.2.

6.1.1 General findings

Air temperature rise leads to higher rates of evaporation. The impact of more evaporation on salinities in the Gulf is dampened by increasing rates of lateral exchange due to increase of oceanic water temperatures, resulting in no effect of climate change on Gulf-averaged salinities. The simulated impact of climate change and desalination capacity increase on salinities at a local scale is of a higher order (>1 PSU) than projected salt accumulation Gulf wide (~0.1 PSU). The strongest effects are simulated at locations of extreme reference salinity. Seasonal variations are simulated to increase. In specific cases, the weekly variation was simulated to increase. Wind climate variation simulations show that wind impacts evaporation rates and internal transport patterns. Thereby influencing the distribution of salt accumulation. In general the results indicate that the Gulf wide salinity is not sensitive to desalination capacity increase and climate change. While local and seasonal extreme salinities tend to become more extreme due to intensified climate and desalination forcing. To give an indication of the severity of salinity rises in the order of two PSU: Al-Said (2017) found a that the species diversity of the phytoplankton community shrank vastly due to a salinity increase of two PSU near Kuwait. The volumetric fish catch halved during this six year period. Increased seasonal extremes contributes to the stress on marine ecology, while increased weekly variation locally reduces stress on marine ecology.

6.1.2 Comparison to AGEDI study

A study by AGEDI (Edson, Wainer & Ferrero, 2016) explored the impact of desalination capacity increase and climate change on salinity in the Arabian Gulf. They found a more severe impact of desalination capacity increase, relative to our findings (section 5.1.2). The main difference between the studies lies in certain modelling assumptions. Namely, while we modelled the desalination plants as fresh water extraction and temperature addition to a brine, AGEDI modelled desalination plants as the dumping of salt from an infinite source. We divided the estimated desalination plants over 126 plants, while AGEDI modelled 14 plants. For boundary conditions, different assumptions were made as well. The boundary of the model by AGEDI was located ~100 km from the Strait of Hormuz (56.4 °E) at a cross section with a maximum depth of < 200 m, while we chose for a boundary condition at ~100 km from the Strait, with a maximum depth of > 3000 m. An artefact of the location of the model boundary so close to the Strait and the limited depth is vorticity east of the Strait (Edson, Wainer & Ferrero, 2016: Figure 6-13), which recirculates saline water into the Arabian Gulf. This ill representation of the transport contributes to the accumulation of salt in the Arabian Gulf and has a large influence on their findings.

The effects of the boundary conditions as modelled in our research is not investigated. The buffer between the Arabian Gulf and the open ocean boundary in the Gulf of Oman seems to stabilise the model results. The fact that the outflow is at a depth of 150m at the AGEDI boundary and at a depth of 3000m at the boundary of our model implies a difference in degree of mixing of in and outflow at the boundary. The effect on local flow patterns at a sheltered location due to addition of salt or extraction of fresh water is undoubtedly different. Our findings suggest that the rate of flushing of an

area dominates the tendency for salt accumulation. This implies that it is important to model desalination plants with optimal representability of reality. Which also counts for the spatial distribution of the plants and the seasonality in their operations.

6.2 Research limitations

There are multiple dimensions of uncertainty that limit the potential of this research. There is uncertainty in the future projections, as it is subjected to strong assumptions, see section 6.2.1. The numerical model has not been validated extensively for the representation of salinity, which introduces uncertainty as well, see section 6.2.2. Simplifications were necessary to keep the computations and output handleable, the uncertainty of the underlying assumptions is discussed in section 6.2.3.

6.2.1 Future projection uncertainty

There is a significant margin of uncertainty for temperature rise predictions by 2080 from 1.5 ^{o}C to 4.5 ^{o}C (see Figure 4). Besides, the future trends of averages and seasonal variation of other drivers of evaporation are uncertain as well. Although no research on future trends in development of the wind climate in the Arabian Gulf region is known at the time of writing this thesis it is possible that a changing climate induces a significantly different wind field by 2050 or 2080 (Eichelberger et al., 2008) compared to the wind field used in the reference case. The analysis on the sensitivity of salinity distribution to wind climate showed that the daily wind fluctuation is important for transport of the inflowing ocean water and flushing of sheltered areas. The predominate wind direction influences the flushing of areas and the wind magnitude impacts both evaporation rate and transport of salt in the Gulf. In multiple ways changing wind climate impacts the accumulation of salt in the coastal regions of the Arabian Gulf. Assuming a constant wind field therefore introduces a limitation to the certainty about climate change driven impact on coastal salinities.

The projections of development of desalination capacity are subject to similarly uncertain factors. The development of water use per capita and the population size is merely approximated as it is a result of a complex system of unpredictable future changes in societal behaviour, policy making and economic development on both a global and regional scale. These factors all influence the increase in demand for desalination capacity and the location where new plants are built. In the simulated scenarios of increased desalination capacity, the assumption was made of a uniform distribution of additional capacity over the existing plants. Technical uncertainties arise when considering what part of the water demand will be met by desalination in 2050 or 2080. Uncertainties in the political, societal, economic and technical domains undermine the certainty of long-term future projections of desalination capacity development.

6.2.2 Model uncertainty

The model showed accurate representation of physical phenomena surface temperatures (see chapter 4 and appendix 13 respectively). The data used for the validation is outdated. Much of the natural forcing has changed since the mt. Mitchel survey in 1992. The simulated salinity distribution both horizontally and vertically showed significant deviation to assimilated data plots, which introduces scepticism to the simulated absolute values of salinity. The reference salinity is subtracted from the results of the projected future forcing simulations, the salinities are regarded relatively. Careful conclusions can be drawn from the simulated relative salinities. Techniques to derive surface salinities from remote sensing reflectance data are emerging (Zhao et al., 2017) and will potentially contribute to increasing model reliability. Large scale surveys or shared databases of measurements of water properties also potentially contribute to limiting the model uncertainty.

6.2.3 Modelling assumptions uncertainty

The assumption that the boundary condition of oceanic temperature adapts uniformly to temperature rise in the atmosphere is a gross simplification. In reality, the distribution of the additional thermal energy is non-uniform and non-linear. The assumption that the upper 100's of meters of the ocean adapt to increased atmospheric temperatures at the same rate as air temperature rise seems valid. It are the surface layers that flow into the Arabian Gulf, while deeper layers recirculate in the Gulf of Oman.

Salinity of the inflow at the open ocean boundary condition is assumed unaffected by the salinity of the outflow, as the outflow is over the bottom (depth: -3000m) and the inflow at the surface, concentrated in the upper 100's of meters. Salinity at the open ocean boundary dominates the salinity of the inflow. Both salinity and temperature at the open ocean boundary have strong influence on the salt balance and are therefore crucial for the accumulation of salt in the Gulf. For the accuracy aimed to achieve in this research the assumptions regarding the boundary conditions are valid.

There is no relation between increasing desalination capacity and increasing rate of evaporation. Therefore the correlation between desalination and water temperature in the Gulf (dashed line in Figure 2) is negligible. The only difference among the model representation of different desalination techniques is the efficiency. The additional temperature of the brine is the same for all techniques, but as efficiency differs, the thermal energy added by an RO plant is 2/7 of the thermal energy added by a MSF plant (see section 2.4.9). The effect of desalination on Gulf temperature is negligible, so it does not matter which techniques are used, which validates the simplification of assumed constant distribution among the desalination techniques.

The model is forced with abrupt change in forcing and given eight years to reach equilibrium. A more accurate representation of reality would be to increase the forcing gradually until 2050 or 2080. All output data is from a single year, which makes conclusions about absolute values indicative. The aim of this research is to understand the long-term development, so it is considered valid to use relative values of the ninth simulated year of alternative scenarios, relative to the ninth year of the simulated reference case.

The local salinity drops larger than 0.5 PSU can be artefacts of the way desalination capacity increase is modelled. In the model results of the reference desalination capacity times five, these salinity drops are not significant, but local flow seems to be affected unrealistically intensive in the case of ten times the reference desalination capacity. This drives locally intense flows, for which the spatial resolution is too coarse to accurately represent the flow, see appendix 14.

7 Conclusions

The research questions introduced in section 1.3, are answered in this chapter. The findings on which the conclusions are based at are presented in chapter 5. Further elaboration upon the limitations of the findings can be found in section 6.2.

1. ***What is the combined impact of increasing desalination capacity and climate change on local salinities in the coastal regions of the Arabian Gulf?***

The combination of future increased desalination capacity and climate change causes salinity rise at sheltered shallow locations along the coastline of the Arabian Peninsula of a much bigger order (>1 PSU) than deviations of Gulf wide salinity (~0.1 PSU). At sheltered shallow locations, where significant desalination brine is discharged, the effects of desalination capacity dominate over the effects of climate change, cumulatively causing local salinity rises in the order of 2 PSU for 10% of the shallow area, simulated for the extreme scenario for 2080. At the majority of locations where salinity is simulated to rise significantly, the reference salinity is also high. Extreme salinities tend to become more extreme due to increased desalination capacity and climate change.

Seasonally, the additional accumulation of salt due to desalination capacity increase or climate change is most severe at seasonal salinity peaks. Typically, seasonal peak values increase by twice the year averaged salinity increase. Depending on the specific location, the seasonal peak is typically in Summer or late Summer. Both on a seasonal scale and on a spatial scale, salinity extreme are projected to become more extreme. This is especially relevant for sheltered locations close to large desalination plants like Kuwait Bay, the Gulf of Salwah and central UAE coast. In specific cases the weekly variation is increased, but not to order of 1 PSU deviation to the weekly mean.

At locations near large desalination plants, the projected effects of desalination capacity increase dominate the effects of climate change. In the Gulf of Salwah the effects of desalination capacity increase and climate change are both severe (> 1.5 PSU) and neither process dominates the other. Sheltered location more remote from outfalls of desalination brine, like the Bay of Iran, the western UAE coast and the southeast of Qatar, experience milder effects of desalination capacity increase and slight salinity increases (< 1.5 PSU) are driven by air temperature rise. Increasing the extremity of the desalination capacity is simulated to increase the area affected by significant salinity rise. Multiplication of the desalination capacity by ten times the reference capacity causes the highly saline plume from Kuwait Bay to stretch to and around Failaka island, offshore of Kuwait Bay.

Shallow, but more open locations, like the east coast of Qatar and the eastern coast of the UAE, profit from high flushing rates due to tidal exchange and are not prone to significant salinity rise. Locations along these shores that are remote from desalination plants, like Khaimah, are even simulated to show drops in salinity due to desalination capacity increase and air temperature rise. The Iranian coastline is not prone to significant salinity deviation due to desalination capacity increase or climate change.

2. ***How do changes in desalination capacity and climate affect salt accumulation in the Arabian Gulf?***

Increases in air temperature rise and resulting increase in the rate of evaporation, drives salinity increase over the entire Gulf (order of 0.5 PSU) with extremes (order of 1.5 PSU and higher) in the Gulf of Salwah, the Bay of Iran and in the marshes near Abu Dhabi. Oceanic temperature rise drives evenly distributed salinity decrease in the Gulf (order of 0.5 PSU). Combined air and oceanic temperature rise barely affect the Gulfs simulated average salinity. Climate change affects the distribution of salt accumulation in the Gulf rather than the total amount of salt in the Gulf.

Desalination, when concentrated and at a sheltered location, drives local salinity increase. Adaptation of the flow patterns on a local scale causes salinity drops at specific locations, more remote from the desalination plants. The distribution of desalination plants is influential to the spatial distribution of salinity development.

Wind climate impacts the accumulation of salt in the coastal regions of the Arabian Gulf through various processes. Daily fluctuations of wind affect the energy intensity and direction of the inflowing ocean water and thereby affect the rates of flushing of sheltered areas. Change in the predominate wind direction influences the flushing of sheltered areas. Changes in the wind velocity impacts both evaporation rate and transport of salt in the Gulf. Therefore, changes in wind velocity impact the salinity distribution in the Gulf. The temperature of the ocean water has a strong driving effect on the gross inflow volume of oceanic water through the Strait of Hormuz. The lateral exchange flushes the Arabian Gulf and therefore has a crucial effect on the Gulf wide scale and along the majority of the coastline in the Arabian Gulf.

8 Recommendations

The findings of this research contribute to both further in-depth research, as well as a public discussion regarding sustainability of desalination. This chapter presents a few recommendations for researchers in section 8.1 and recommendations for policy makers in section 8.2.

8.1 Recommendations for researchers

- Numerical experiments focussing on the relation between boundary conditions and mixing patterns in the Gulf of Oman can improve the accuracy of representation of climate change at the boundary and limit artificial dependencies on the boundary conditions.
- Output with a frequency in the order of hours instead of days, would help to interpret local flow patterns. Increased understanding of the flow will help to gain more detailed knowledge on flushing of sheltered areas.
- An elaborate set of simulations with a downscaled global climate model could provide valuable information on what to expect of the future wind climate. Subsequently more profound climate scenarios can be generated, which provide more realistic future impact assessments.
- The impact of desalination capacity increase and climate change are most interesting on a more local scale. Therefore refinement in sheltered areas would be a logical next step in understanding the impact on vulnerable coastal areas.

8.2 Recommendations for policy makers

- The local extreme salinity increases modelled in Kuwait Bay, the Gulf of Salwah and along the western UAE coast, provides a reason for municipalities or desalination plant operators to investigate possibilities of strategic locations for future construction of desalination plants.
- Locally a lot of valuable hydrodynamic data is gathered in the Arabian Gulf. The availability of this data is limited to private users. The academic community at first, but thereby also local stakeholders, would benefit from increased cooperation and data sharing. Among other parameters, the diffusivity and viscosity coefficients could be further calibrated. Calibration and more extensive validation of flow and salinity in the model would increase the value of the model simulations.
- Numerical and field experiments on the ecological response on salinity increase would provide valuable knowledge, with which more effective guidelines and norms can be set for future desalination plants.

References

Al-Asadi, S.A.R. (2017). The future of fresh water in Shatt Al-Arab river (southern Iraq). Journal of Geography and Geology 9 (2), 24-38 http://dx.doi.org/10.1016/j.marpolbul.2015.11.033

Al Sarmi, S., & Washington, R. (2011). Recent observed climate change over the Arabian Peninsula, 116 (December 2010), 1–15. https://doi.org/10.1029/2010JD015459

Al Senafi, F., & Anis, A. (2015). Shamals and climate variability in the Northern Arabian/Persian Gulf from 1973 to 2012. International Journal of Climatology, 35(15), 4509–4528. Doi: 10.1002.4302

Alosairi, Y., & Pokavanich, T. (2017). Seasonal circulation assessments of the Northern Arabian/Persian Gulf. Marine Pollution Bulletin, 116(1–2), 270–290. https://doi.org/10.1016/j.marpolbul.2016.12.065

Altayaran, A. M., & Madany, I. M. (1992). Impact of a desalination plant on the physical and chemical properties of seawater, Bahrain. Water Research, 26(4), 435–441. https://doi.org/10.1016/0043-1354(92)90043-4

Bleck, R. (1998). Ocean modelling in isopycnic coordinates. Ocean Modelling and Parametrization, 423–424.

Bleck, R. (2002). An oceanic general circulation model framed in hybrid isopycnic-Cartesian coordinates. Ocean Modelling, 37, 55–88.

Brewer, P., & Dryssen, D. (1985). Chemical Oceanography of the Persian Gulf. Progress in Oceanography, 14, 41-55.

Buchanan, J.R., Krupp, F.,Burt, J.A., Feary, D.A., Ralph, G.M. & Carpenter, K.E. (2016). Living on the edge: Vulnerability of coral-dependent fishes in the Gulf. Marine pollution bulletin 105, 480-488. http://dx.doi.org/10.1016/j.marpolbul.2015.11.033

Carrere, L., Lyard, F., Cancet, M. & Guillot, A. (2015). FES 2014, a new tidal model on the global ocean with enhanced accuracy in shallow seas and in the Arctic region. Journal of Geophysical research 17.

Chartrand, K., Durako, M. & Blum, J. (2009). Effect of hyposalinity on the photophysiology of *Siderastrea radians*. Marine Biology 156, 1691–1702. doi:10.1007/s00227-009-1204-3

Chao, S., Kao, T., & Al-Hajri, A. (1992). A numerical investigation of circulation in the Arabian Gulf. Journal of Geophysics, 97(11), 219-236.

Coles, S. (2003). Coral species diversity and environmental factors in the Arabian Gulf and the Gulf of Oman. Atoll Research Bulletin (507), 1-19.

Dawoud, M. A., & Al Mulla, M. M. (2012). Environmental Impacts of Seawater Desalination: Arabian Gulf Case Study. International Journal of Environment and Sustainability, 1(3), 22–37. https://doi.org/10.24102/ijes.v1i3.96

Dee, D., and Coauthors, 2011: The ERA-Interim reanalysis: Configuration and performance of the data assimilation system. Quarterly Journal Royal Meteorological Society, 137, 553–597.

Deltares. (2018). Delft3D-FLOW User Manual. version 3.15. Delft, the Netherlands: Deltares.

Edson, J. P., Wainer, I., & Ferrero, B. (2015). Regional Ocean Modeling: A Numerical Study of the Impact of Climate Change on the Arabian Gulf. University of Sao Paolo Sao Paolo.

Edson, J., Wainer, I., & Ferrero, B. (2016). Socioeconomic System: Desalinated Water Supply: Full Technical Report. AGEDI, Abu Dhabi, United Arabian Emirates.

Eichelberger, S & Mccaa, J. & Nijssen, B. & Wood, A. (2008). Climate change effects on wind speed. NA Wind Power. 7. 68-72.

Elhakeem, A., & Elshorbagy, W. (2015a). Hydrodynamic evaluation of long term impacts of climate change and coastal effluents in the Arabian Gulf. Marine Pollution Bulletin, 101(2), 667–685. https://doi.org/10.1016/j.marpolbul.2015.10.032

Elhakeem, A., Elshorbagy, W., & Bleninger, T. (2015b). Long-term hydrodynamic modeling of the Arabian Gulf. Marine Pollution Bulletin, 94(1–2), 19–36. Doi:10.1016.2015.03.020

Elhakeem, A., Elshorbagy, W., & Al-Naser, H. D. (2015c). Downscaling Global Circulation Model Projections of Climate Change for the United Arab Emirates. Journal for Water Resource Planning and Management, Volume 141, Issue 9.

Erftemeijer, P.L.A. & Shuail, D.A. (2012). Seagrass habitats in the Arabian Gulf: Distribution, tolerance thresholds and threats. Journal of Aquatic ecosystem health and management 15(1), 73-83.

Hashim, A., & Hajjaj, M. (2005). Impact of desalination plants fluid effluents on the integrity of seawater, with the Arabian Gulf in perspective. Desalination, 182, 373–393. Doi: 10.1016.2005.04.020

Hunter, J. (1982). The physical oceanography of the Arabian Gulf: a review and theoretical interpretation of previous measurements. First Gulf Conference on Environment and Pollution. Kuwait: First Gulf Conference on Environment and Pollution.

Hunter, J. (1983). Aspects of the dynamics of the residual circulation of the Arabian Gulf (1st ed.). New York, London: Plenum Press.

IPCC. (2014). Climate Change 2014: Impacts, Adaptation, Vulnerability and Sectoral Impacts. Contribution of Working Group II to the Fifth Assessment Report of the Intergovernmental Panel on Climate Change. (C. W. Team, R. K. Pachauri, & L. A. Meyer, Eds.). Geneva, Switzerland: IPCC.

John, V. C., Coles, S. L., & Abozed, A. I. (1990). Seasonal cycles of temperature , salinity and water masses of the western Arabian Gulf. Oceanologica Acta, 13(3), 273–282.

Johns, W. E., Yao, F., Olson, D. B., Josey, S. A., Grist, J. P., & Smeed, D. A. (2003). Observations of seasonal exchange through the Straits of Hormuz and the inferred heat and freshwater budgets of the Persian Gulf. Journal of Geophysical Research, 108(C12), 3391. Doi: 10.1029/2003JC001881.

Lardner, R. W., & Das, S. K. (1991). On the computation of flows driven by density gradient: Residual currents in the Arabian Gulf. Applied Mathematical Modelling, 15(6), 282–294. Doi: 10.1016/0307-904X(91)90043-O

Loutatidou, S., Mavukkandy, M. O., Chakraborty, S., & Arafat, H. A. (2017). Desalination sustainability: a technical, socioeconomic, and environmental approach. In Desalination Sustainability (pp. 1–30). Elsevier Inc. https://doi.org/10.1016/B978-0-12-809791-5.00001-8

Mansour, S., Arafat, H. A., & Hasan, S. W. (2017). Desalination sustainability: a technical, socioeconomic, and environmental approach. In Desalination Sustainability (pp. 207–236). Elsevier Inc. https://doi.org/10.1016/B978-0-12-809791-5.00005-5

Marshall, J., Jones, H., Karsten, R., & Wardle, R. (2002). Can Eddies Set Ocean Stratification?, Journal of physical oceanography 32, 26–38.

Martyr-koller, R. C., Kernkamp, H. W. J., Dam, A. Van, & Wegen, M. Van Der. (2017). Estuarine , Coastal and Shelf Science Application of an unstructured 3D finite volume numerical model to flows and salinity dynamics in the San Francisco Bay-Delta. Estuarine, Coastal and Shelf Science, 192, 86–107. https://doi.org/10.1016/j.ecss.2017.04.024

Mazzoni, A., Heggy, E. & Scabbia, G. (2018). Forecasting water budget deficits and groundwater depletion in the main fossil aquifer systems in North Africa and the Arabian Peninsula. Journal of Global Environmental Change 53, 157-173. https://doi.org/10.1016/j.gloenvcha.2018.09.009

Peng, Z., & Bradon, J. (2016). 3-D Comprehensive Hydrodynamic Modelling in the Arabian Gulf. Journal of Coastal Research, 75(sp1), 547–551. https://doi.org/10.2112/SI75-110.1

Pokavanich, T., Alosairi, Y., Morelissen, R., Verbruggen, R., Al- Rifaie, K., Altaf, T., & Al-said, T. (2015). Three-Dimensional Arabian Gulf Hydro-Environmental Modelling Using Delft3d. the Hague, the Netherlands: Proceedings Of The 36th IAHR World Congress.

Pous, S. P. (2012). A Process Study of the Tidal Circulation in the Persian Gulf. Open Journal of Marine Science, 02(04), 131–140. https://doi.org/10.4236/ojms.2012.24016

Pous, S. P., Carton, X., & Lazure, P. (2015). A model of the general circulation in the Persian Gulf and in the Strait of Hormuz: Intraseasonal to interannual variability. Journal of Continental Shelf Research 94, 55- 70. http://dx.doi.org/10.1016/j.csr.2014.12.008

Rao, P. G., Al-Sulaiti, M., & Al-Mulla, A. H. (2001). Winter shamals in Qatar, Arabian Gulf. Weather, 56(12), 444–451. https://doi.org/10.1002/j.1477-8696.2001.tb06528.x

Rao, P. G., Hatwar, H. R., Al-Sulaiti, M. H., & Al-Mulla, Avia, A. H. (2003). Summer shamals over the Arabian Gulf. Weather, 58(12), 471–478. https://doi.org/10.1002/wea.6080581206

Reynolds, M. R. (1993). Physical oceanography of the Gulf, Strait of Hormuz, and the Gulf of Oman-Results from the Mt Mitchell expedition. Marine Pollution Bulletin, 27(C), 35–59. https://doi.org/10.1016/0025-326X(93)90007-7

Roberts, D. A., Johnston, E. L., & Knott, N. A. (2010). Impacts of desalination plant discharges on the marine environment: A critical review of published studies. Water Research, 44(18), 5117–5128. https://doi.org/10.1016/j.watres.2010.04.036

Service, R. F. (2006). Desalination Freshens Up. Science, 313, 1088–1090. Doi: 10.1126.313.5790.1088

Sheppard C. & co-authors (2010). The Gulf: A young sea in decline. Marine pollution bulletin 60, 13-38. doi:10.1016/j.marpolbul.2009.10.017

Swift, S. A., & Bower, A. S. (2003). Formation and circulation of dense water in the Persian/Arabian Gulf. Journal of Geophysical Research, 108(C1), 3004. https://doi.org/10.1029/2002JC001360

Talley, L., Pickard, G., Emery, W., & Swift, J. (2011). Descriptive Physical Oceanography (6th ed.). Amsterdam, the Netherlands: Elsevier.

Tan, W.Y. (1992). Shallow Water Hydrodynamics: Mathematical Theory and Numerical solution for a Two-dimensional system of Shallow Water Equations. (Cunli, Y. & Xinhua, T., Ed.) (1st ed., pp. 21) Amsterdam, Elsevier science publishers.

Fernández-Torquemada, Y., Sánchez-Lizaso, J.L., González-Correa, J.M., 2005. Preliminary results of the monitoring of the brine discharge produced by the SWRO desalination plant of Alicante (SE Spain). Desalination 182 (1–3), 395–402.

Odhiambo, G.O. (2016). Water scarcity in the Arabian Peninsula and socio-economic implications. Journal of applied water science 7: 2479-2492. Berlin. DOI: 10.1007/s13201-016-0440-1

Vaughan, G. O., Al-Monsoori, N., & Burt, J. A. (2018). World Seas: an Environmental Evaluation: Volume II: the Indian ocean to the Pacific. (C. Sheppard, Ed.) (2nd ed., Vol. 5). Cambridge, Massachusetts, USA: Academic Press.

Water UN (2012) Global Annual Assessment of Sanitation and drinking-water (GlAAS) 2012 report: the challenge of extending and sustaining services. UN, New York

World Bank (2005) A Water Sector Assessment Report on the Countries of the Cooperation Council of the Arab States of the Gulf. World Bank Report No. 32539-MNA, Washington, DC

Xue, P., & Eltahir, E. A. B. (2015). Estimation of the heat and water budgets of the Persian (Arabian) gulf using a regional climate model. Journal of Climate, 28 (13), 5041–5062. Doi: 10.1175/JCLI-D-14-00189.1

Yao, F., & Johns, W. E. (2010). A HYCOM modeling study of the Persian Gulf: 1. Model configurations and surface circulation. Journal of Geophysical Research: Oceans, 115(11). Doi: 10.1029.005781

Zhao, J., Temimi, M., & Ghedira, H. (2017). Remotely sensed sea surface salinity in the hyper-saline Arabian Gulf: Application to landsat 8 OLI data. Estuarine, Coastal and Shelf Science, 187, 168–177. https://doi.org/10.1016/j.ecss.2017.01.008

Appendices

Appendix 1: Overview of alternative model forcing

Table 8: Overview of alternative model forcing, with every cell representing a run of alternative conditions. With all other forcings similar to the reference case.

Mild 2050: Air+ocean temp. +1.5 °c desalination cap. x2	**Extreme 2050:** Air+ocean temp +3°c desalination cap. x4	**Mild 2080:** Air+ocean temp. +1.5°c desalination cap. x5	**Extreme 2080:** Air+ocean temp. +4.5°c desalination cap. x10
Air temp.+1.5°c	**Air temp.+3°c**	**Air temp.+4.5°c**	
Ocean temp. +1.5°c	**Ocean temp. +3°c**	**Ocean temp. +4.5°c**	
Air+ocean temp +1.5°c	**Air+ocean temp. +3°**	**Air+ocean temp. +4.5°c**	
Desalination cap. X0	**Desalination cap. X2**	**Desalination cap. X5**	**Desalination cap. X10**
Uniform wind field	**Wind direction +20°**	**Wind direction -20°**	
Wind velocity +50%	**Wind velocity -50%**		
River discharge x0	**River discharge x2**		

Appendix 2: Development of Gulf wide bottom and surface salinity

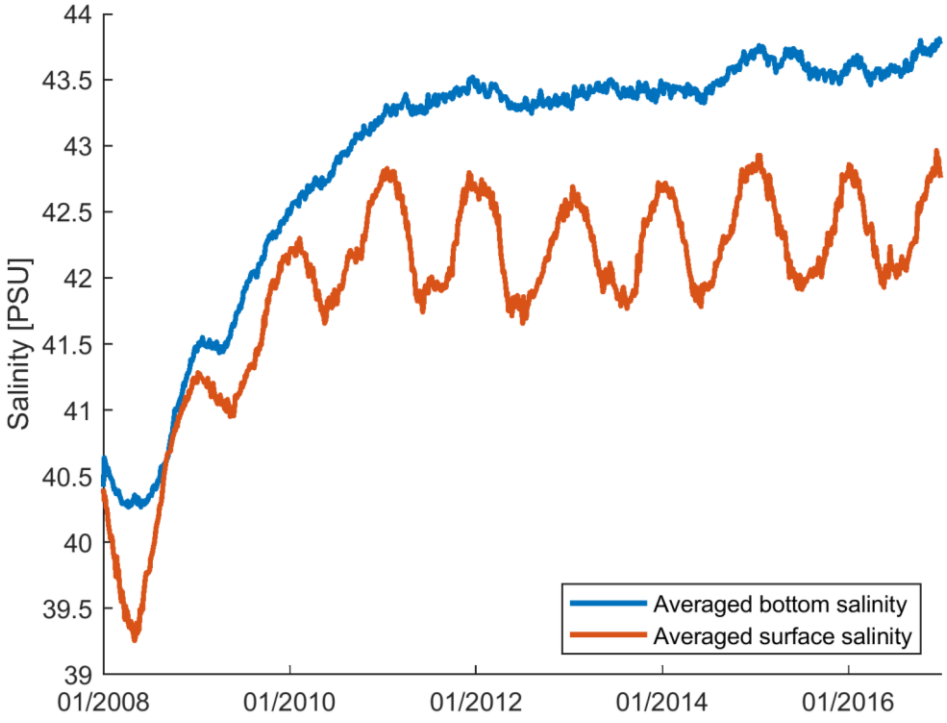

Figure 31: Long term salinity development of Gulf averaged bottom salinity (blue line) and surface salinity (orange line).

Appendix 3: IPCC projections

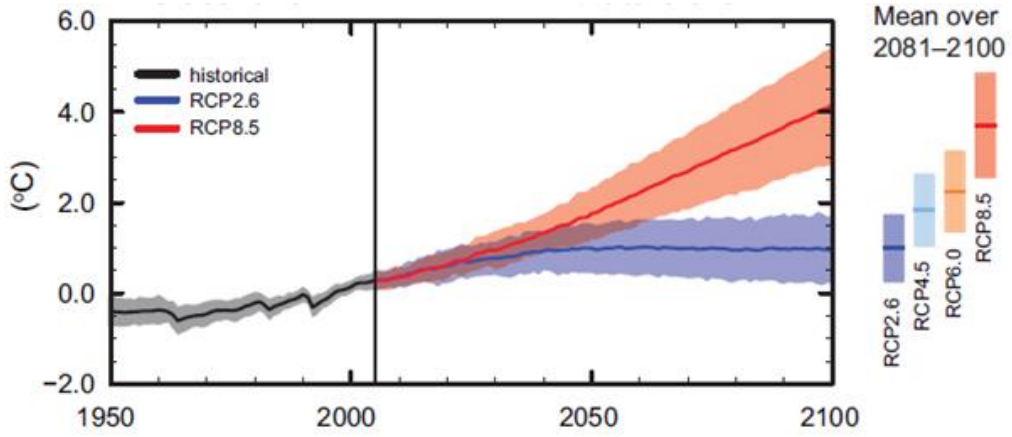

Figure 32: Global mean air temperature predictions normalized to 2005 (IPCC, 2014)

Appendix 4: Model set up

Table 9: Overview of physical and numerical parameters as set in the Delft3D FMl simulations.

Physical parameters		**Numerical parameters**	
Uniform friction coefficient (-)	0.02	Maximum computational time step (s)	120
Uniform horizontal eddy viscosity (m^2/s)	0.5	Courant number limiter (-)	0.9
Uniform horizontal eddy diffusivity (m^2/s)	0.5		
Uniform vertical eddy viscosity (m^2/s)	0		
Uniform vertical eddy diffusivity (m^2/s)	0		
Smagorinsky factor (-)	0.15		
Secchi depth (m)	3		
Air density (kg/m^3)	1.25		

Appendix 5: Wind climate in the Arabian Gulf

Figure 33: Map of the Arabian Gulf, with wind roses showing the annual distribution of wind directions. based on ERA-interim data Dee et al., 2011).

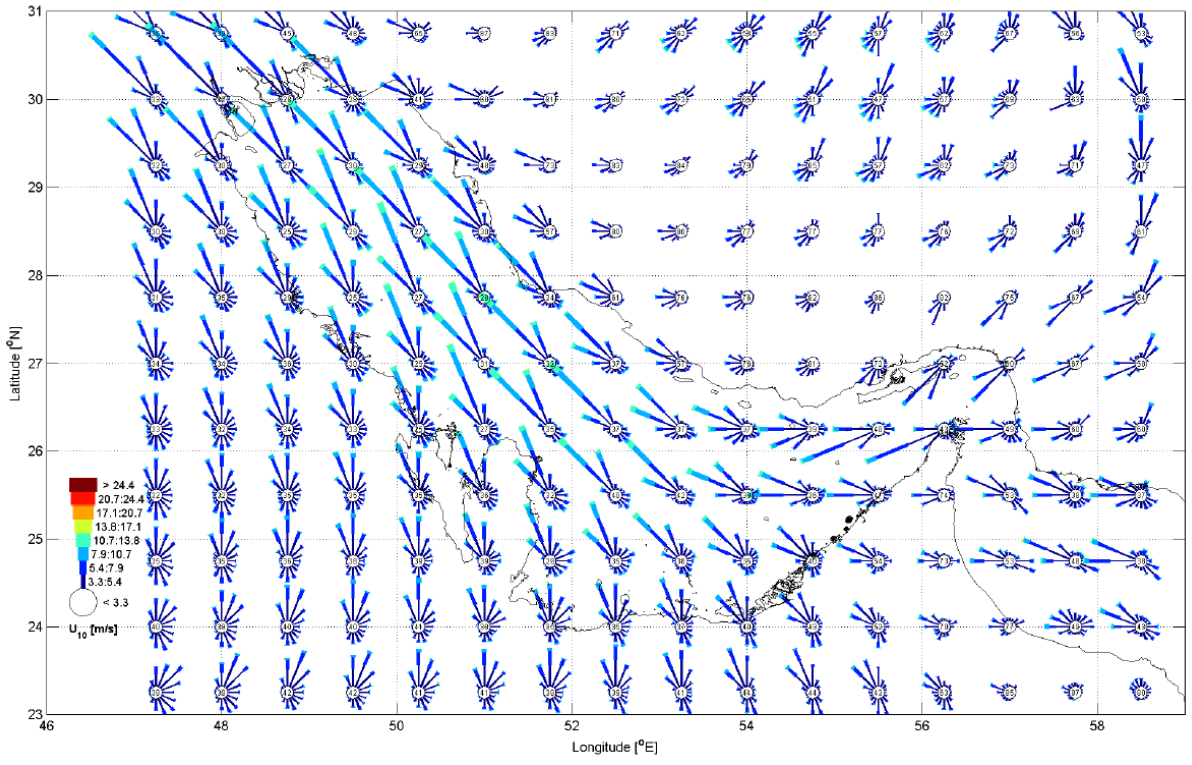

Appendix 6: Locations of modelled rivers in the Arabian Gulf

River	Q [M³/s]
Shatt al Arab	70-250
Karun	20
Hendijan	30-100
Hilleh	50-80
Mand	50-200
Mehrun	50-80
Shur	50-80
Minab	50-80

Figure 34: River locations and discharges around the northern and eastern Arabian Gulf coasts.

Appendix 7: Location of desalination plants in the Arabian Gulf

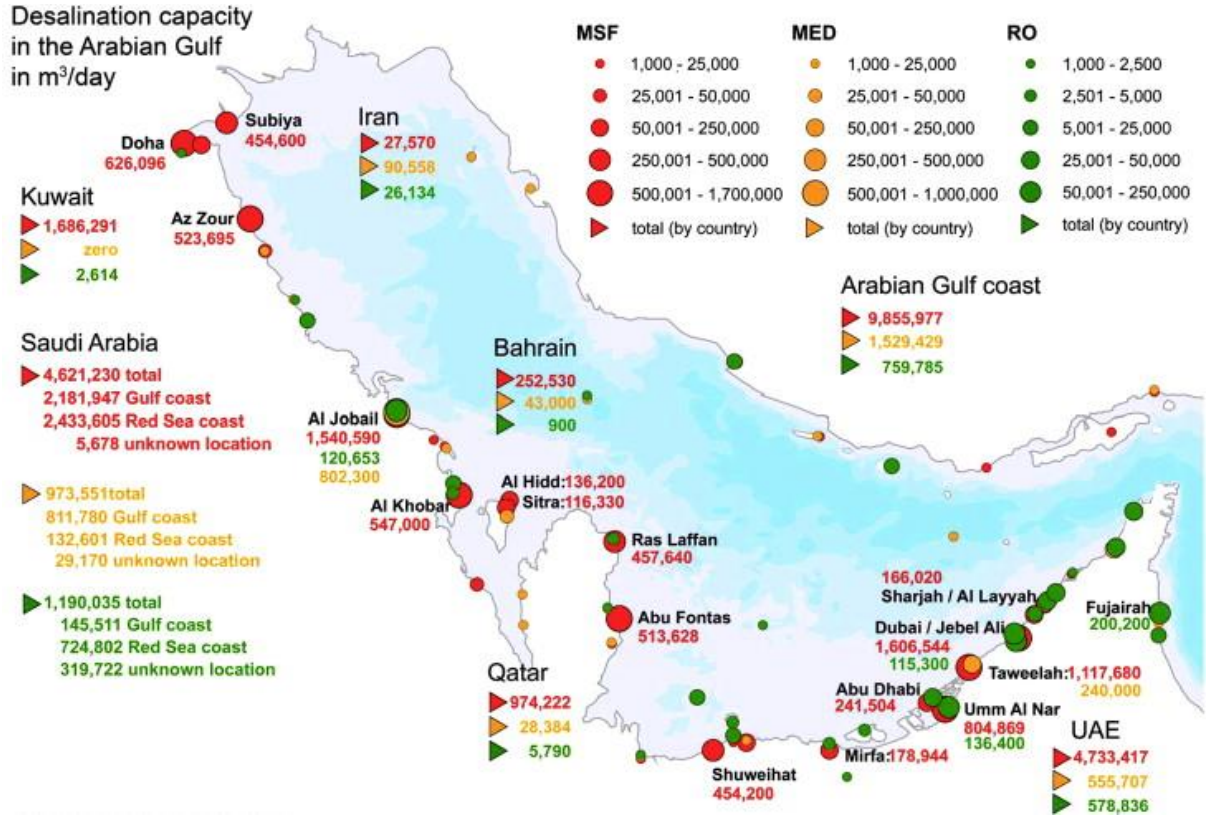

Figure 35: Desalination plant locations and capacities around the Arabian Gulf (Latteman & Höpner, 2010).

Appendix 8: Heat exchange model

Solar radiation

The sun emits thermal energy through short-wave radiation. The incoming energy flux (Q_s) at the earth's surface level depends on the atmospheric absorption and the angle of inclination between the incoming radiation and the water surface. The angle inclination at a certain position is obviously dependent on the location and rotation of the earth relative to the sun and varies over time with dominating annual and diurnal variations. Before reaching the earth's surface, the solar radiation is partly absorbed in the atmosphere. Solar radiative energy at the earth's surface is distinguished into two wavelength classifications:

1. Longwave radiation: radiative energy that has been absorbed by water vapour and carbon dioxide in the atmosphere,
2. Shortwave radiation: direct solar radiation.

The solar radiation absorption model by Gill (1982) describes that under clear sky conditions approximately 76% of the shortwave radiation reaches the earth's atmosphere. The incoming solar radiation at the earth's surface at clear sky conditions is calculated by equation VIII:

$$Q_{sc} = 0.76 * S * \sin(\gamma) \qquad \text{(VIII)}$$

With:

S Solar constant, or average heat flux at the mean radius of the Earth 1368 J/(m^2 s)

γ Solar elevation angle, depending on time and latitude

The cloud cover F_c reduces the magnitude of radiation flux that reaches the earth's surface. Solar radiation that reaches the surface Q_s is calculated by the empirical equation IX.

$$Q_s = Q_{sc} * (1 - 0.4F_c - 0.38{F_c}^2) \qquad \text{(IX)}$$

The albedo reflection coefficient α (=0.06) represents the portion of shortwave radiation energy that is not absorbed by the water. The net radiation heat flux through the surface of the water body is calculated by equation X.

$$Q_{sn} = (1 - \alpha) * Q_s \qquad \text{(X)}$$

Of the sun's radiative energy that reaches the sea surface a part $(1 - \beta)$ is short wave solar energy, while another part (β) has been transformed into longwave radiation by atmospheric absorption. The longwave solar radiation is absorbed in the water's surface layer (~cm's). Short wave solar radiation reaches till depths of up to 30 meter into the water column, depending on the clarity of water. The absorption of short wave solar radiative energy in the water column (Q_{sn}) is calculated by equation XI:

$$Q_{sn}(h) = \frac{\gamma e^{-\gamma h}}{1 - e^{-\gamma H}}(1 - \beta)Q_{sn} \qquad \text{(XI)}$$

With:

β The portion of solar radiative energy that is absorbed into the atmosphere, default value: *0.06*

γ The extinction coefficient, related to the Secchi depth: $1.7 / H_{Secchi}$ [m^{-1}]

h Distance to water surface [m]

H Total water depth.

From which can be derived that short wave solar radiation that penetrates the water surface is absorbed over the water column, exponentially decreasing with increasing water depth until the Secchi depth, describing water clarity.

Evaporation

Solar radiative energy that is absorbed over the Secchi depth in the top of the water column is partly transformed into thermal energy and partly forces evaporation. The endothermic process called evaporation changes the state of water molecules at the surface from liquid into vapour. Vaporised water molecules 'escape' from the water surface into the atmosphere, which is analogue to both a mass flux and a heat flux from water to atmosphere. This particular process is called 'forced' evaporation. Forced evaporative mass flux is calculated with equation XII:

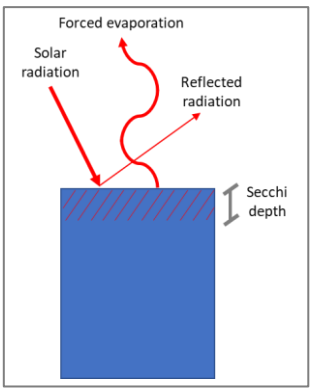

Figure 36:Schematization of forced evaporation.

$$M_{ev,forced} = \rho_a * c_e * U_{10} * (q_s - q_a) \qquad \text{(XII)}$$

With:

ρ_a	Air density:	$\rho_a = 1.25\ kg/m^3$
c_e	Dalton number, calibrated to the North Sea:	$c_e = 0.0015$
U_{10}	Wind speed, 10 meters above water level:	meteorological input
q_s	Specific humidity of sutured air:	function of T_s and P_{atm}
q_a	Specific humidity of air at 10 m above water level:	function of T_a and r_{hum}
T_s	Water surface temperature:	model output
T_a	Air temperature:	meteorological input
P_{atm}	Atmospheric pressure:	meteorological input
r_{hum}	Relative humidity:	meteorological input

Evaporation of water molecules can also be driven by buoyant forces, leading to 'free' convection of water molecules into the air, which is called free evaporation. Buoyant forces are a result of instabilities in the atmosphere layer from 0 to 10 meter above the water surface, these instabilities are caused by inverse density gradients due to relatively high vapour content high in the atmosphere layer or high temperatures low in the atmosphere layer.

Neglecting free convection causes underestimating the heat flux from the water column into the atmosphere (Ryan et al., 1974), especially in conditions with low wind speed and high surface water temperature. The free evaporative heat flux is calculated with equation XIII:

$$M_{ev,free} = k_s * \overline{\rho_a} * (q_s - q_a) \qquad \text{(XIII)}$$

With heat transfer coefficient:

$$k_s = c_{fr.conv.} \left\{ \frac{g(0.7 * \nu_{air})^2}{\overline{\rho_a} * \nu_{air}} (\rho_{a10} - \rho_{a0}) \right\}^{1/3} \qquad \text{if } (\rho_{a10} - \rho_{a0}) > 0 \text{ , otherwise } k_s = 0$$

$c_{fr.conv.}$	Coefficient of free convection, calibrated:	0.14
ν_{air}	Diffusivity of air, calibrated:	$16*10^6$ m^2/s

$\overline{\rho_a}$ Average air density over atmospheric layer: $(\rho_{a10} + \rho_{a0})/2$

ρ_{a10} Air density at 10 meters above water level, while ρ_{a0} is air density at water level.

The total evaporative mass flux is the summation of free and forced evaporation:

$$M_{ev} = M_{ev,free} + M_{ev,forced} \quad \text{(XIV)}$$

To vaporize air energy was required, which is analogue to heat loss at the water surface. The thermal energy flux by evaporation is calculated with equation XV:

$$Q_{ev} = L_v * M_{ev} \quad \text{(XV)}$$

With L_v the latent heat required for vaporization of water:

$$L_v = 2.5 * 10^6 - 2.3 * 10^3 T_s \quad \text{(XVI)}$$

The higher the temperature of the surface water the smaller the amount of energy needed for evaporation, though an increase of 10 ^{O}C only leads to a reduction in energy needed of 1%.

Appendix 9: Water clarity

Short wave solar radiation is absorbed in the water column. The depth until which the solar energy waves reach is analogue to the clarity of the water and described by the depth until which people can distinct black from white. This depth is called the Secchi disk depth. Water clarity dependents on the degree of presence of vegetation, sediment suspension, algae bloom, dissolved organic matters and phytoplankton. Kaabi, Zhao & Ghedira (2017) based maps of seasonal average Secchi depths on satellite data, that indicate clear seasonal and spatial patterns. For the offshore, deeper regions in the Arabian Gulf the Secchi disk depth is typically in the order of 7 to 20 meter, depending on the season. For coastal regions the Secchi disk depth is much smaller, typically in the order of 3 to 4 meter. In Delft3D FM the assigned Secchi depth is spatially uniform. As the focus lies on the coastal regions, the Secchi depth in the model is decided to be 3 meter.

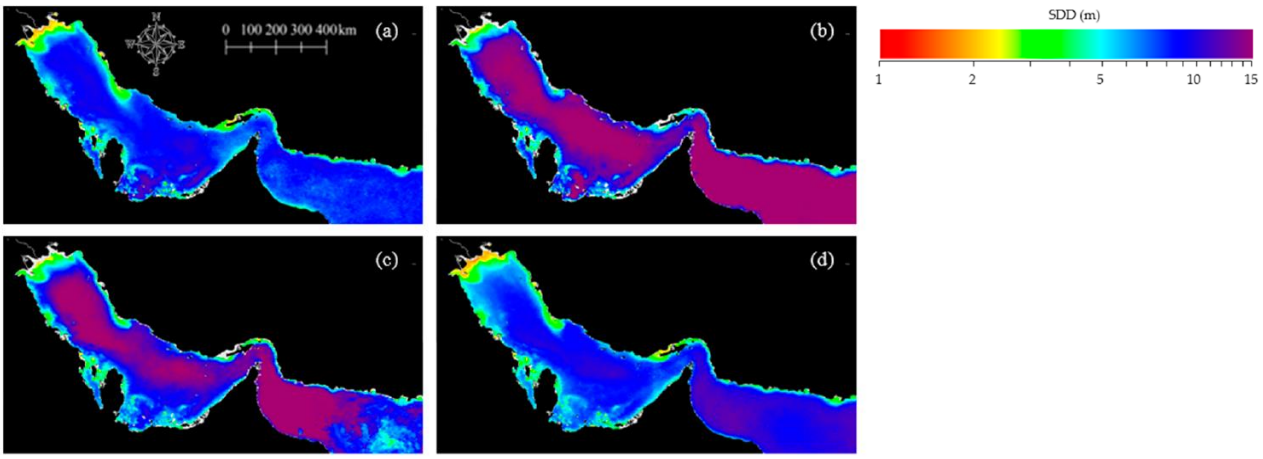

Figure 37: Seasonal Secchi Disk Depth maps based on NASA's aqua satellite data, averaged over the period of 2002-2015 for (a) spring, (b) summer, (c) fall and (d) winter (Kaabi, Zhao and Ghedira 2017).

Appendix 10: Geostrophic flow

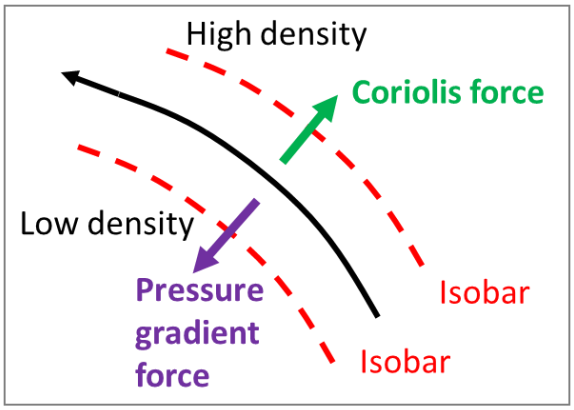

Figure 38: Schematic depiction of geostrophic flow.

Appendix 11: Ekman transport

Winds that blow over a water surface, induce sheared flows and waves, that generate turbulence. The turbulence increase the amount of momentum transfer from the atmosphere to sub-surface layers in the water body, causing both vertical mixing and propagation in sub-surface layers. The Ekman principle is schematised as follows with the Ekman transport in vector notation:

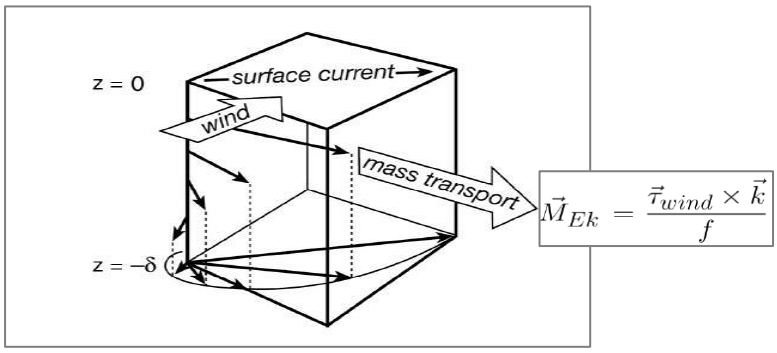

Figure 39: schematization of Ekman transport with the direction of wind; surface current and sub-surface currents until the depth equals $-\delta$.

Appendix 12: Monthly hydrological values

Table 10: Monthly water fluxes for the Gulf, averaged over 1981 to 1990 (Xue & Eltahir, 2015). The unit is in in m/month and is a practical unit for volume flux per month [m3/month], divided over the assumed constant surface area.

Month	Evaporation	Precipitation	River	Lateral (in)	Lateral (out)	Net
January	−0.1325	0.0083	0.0167	3.3833	−3.2892	−0.0133
February	−0.1308	0.0175	0.0217	3.4708	−3.3925	−0.0133
March	−0.1108	0.01	0.03	3.555	−3.5317	−0.0475
April	−0.1125	0.0025	0.0358	3.5575	−3.4425	0.0408
May	−0.1375	0.0008	0.0308	3.4233	−3.3275	−0.01
June	−0.1375	0	0.0183	3.3167	−3.115	0.0833
July	−0.1458	0	0.0108	2.8283	−2.675	0.0192
August	−0.17	0	0.0083	2.31	−2.1283	0.0217
September	−0.175	0	0.0075	1.8558	−1.7167	−0.0275
October	−0.19	0.0075	0.0083	1.6158	−1.4175	0.0242
November	−0.2017	0.0208	0.01	1.835	−1.7375	−0.0733
December	−0.1992	0.015	0.0133	2.5033	−2.3383	−0.0067
Average	−0.1533	0.0067	0.0175	2.805	−2.6758	0

Appendix 13: Model validity

Data from *Conductivity-Temperature-Density* devices (CTD's) has been essential for the research on pressure driven flow in the Arabian Gulf. CTD's measure electrical conductivity, water temperature and pressure. Salinity values can be extracted by measuring electrical conductivity (Talley, Pickard, Emery, & Swift, 2011). The first large scale field survey, using 273 CTD casts, was in July and August 1968. The best documented survey is the R.V. Atlantis II survey in February of 1977 (Brewer & Dryssen, 1985). The geographically most inclusive data set was gathered during the Mt Mitchell surveys in winter and spring 1992, CTD samples were gained for the Strait of Hormuz and the shallow southern banks for the first time (Reynolds, 1993). Follow-up CTD surveys were done in April of 1994 and March/April of 1996, but the area investigated by these cruises is not as wide as that covered by the Mt Mitchell *(Swift & Bower, 2003)*. Researchers that were interested in wind driven surface flows in the late 20th century *e.g. Hunter, 1983, Chao et al., 1992)* used historical ship drift data to calibrate, but this was rather inaccurate. The U.S. Naval Oceanographic Office maintains a database called the *Master Oceanographic Observations Data Set* (MOODS), containing most of the known CTD samples from field surveys. The data set shows wide gaps in space and time, which causes the set to be both spatially and temporally biased *(Swift & Bower, 2003)*. Figure 40 shows the non-uniform spatial and temporal distribution of CTD casts. Table 11 gives an overview of the gathered casts during the 20th century, included in the MOODS database. This spatial and temporal bias of the data has limited the statistical certainty and ability to calibrate imperfect models.

Table 11: Number of CTD casts gathered per decade and per month in the Arabian Gulf (Swift & Bower, 2003).

decade	40's	50's	60's	70's	80's	90's						
casts	16	96	644	61	0	941						
	Jan	Feb	Mar	Apr	May	Jun	Jul	Aug	Sep	Oct	Nov	Dec
cast	148	223	287	542	114	64	160	161	26	0	27	0

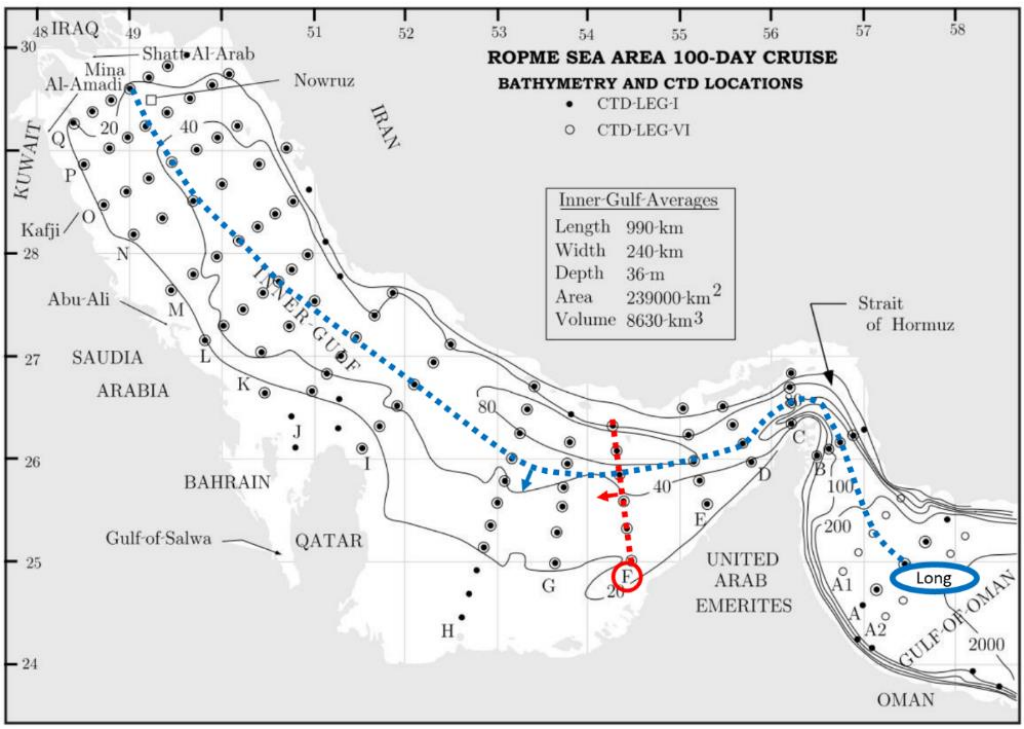

Figure 40: Map of the Arabian Gulf with CTD casts from the winter survey (black dots); casts from the early summer survey (black circles). The red dotted line indicates the location of the vertical slice through the southern Gulf and the blue dotted slice indicates the slice along the longitudinal axis. The arrows represent the direction at which one looks when looking in the vertical sections (Figure 18, Figure 41, Figure 42, Figure 43 and Figure 44).

Comparison to mt. Mitchell survey data

Temperature, velocity and density data was gathered by the mt. Mitchell surveys in winter (late February) and early summer (late May) 1992. The results were presented by *Reynolds* (1993). Cross section F (red in Figure 40) and the longitudinal section (blue in Figure 40) are used for validation of the spatial output of the numerical model. Plots of cross sections containing temperature, salinity and density data of model results (2016) and the mt. Mitchel survey (1992).

Winter

The vertical cross section of temperatures, Figure 41a, shows that the Gulf is close to isothermal. Compared the cross section based on the 1992 field measurements by Reynolds, the modelled temperatures at the surface are slightly higher (~1-2^{o}C). The modelled salinity cross section, Figure 41b, shows a similar pattern to the findings by Reynolds, while the salinity in the shallow region, the south-eastern banks is much higher than measured in 1992. The simulated salinity reaches up to 45 PSU, while the maximum measured salinities are 41.5 PSU. The lowest simulated salinity is situated right above the deepest part of the Gulf and represents the jet of inflowing Indian ocean water. The daily variation of salinity is much smaller, as processes of dispersion of salt and adaptation of salinities are much slower than for the convection of temperature.

The longitudinal slices in Figure 42 show a dominant horizontal temperature gradient in de modelled results and a dominant vertical temperature gradient in the measured plot. The salinity plots show the same diagonal pattern of oceanic water from the right upper corner, the surface at the Strait of Hormuz, intruding the Gulf. The salinities are again in a different order as in the modelled longitudinal section the salinities reach up to levels of 44 PSU in the north of the section, while Reynolds measured maximum salinities of 41 PSU.

Summer

The vertical cross-section shows of temperature in Figure 44 shows a stratification pattern, similar to the measured temperature cross-section, with temperatures being ~1-2 ^{o}C higher than measured. The modelled cross-section does not show temperature stratification at the shallow banks, while thermal stratification was measured there in 1992. The disrupted surface salinity pattern in marks the location of the first MSE. The bottom salinity and the salinity in the shallow banks are simulated higher for 2016 than measured in 1992. The disconnection between these two high salt concentrations indicates the longshore salt transport at the shallow southern banks. The decreasing salinity in the measured figure to the top right (north) suggests that the Iranian jet is located north of the trough, but unfortunately no measurements were taken in the northern part of the section. The density plot of the simulation shows that, like the density plot of the measurements the steepest density gradient is situated at a depth of approximately 15-25 meter.

The vertical section longitudinal to the Gulf of measured and modelled temperature show a distinction between the simulated and measured reach of the Iranian jet. The surface temperature in the centre of the Gulf (position -400km) are over 32 ^{o}C, while the measured surface temperature at this location were between 26 and 28 ^{o}C. In general a similar stratification pattern can be observed in both the measured and simulated longitudinal sections, but the simulated section shows disturbances at -200km, -350 km and -525km, where bottom water seems to have been lifted. These locations of intensified vertical mixing are as evident in the salinity and density plots. The cause of the uplift of bottom flow and vertical mixing are the MSE's, see Section 4.1.2. Both bottom and surface of the modelled water column, left of position -200 km are much more saline and dense.

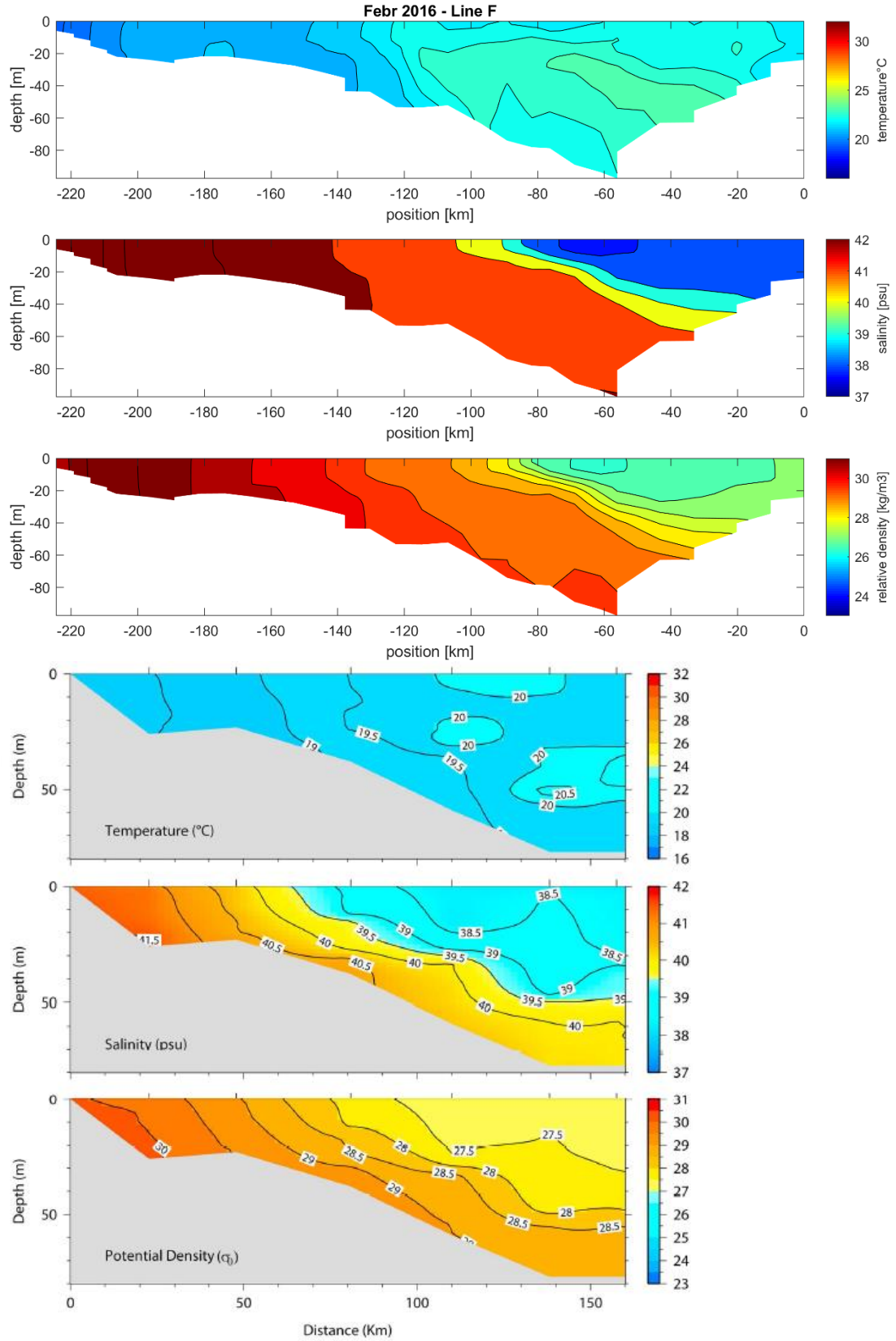

Figure 41: Vertical cross sections along line F of the simulated reference case in the top three panels and of 1992 measuring data in February.

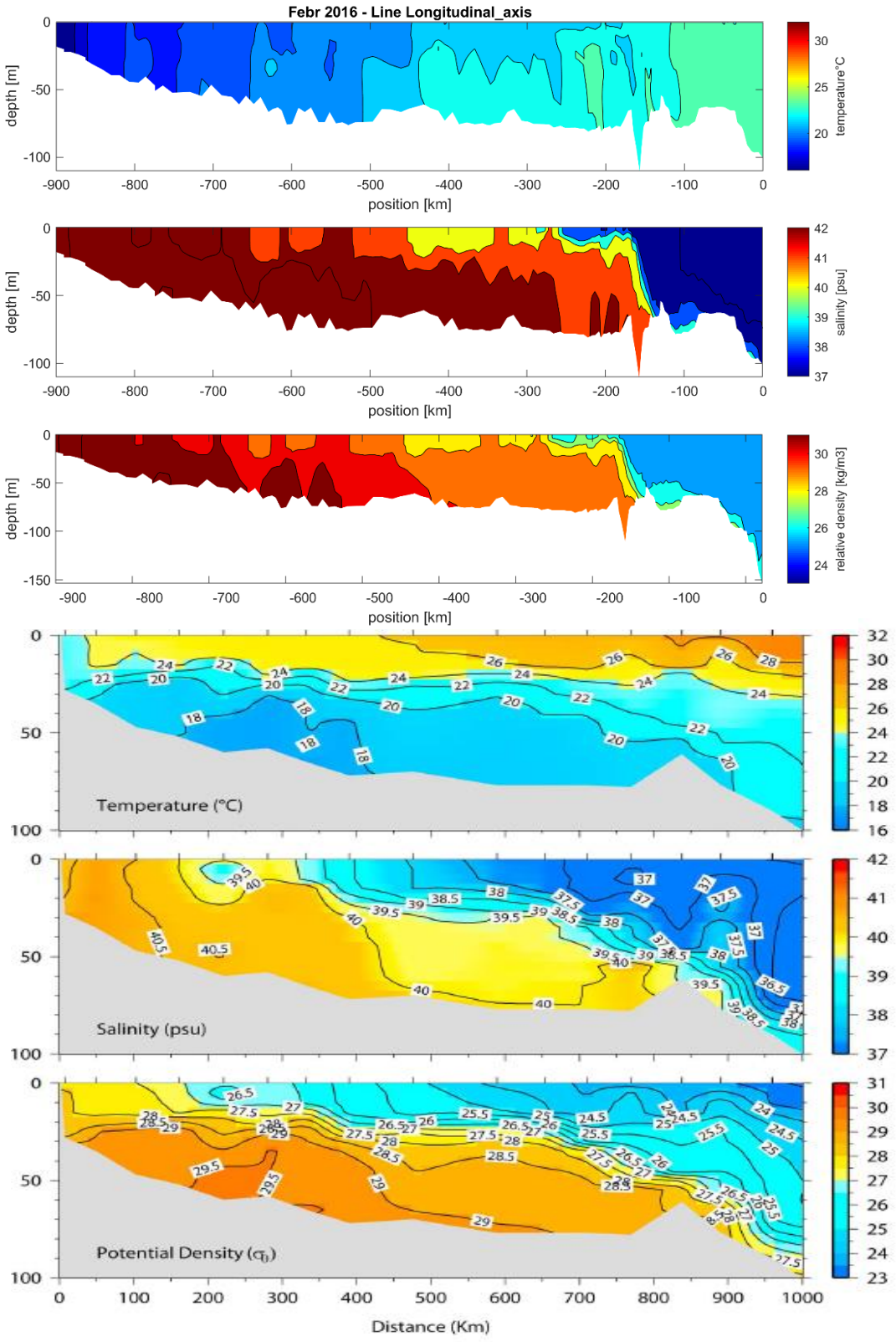

Figure 42: Vertical longitudinal cross section of the simulated reference case in the top three panels and of 1992 measuring data in February.

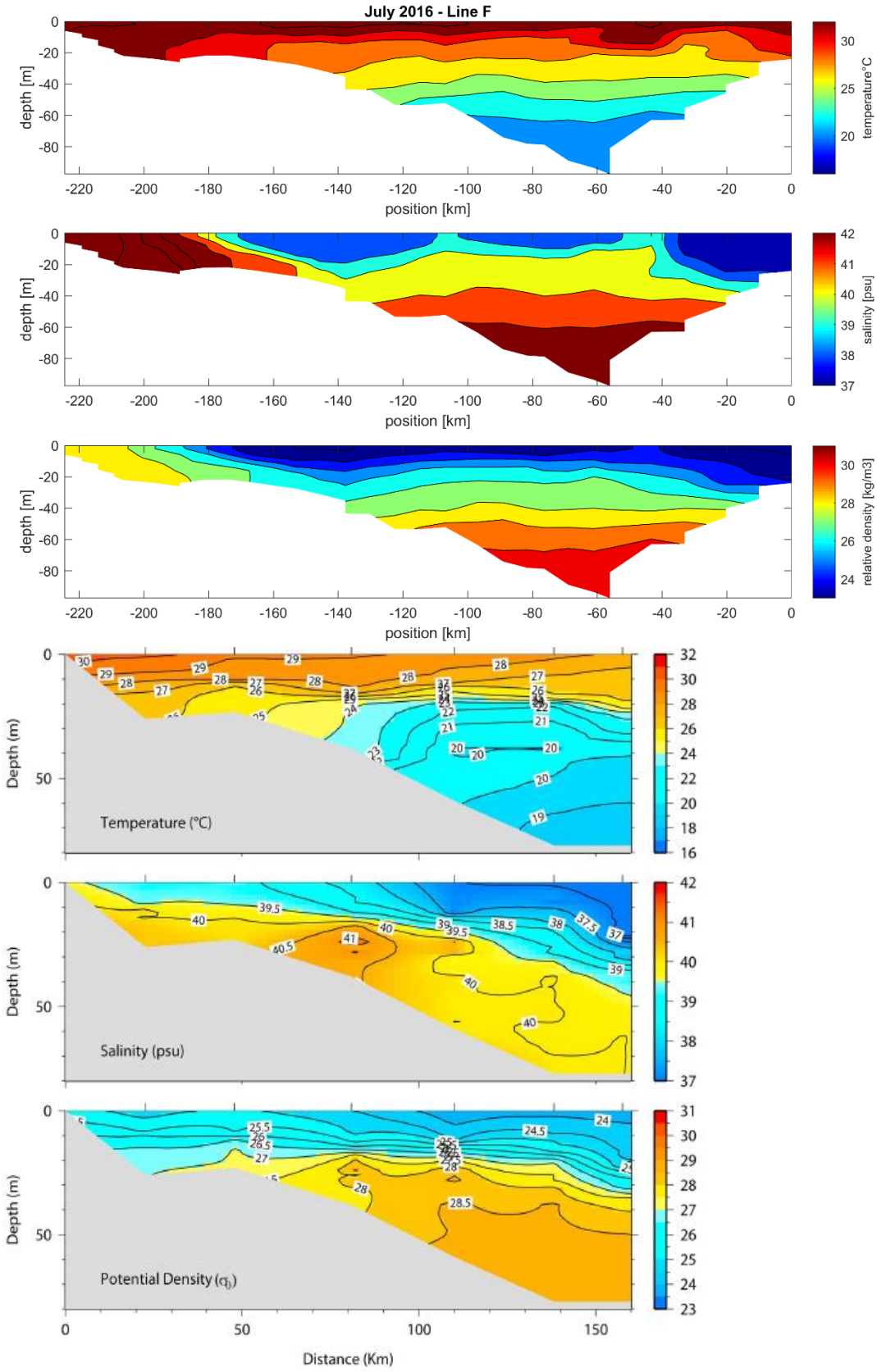

Figure 43: Vertical cross sections along line F of the simulated reference case in the top three panels and of 1992 measuring data in July.

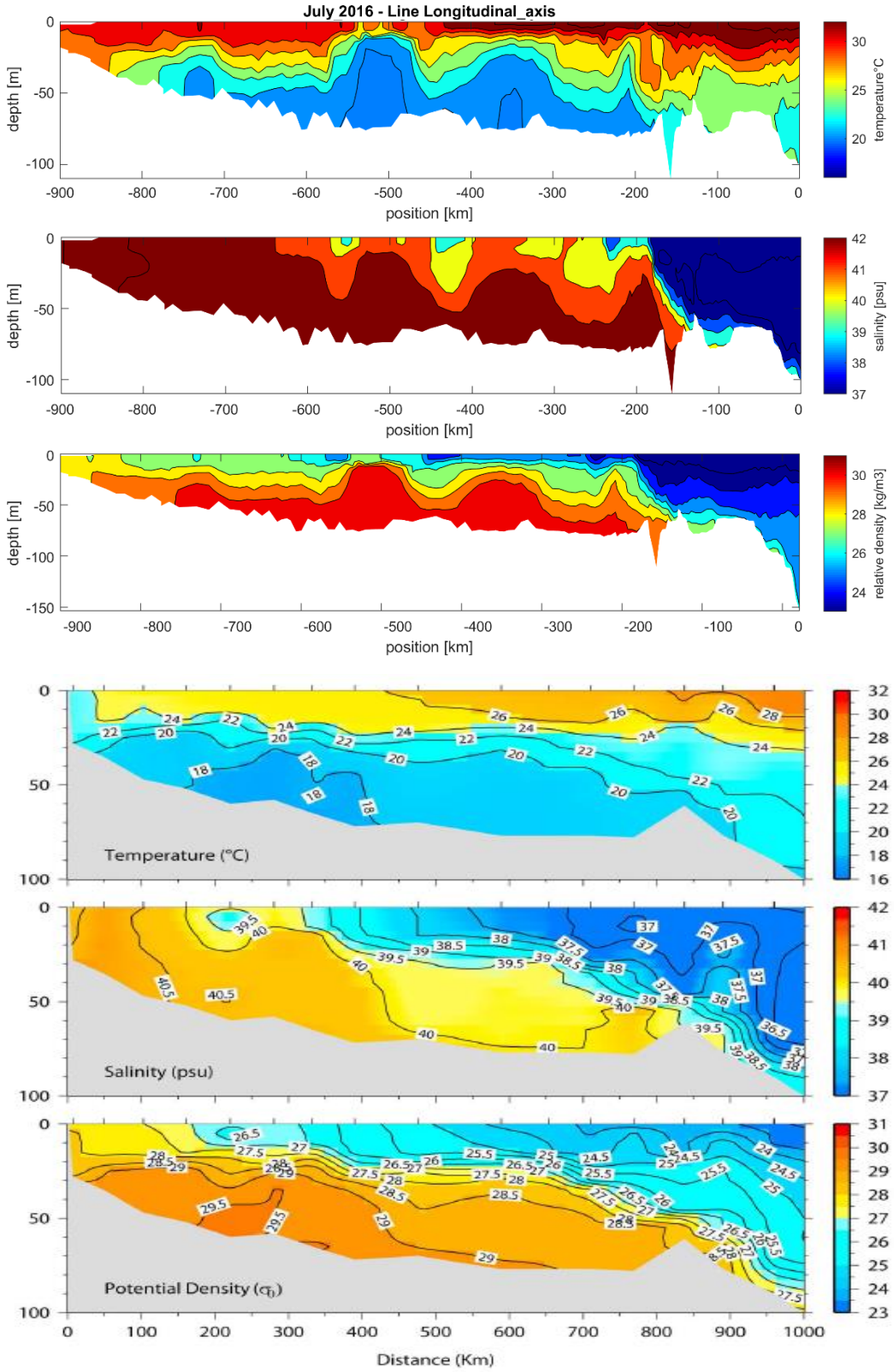

Figure 44: Vertical longitudinal cross section of the simulated reference case in the top three panels and of 1992 measuring data in February.

Comparison to assimilated field data

The assimilated database called *Master Oceanographic Observations Data Set* (MOODS) offers a valuable resource for validation. By interpolation, *Swift* and *Bower (2003)* created spatial maps that represent a two-month-mean surface salinity.

Surface salinity validation

The simulated salinities in 2016 (lower 4 panels) were much higher than the averaged measured salinities during the period of 1960-2000 upper 4 panels) over almost the entire Gulf *(<55 °E)*. The salinity stratification in the summer, causing low surface salinities is not modelled, suggesting that the difference in surface salinity is not an artefact of the exclusion of rainfall, as rainfall is extremely rare during dry season (May to October). The higher temperature of the inflow in summer is modelled similar to measured, which suggests that difference in Gulf surface salinity are not an artefact of boundary conditions difference between 2016 from the 20th century.

Typical depth profile validation

The MOODS database has also been used to sample typical depth profiles. Swift and Bower artificially assigned multiple boxes along the Gulfs longitudinal axis. Plots of depth profiles per set of boxes were drawn per two month period. Coherent with the plots in Swift & Bower (2003) four temperature-salinity sets are compared with simulated data. Boxset 13-14 represents an area adjacent to the strait of Hormuz and will be called '*Gulf entry*'. Boxset 8-9 represents a typical situation in the centre of the Gulf and will be called *'Gulf centre'*. For both areas, depth plots for Salinity and temperature, averaged over May and June as well as over July and August are presented.

Within the boxed areas 50 locations with a minimum depth of 40 meters are randomly selected. The two-month average depth profiles of salinity and temperature for each of the 50 locations are used to calculate a typical depth profile for that box, representing the mean variable value per computational layer.

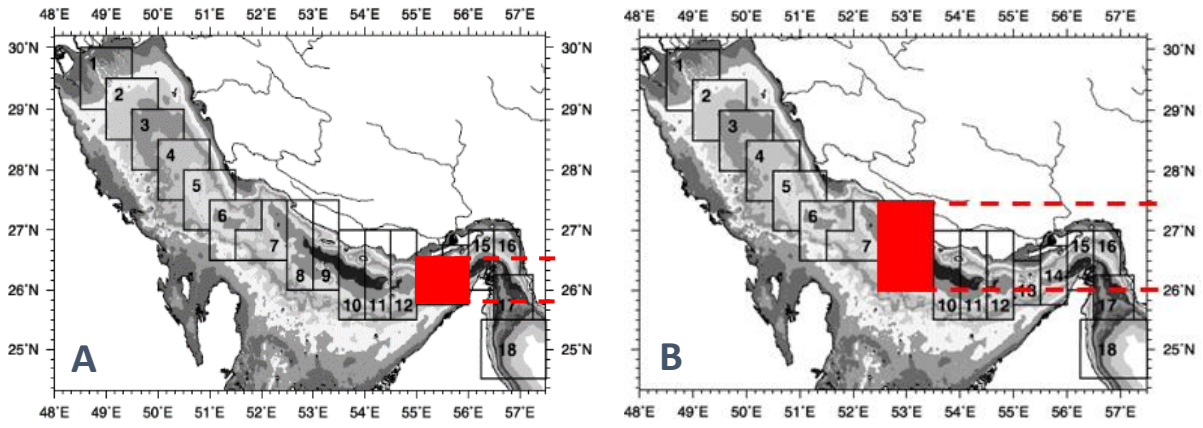

Figure 45: the locations of a) the Gulf entry area and b) the location of the Gulf centre area.

Gulf entry

The water entering the Gulf is modelled in correspondence to MOODS data, except for the temperatures in relatively deep water (> 30m) in the May & June period. The salinities at the water surface are simulated conform to measurements for both periods. The salinities in deep water (> 60 m) are higher than salinity derived from MOODS. This indicates that the 2016 simulated outflow is more saline than the measured outflow over the second half of the 20th century. The discrepancy is larger (~1 PSU) for the simulation with desalination.

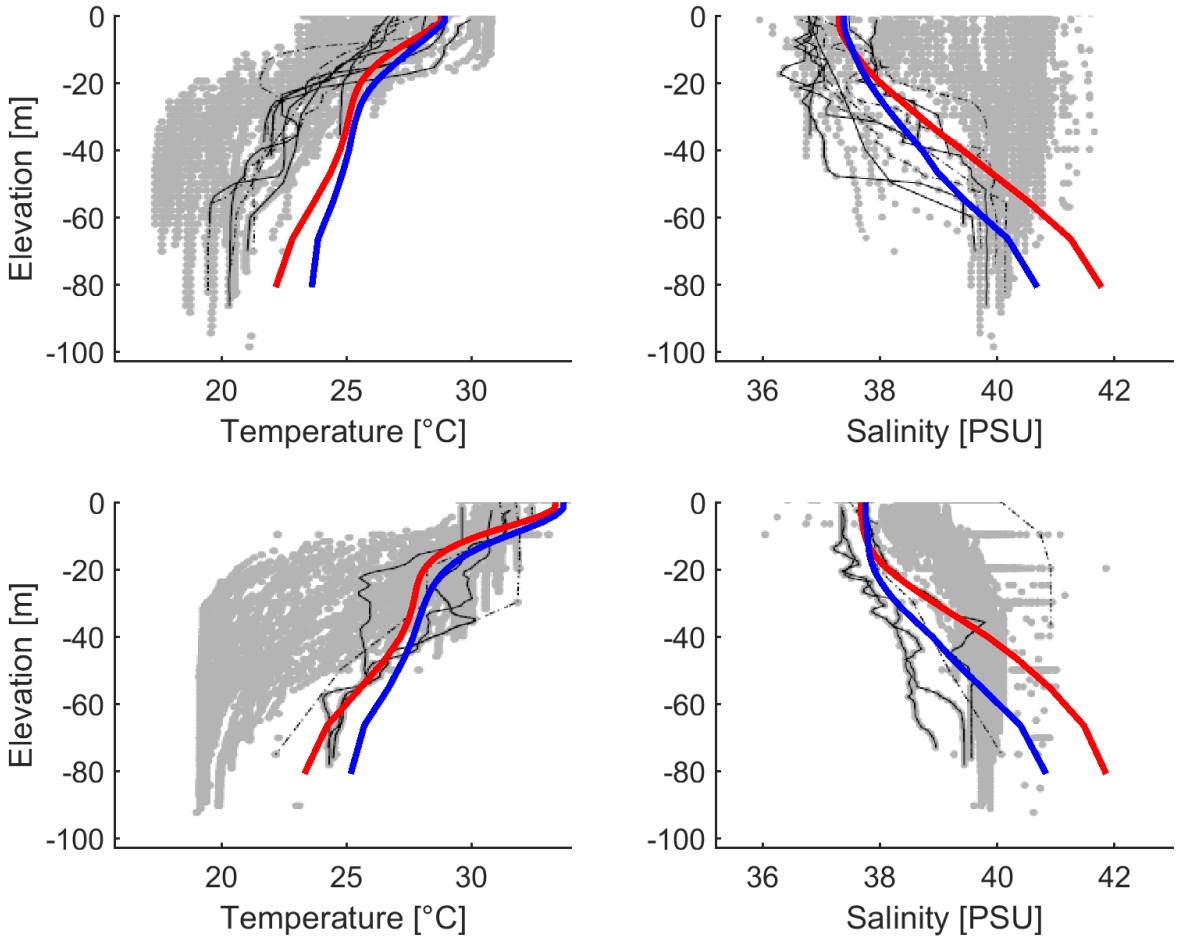

Figure 46: depth profile of Temperature (left column) and Salinity (right column) for the Gulf entry area in May and June (upper row) and July and August (lower row). With in grey: depth profile over the entire Gulf from MOODS, in black the profiles measured in the Gulf entry area. The blue line represents the simulation results of the reference case. In red the simulation results of a model with incorrect representation of brine discharge are showed, but can be disregarded.

Gulf centre

The temperature-depth profiles of the Gulf centre simulated for the period of May and June in 2016 show a lesser stratified flow than the typical measured profiles (black lines in Figure 46). For the period of July & August the vertical temperature gradient is simulated similar to measured, but the depth profiles are shifted up 1 to 2 °C.

The simulated salinity-depth profiles show very little correspondence to the measured profiles. Both surface and bottom salinities are overestimated, the pycnocline is less evident and deeper. This suggest better mixing of the water column and more salt fed from the nearshore areas to the deeper Gulf centre area.

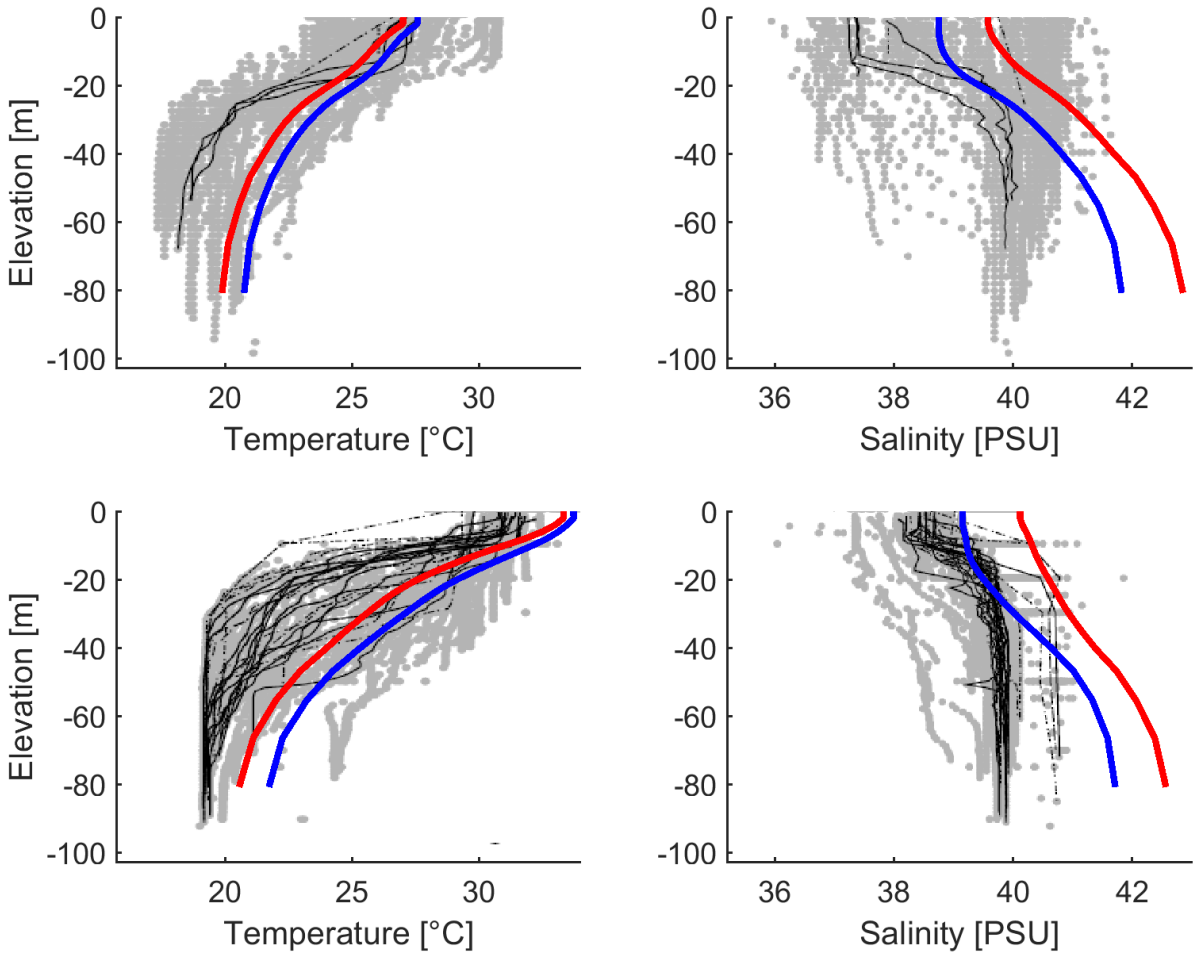

Figure 47: Figure depth profile of Temperature (left column) and Salinity (right column) for the Gulf centre area in May and June (upper row) and July and August (lower row). With, in grey: depth profile over the entire Gulf from MOODS, in black the profiles measured in the Gulf centre area. The blue line represents the simulation results of the reference case. In red the simulation results of a model with incorrect representation of brine discharge are showed, but can be disregarded.

Sea surface temperature comparison

The average simulated surface temperature of February 2009and the a satellite image of 13 February 2009 correspond well (See Figure 49), as do the timelines of simulated and satellite based monthly mean SST. The model shows a high level of agreement considering the temperature and salinity of the inflow water and considering the surface temperature. The model formulations of ocean-atmosphere heat exchange, the boundary conditions and the propagation thereof through the Gulf of Oman are valid. The locations and dimensions of meso-scale eddies (MSE's) in the Arabian Gulf are represented well by the model, but the validity of its strength and the extend of horizontal eddy induced vertical mixing are is sure. Climate conditions have great impact on the MSE's.

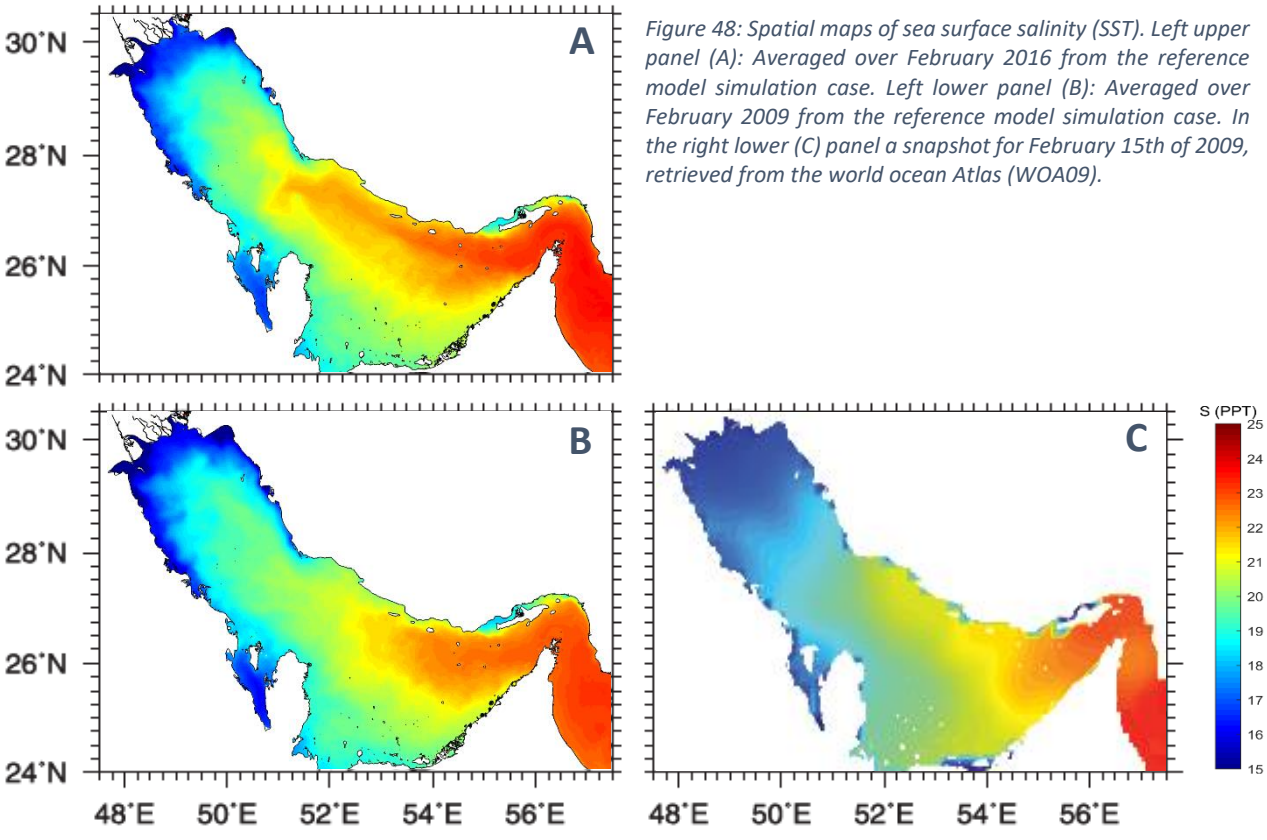

Figure 48: Spatial maps of sea surface salinity (SST). Left upper panel (A): Averaged over February 2016 from the reference model simulation case. Left lower panel (B): Averaged over February 2009 from the reference model simulation case. In the right lower (C) panel a snapshot for February 15th of 2009, retrieved from the world ocean Atlas (WOA09).

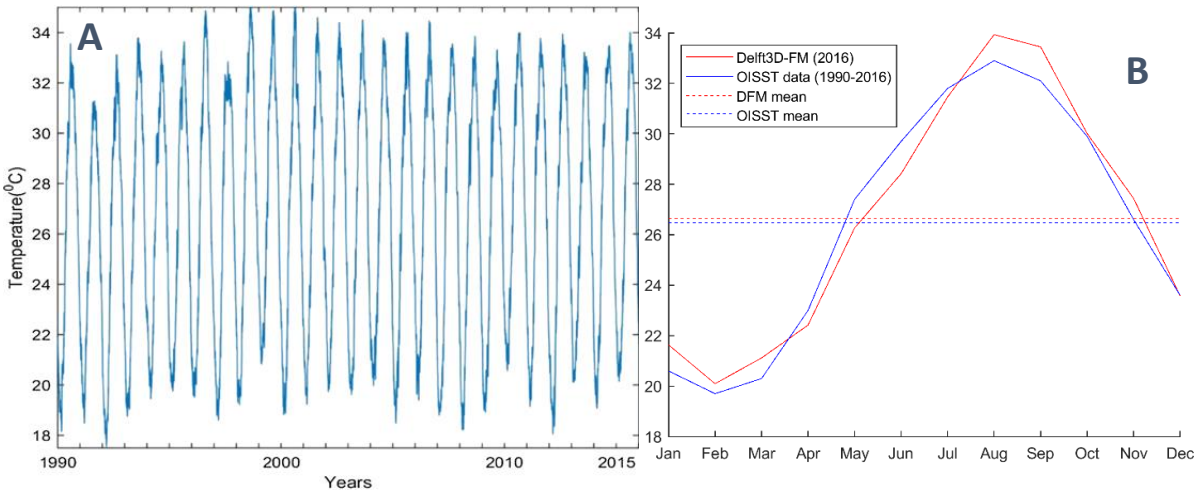

Figure 49: A (left panel) timeline of Gulf averaged sea surface temperature (SST), measured by OISST satellite data (Abbasi, 2018). B (right panel) monthly values of Gulf averaged SST simulated for 2016 with the simulated reference case in red and OISST data averaged over 1990-2016 in blue.

Appendix 14: Simulated year averaged flow velocities of desalination capacity x10 scenario

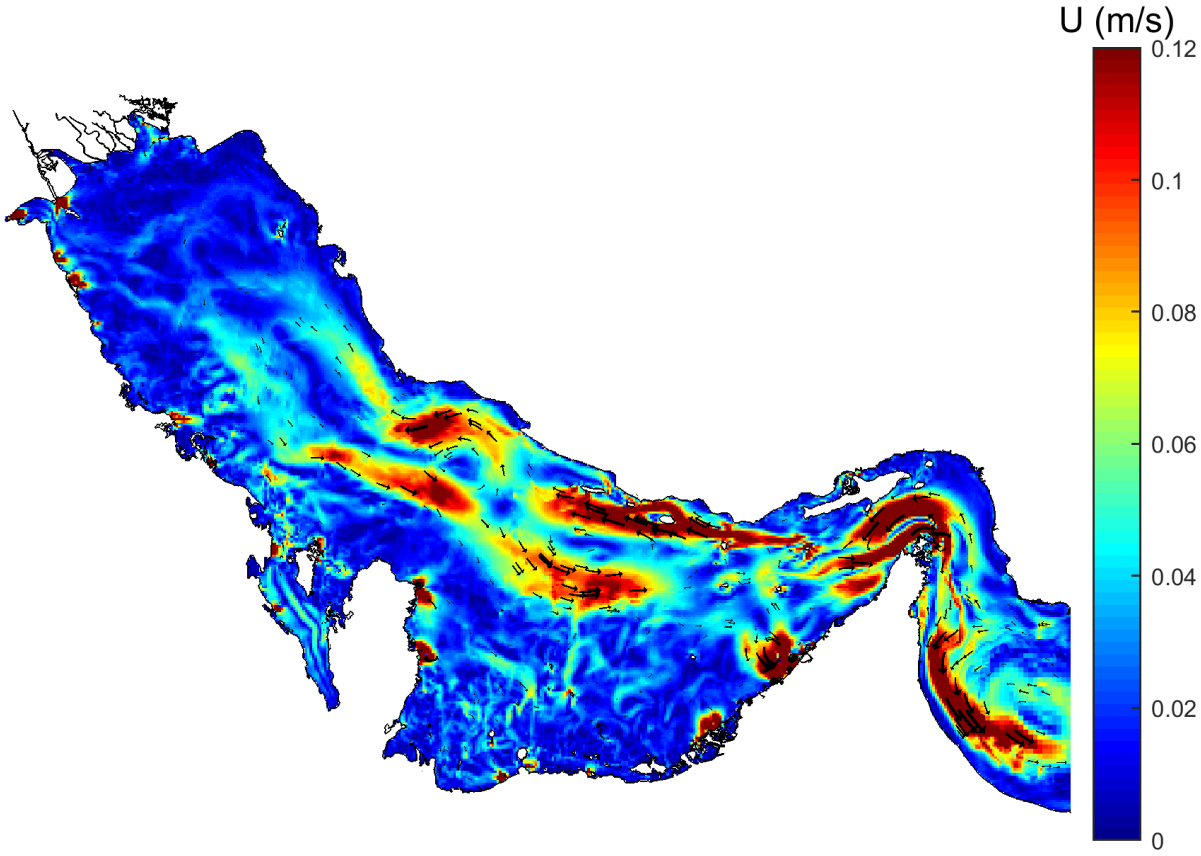

Figure 50: Year averaged, depth averaged simulated flow velocities in case of 10x reference desalination capacity gained by Fourier Analysis.